GROUND-BASED REMOTE SENSING FOR THE DETECTION OF GREENHOUSE GASES BY FOURIER TRANSFORM INFRARED SPECTROMETRY: OPTIMIZATION OF RETRIEVAL STRATEGIES AND ITS VALIDATION

ELIEZER SEPÚLVEDA HERNÁNDEZ

Departamento de Física – Facultad de Física
Universidad de La Laguna
Santa Cruz de Tenerife

February 2014

Doctoral thesis to obtain the degree of Doctor in Physics

Eliezer Sepúlveda Hernández: *Ground-based Remote Sensing for the Detection of Greenhouse Gases by Fourier Transform InfraRed Spectrometry: Optimization of Retrieval Strategies and its Validation*

SUPERVISOR:
Dr. Matthias Schneider
CO-SUPERVISOR:
Dr. Juan Carlos Guerra García

Departamento de Física
Facultad de Física – Universidad de La Laguna
Santa Cruz de Tenerife

February 2014

DECLARATION

Dr. Matthias Schneider from the Karlsruhe Institute of Technology and *Dr. Juan Carlos Guerra García* from the University of La Laguna,

DECLARE,

that *Eliezer Sepúlveda Hernández* with the Degree of Physics by the University of La Laguna, has done the doctoral thesis *'Ground-based Remote Sensing for the Detection of Greenhouse Gases by Fourier Transform InfraRed Spectrometry: Optimization of Retrieval Strategies and its Validation'* under our supervision.

In witness thereof, we authorize the submission of the here presented thesis and sign it,

Supervisor:
Dr. Matthias Schneider

Co-supervisor:
Dr. Juan Carlos Guerra García

Santa Cruz de Tenerife, February 2014

ABSTRACT

This manuscript presents the dissertation of Eliezer Sepúlveda Hernández to obtain the title of Doctor in Physics by the University of La Laguna, according to the modality of compendium of publications. Three peer-reviewed articles published in scientific journals are presented and a summary of the thesis work is given.

The work is based on the high-quality ground-based remote sensing Fourier Transform InfraRed spectrometer for the inversion of precise total column amounts and vertical profiles of different atmospheric trace gases. The thesis is focused on the optimization of the retrieval strategies for the greenhouse gases water vapour and methane. For this purpose the inversion code PROFFIT is applied. The vertical distribution of water vapour and tropospheric methane as derived from our remote sensing measurements are compared against very precise in-situ measurements. Thus, the quality of our retrieved products are documented. These studies have been carry out at the Izaña Atmospheric Research Center (IARC-AEMET), Canary Island, 28.30°N, 16.50°W.

The first article presented in this dissertation, Schneider et al. [37], shows for the first time the capability of the international network TCCON (Total Carbon Column Observing Network) to derive the vertical distribution of tropospheric water vapour (the lower and the middle/upper troposphere can be distinguished). The second article, Sepúlveda et al. [41], presents a novel strategy for the inversion of tropospheric methane independent on the stratospheric methane contribution. This study applies NDACC (Network for the Detection of Atmospheric Composition Change) spectra for the subtropical site of Izaña. The third article, Sepúlveda et al. [42], extends the previous study to a set of nine globally distributed NDACC sites from the Arctic to the Antarctic, and thus under different contrasting atmospheric conditions. We introduced an aposteriori correction that further reduce the stratospheric methane variations. This study demonstrates the feasibility of our proposed inversion strategy.

The manuscript is organize in two parts. The first part (*Dissertation Summary*) gives an overview of the thesis work. It introduces the motivation and objectives, the methodology of work, and summarizes the results and discussion in separate chapters. The second part (*Articles*) presents the three peer-reviewed articles as they have been published in the scientific journals.

There is no favourable wind
for those who do not know
which port one is sailing.

— Séneca

ACKNOWLEDGEMENTS

I would like to thank everybody who has been close by for one or another reason during these years of PhD!! Family, friends, colleagues, and pets...

Special thanks to my supervisor *Dr. Matthias Schneider* from Karlsruhe Institute of Technology. He has conducted this thesis work from its beginning... always with good suggestions, comments and corrections. I really acknowledge his active dedication and patience during the whole thesis period.

I would like to thank my co–supervisor *Dr. Juan Carlos Guerra García* from La Laguna University for supporting this thesis with his rewarding help.

I would like to thank *Dr. Emilio Cuevas Agulló*, Head of the Izaña Atmospheric Research Center (AEMET), for having given me the opportunity to start this thesis work and successfully finish it. I would also like to give my sincere thanks to my colleague *Dr. Omaira García Rodríguez* for her extremely valuable contributions.

I would like to thank *Dr. Thomas Blumenstock* and *Dr. Frank Hase* for hosting me during five months at the IMK-ASF of the Karlsruhe Institute of Technology and teaching on the FTIR technique, PROFFIT code, and their valuable comments on the articles.

I would like to thank *Prof. David Griffith* for hosting me during three months at the University of Wollongong and teaching on the FTIR instrument.

Thanks to the many colleagues from the Izaña Atmospheric Research Center, Karlsruhe Institute of Technology, and University of Wollongong not only for sharing the office time but also the coffee time...

I would like to thank the Spanish Ministry of Education for the financial support received during the years 2009-2013 with the awards of the FPU grant. And also for supporting three brief stays at interna-

tional institutions.

I would also like to thank the many people involved in the FTIR and surface in-situ communities for their works in measuring, improving, maintenance of the instruments and providing the data. This thesis work would not have been possible without these efforts.

And. . . , thanks to the wind for being blowing!!

CONTENTS

LIST OF TABLES

ACRONYMS

ACE Atmospheric Chemistry Experiment

AEMET Agencia Estatal de METeorología

ATMOS Atmospheric Trace MOlecule Spectroscopy experiment

CDRS Cavity Ring-Down Spectroscopy

DOFS Degree Of Freedom of Signal

DPC Dry Pressure Column

ECC Electro Chemical Cell

FID Flame Ionization Detection

FPU Formación de Profesorado Universitario

FTIR Fourier Transform InfraRed

GAW Global Atmosphere Watch

GC Gas Chromatography

GHG GreenHouse Gas

GOSAT Greenhouse gases Observing SATellite

HITRAN HIgh resolution TRANsmission

IARC Izaña Atmospheric Research Center

IASI Infrared Atmospheric Sounding Interferometer

IMK-ASF Institute for Meteorology and Climate Research-Atmospheric Trace Gases and Remote Sensing

ILAS Improved Limb Atmospheric Spectrometer

ILS Instrumental Line Shape

KIT Karlsruhe Institute of Technology

METOP METeorological OPerational satellite program

NCEP National Centers for Environmental Prediction

NDACC Network for the Detection of Atmospheric Composition Change

OCO Orbiting Carbon Observatory

OPD Optical Path Difference

PR Profile Retrieval

SCIAMACHY SCanning Imaging Absorption spectroMeter for Atmospheric CHartographY

SR Scaling Retrieval

TANSO Thermal And Near infrared Sensor for carbon Observation

TCCON Total Carbon Column Observing Network

UOW University of Wollongong

UTC Coordinated Universal Time

UTLS Upper Troposphere / Lower Stratosphere

VMR Volume Mixing Ratio

WACCM Whole Atmosphere Community Climate Model

WMO World Meteorological Organization

Part I

DISSERTATION BY COMPENDIUM OF PUBLICATIONS: DISSERTATION SUMMARY

This first part of the manuscript gives an overview of the thesis work accordingly to the three articles presented. The first chapter introduces the background, the motivation, and objectives of the studies. The second chapter presents the methodology followed during the thesis. The third chapter presents and discusses the main results of the three articles. Finally, the summary and conclusions of the thesis are presented in the fourth chapter.

1 INTRODUCTION

1.1 AN OVERVIEW

The human activities during the last decades has provoked strong modifications in the Earth's atmosphere. Prominent examples are the stratospheric ozone depletion and the upward trend in the concentration of greenhouse gases (GHG). While studies about the stratospheric ozone depletion have progressed rather well, there still exists a considerable deficiency in understanding the sources and sinks of the GHG and the complex interplay between GHG concentrations and climate.

Understanding the global carbon cycle, and predicting its evolution under future climate scenarios is one of the biggest challenges facing science today. The feedbacks between climate change and the carbon reservoirs are not well known or understood. The spatial and temporal distribution of natural sinks over land and oceans remains elusive, which makes impossible a better quantification of their underlying mechanisms and drivers. In addition to natural sinks, anthropogenic emissions from fossil fuel burning and land use change need to be known at regional level and with better accuracy (Ciais et al. [3]). The uncertainty in the sources and sinks of the carbon cycle is a major contributor to the uncertainty in climate predictions. These uncertainties must be reduced to better understand global climate change. In this context, inverse models are applied (e.g. Bousquet et al. [1], Tans et al. [45]). They use atmospheric measurements of GHG concentrations in combination with an atmospheric transport model for estimating the surface fluxes. Currently surface in-situ concentration measurements are the primary data used to constrain these inverse model estimates. Accuracy is extremely good, but there are sampling issues which limit the value of these data for estimating sources and sinks. GHG concentrations measured near the surface are significantly influenced by vertical transport, which is highly variable and poorly simulated in global models. Moreover, these measurements only cover a fraction of Earth's atmosphere. A great number of surface in-situ measurements are therefore required. For instance, the Global Atmosphere Watch (GAW) program has been established by the World Meteorological Organization (WMO).

In this context, remote sensing observations are very important datasets to improve surfaces flux estimations. For instance, O'Brien and Rayner [25] showed that high precision measurements of GHG column-averaged amounts can improve the source/sink estimates

compared to estimates based on the surface layer data.Olsen and Randerson [26] proposed using total column-averaged observations of carbon dioxide (CO_2) as valid input for inverse models. However, given the long atmospheric lifetimes of most GHG (e.g. CO_2 about 30-95 yr and methane (CH_4) about 12 yr), the fluxes are small compared to the resident quantity in the atmosphere. Therefore, the remote sensing accuracy requirements are very demanding, since small errors in the retrieved total column concentrations may result in significant errors in the derived fluxes (e.g. Chevallier et al. [2]).

Remote sensing observations can well complement the surface in-situ data

Currently ground- and space-based remote sensing techniques can provide this kind of data on a regular basis. With the implementation of the Total Carbon Column Observing Network (TCCON, Wunch et al. [52]), the consolidation of the Network for the Detection of Atmospheric Composition Change (NDACC, Kurylo and Zander [19]), and with the new generation of the space-based sensors (e.g. GOSAT, OCO-2...) the remotely-sensed column-averaged GHG amounts are becoming very attractive for inverse modelling and indispensable for climate monitoring.

High-precision Fourier Transform Infrared (FTIR) spectrometer is one of the most suitable instruments to measure GHG concentrations from remote sensing techniques. In fact, it is the technique used by the ground-based TCCON and NDACC networks as well as by several space-based remote sensors like IASI onboard METOP and TANSO onboard GOSAT. This advanced instrument, based on a Michelson Interferometer, measures high-resolution solar absorption spectra with combines a high spectral resolution and a very good signal-to-noise ratio. As a result, it is able to simultaneously detect many different atmospheric constituents.

The ground-based FTIR technique allows for measuring column amounts and volume mixing ratio (VMR) profiles of many different atmospheric gases often with an unprecedented precision. For instance, total column amounts of ozone (O_3), water vapor (H_2O) or CH_4 with a precision of $0.5-1\%$ (Schneider et al. [34], Schneider and Hase [32], Sepúlveda et al. [41]). During the last years there have been a lot of efforts for assuring the high quality of these data: e.g. monitor the instrumental line shape (Hase et al. [15]), monitor and improve the accuracy of the applied solar trackers, thereby improving the knowledge of the observed airmass (Gisi et al. [10]) as well as for developing sophisticated retrieval algorithms (Hase et al. [16]). The good quality of this long-term ground-based FTIR data sets has been extensively documented by theoretical and empirical validation studies (e.g., Schneider et al. [35], García et al. [8], Sepúlveda et al. [41]). Furthermore, these ground-based FTIR products have been used to validate remote sensing products from space. For example, validation of carbon monoxide (CO), H_2O, and isotopes of H_2O measured by SCIAMACHY (Frankenberg et al. [7], Laat et al. [20]); CO measured

by ACE (Clerbaux et al. [4]), validation of O_3, nitric acid (HNO_3), nitrous oxide (NO), CH_4 measured by ILAS (Griesfeller et al. [12]) and in particular the validation for the IASI sensor of O_3, H_2O, and isotopes of H_2O and CH_4 (Viatte et al. [46], Schneider and Hase [33], García et al. [9]).

Water vapour is the dominant greenhouse gas while carbon dioxide followed by methane are the most important anthropogenic greenhouse gases

Among these GHG, water vapour and methane play an important role in this thesis. Water vapour is the dominant GHG in the atmosphere, and in particular its concentration and evolution in the upper troposphere and lower stratosphere (UTLS) are of great scientific interest for climate modelling (Spencer and Braswell [43]). Water vapour is the main responsible atmospheric gas that regulates the weather and climate and contributes with about 90% of the Earth's natural greenhouse effect. The continuous cycle of evaporation, vapour transport, cloud formation, and precipitation distributes water and energy around the globe. The quick changes of atmospheric water vapour concentrations with time, their large horizontal gradients, and their decrease of several orders of magnitude with height makes their accurate detection a challenging task for any measurement technique.

Although GHG concentrations as CO_2 and CH_4 have changed naturally over the past several thousand years, human activities are responsible for its recent strong increase. The increased anthropogenic emissions are mainly due to extraction and distribution of fossil fuels, industry, agriculture (including biomass burning), and waste. CO_2 is the most important anthropogenic GHG followed by CH_4. Their concentrations have been continuously modified by human activities since pre-industrial times (1750): for CO_2 from about 280 ppm to more than 400 ppm nowadays, and for CH_4 from 715 ppb to about 1900 ppb nowadays. As consequence these two GHG show the highest radiative forcing: for CO_2 1.66 ± 0.17 Wm^{-2} and for CH_4 of 0.48 ± 0.05 Wm^{-2}. Although CH_4 is less abundant than CO_2, it is more efficient than CO_2 to trap outgoing long wave radiation (IPCC [17]).

1.2 MOTIVATION

The Izaña Atmospheric Research Center (IARC), located in the Tenerife island is a worldwide reference station. Since almost three decades, the IARC aims at monitoring atmospheric constituents that are capable of forcing change in the climate of the Earth, through modification of the atmospheric radiative environment (GHG and aerosols), and those that may cause depletion of the global ozone layer. This site takes part in the ground-based FTIR international networks NDACC and TCCON since 1999 and 2007, which measure high- and low- resolution solar absorption spectra, respectively. It is a global GAW station since 1984 and belongs to other many international and national networks. This station is usually located above a strong subtropical

temperature inversion layer, acting as a local barrier pollution and being very well situated to study the free troposphere. This fact only occurs in few stations around the world. The high-precision ground-based FTIR measurements at the IARC are excellent for monitoring subtropical long-term time series of many different GHG concentrations and for validating satellite measurements. These FTIR measurements are also very valuable as inputs for estimating surfaces carbon fluxes of the subtropical North Atlantic region. Moreover, the possibility to empirically validate our FTIR products with in-situ measurements, taken at the same station, make our results more valuable.

Very recently, retrieval strategies for determining H_2O vertical distribution have become feasible within NDACC (e.g. Schneider et al. [34, 36, 39]). However, within TCCON no H_2O profiles have been shown. TCCON H_2O profiles would be very desirable for complementing the NDACC H_2O dataset as might provide tropospheric H_2O data with an unprecedented high measurement frequency.

On the other hand, the establishment of an improved NDACC CH_4 retrieval guideline is under discussion. The objective is an NDACC CH_4 product that approaches the high precision requirements of TCCON (a few per mil). Different studies have been developed (e.g. Sussmann et al. [44]) without finding a general agreement within the network. The CH_4 total column-averaged is affected by the strong vertical gradient in the stratosphere. Therefore, strongly dependent on the tropopause altitude. The uncertainty in modelling the variations of the tropopause altitude and of stratospheric CH_4 significantly limits the usefulness of the CH_4 total column-averaged observations for inverse modelling purposes.

We face this thesis work with the idea of contributing to these two important issues.

1.3 OBJECTIVES

The general aim of this dissertation is the determination of total column amounts and profiles of different GHG concentrations from ground-based FTIR measurements obtained at the super-site of Izaña and its validation against in-situ measurements. In order to achieve precise total column amounts and profiles of any infrared absorber, a dedicated retrieval set up must be carefully developed. In this thesis we aim to optimize the inversion of two main GHG absorbers, H_2O, and CH_4. Firstly, we will investigate the possibilities of the low-resolution near-infrared TCCON spectra to determine the vertical distribution of the tropospheric H_2O. Secondly, we will investigate the possibilities of the high-resolution mid-infrared NDACC spectra to determine precise total column amounts and tropospheric CH_4 being independent from the stratospheric contribution.

2

WORKING METHODOLOGY

This chapter presents the working methodology applied during the thesis. The measurement site, its situation and the activities related with the thesis work will be given. A detailed information about the FTIR instrument will be presented. We will explain how the FTIR spectra are evaluated in order to retrieve the different atmospheric gas concentrations and how we estimate the theoretical error of the FTIR products. Finally, we will show the independent techniques used to validate our FTIR data.

2.1 THE MEASUREMENT SITE

This thesis has been carried out at the high mountain super-site observatory of the Izaña Atmospheric Research Centre (IARC) in the Canary Island of Tenerife, located at 2370 m a.s.l., at 28.30°N, 16.50°W and about 300 km from the African West coast (Figure 1). The IARC belongs to the Spanish State Agency of Meteorology (AEMET is its Spanish acronym). The observatory is located in the subtropical North Atlantic Ocean and above a stable trade wind inversion layer (typically located between 800 and 1500 m a.s.l.) that works as a natural barrier for local pollution. Its situation provides clean air and clear sky conditions, during almost the whole year, offering excellent conditions for in-situ and remote sensing observations. Generally, during daytime the strong diurnal insolation generates a slight upslope flow of air originating from below the inversion layer, but during nighttime the inverse circulation is established (downslope flow). During the latter conditions, the airmasses at Izaña are well representative for the free troposphere of subtropical North Atlantic region. In winter (December to April) the mean dynamical tropopause height is 10.5 km, although large variations are observed, i.e. both typical midlatitudinal values of 8–10 km and typical tropical values of 13–16 km are possible. In summer (July to September), when there are less disturbances in the ULTS, the tropopause height is relatively stable and is located around 14.5 km. This pronounced inter-seasonal and day-to-day variability in winter is typical of a subtropical region, since it is the transition area from the high tropical tropopause to the lower mid-latitude tropopause (Rodriguez-Franco and Cuevas [30]).

This thesis work has been carried out at the Izaña Atmospheric Research Centre, located in the Tenerife island, Spain.

The IARC is one of the world-wide leading atmospheric monitoring facilities that offers perfect scientific infrastructures. It has a comprehensive measurement program of a large variety of atmospheric constituents. Detailed information of the activities, programs, projects,

etc. of the observatory can be found in its official website `http://www.izana.org/`. Here, only the activities directly related with the thesis work are discussed.

In 1999 a collaborative agreement was signed between the IMK-ASF (KIT, Germany) and the AEMET-IARC and, as result, a Bruker IFS 120M FTIR spectrometer was installed in the observatory. In 2005 this spectrometer was replaced for the upgrated version, a Bruker IFS 120/5HR, one of the most complete remote sensing instrument available (Figure 1). An intercomparison study between both instruments (IFS 120M - IFS 120/5HR) can be found in Sepúlveda et al. [41] and García et al. [8]. The ground-based FTIR spectrometer in the IARC is the only one dedicated exclusively to atmospheric research in Spain.

The IARC FTIR actively contributes to the international remote sensing networks of NDACC and TCCON and participates in national and international projects (e.g. currently NOVIA,... as nationals and NORS, INGOS, MUSICA, VALIASI,... as internationals projects, respectively). The IARC is a global station of the GAW program since 1984, when it started measuring continuously surface in-situ CO_2 and CH_4, followed by N_2O and SF_6 in 2007.

TOTAL CARBON COLUMN OBSERVING NETWORK (TCCON) is focused on the measurement of accurate and precise total column abundances of GHG concentrations (mainly CO_2, CH_4 and N_2O) and aims at a precision of 1-2 per mil. TCCON measures in the near-infrared spectral region with high-quality ground-based FTIR spectrometers and applies the same measurement protocols and retrieval set up through the whole network. Currently there are about 19 globally distributed sites. Details on this network can be found in Wunch et al. [52].

NETWORK FOR THE DETECTION OF ATMOSPHERIC COMPOSITION CHANGE (NDACC) provides long-term observations of many trace gases and allows assessment of their impact on global climate. It is composed of more than 70 high-quality remote-sensing research stations operating several different measurement techniques. Currently, 22 NDACC sites operate high-quality ground-based FTIR spectrometers measuring in the mid-infrared spectral region. Details on this network can be found in Kurylo and Zander [19].

GLOBAL ATMOSPHERE WATCH (GAW) program has been established by the World Meteorological Organization (WMO) in order to ensure consistent high quality standards. It measures high quality in-situ GHG concentrations (e.g. compatibility between laboratories of ± 2 ppb for CH_4, ± 0.1 ppm for CO_2, and ± 0.1 ppb for N_2O).

The AEMET has a well established radiosondes program since 1970 in the Tenerife island. The meteorological radiosondes are launched

twice a day (00 and 12 UTC) from the Güimar station (WMO station #60018, 105 m a.s.l.), 15 km southeast of the observatory. Until June 2005 the Vaisala RS80 was employed but since then, the Vaisala RS92 have been used.

Figure 1: a) Main building of the Izaña observatory. b) Scientific container hosting the Bruker IFS 120/5HR instrument at IARC. c) The FTIR experiment inside the container (the temperature and humidity conditions are controlled).

This thesis has also used data from others atmospheric measurement stations. From eleven surface in-situ GAW stations and from nine globally distributed NDACC FTIR sites (that take part on the project MUSICA[1]). The doctoral student has visited and worked for a period of eight months at two of those NDACC FTIR stations: at the Karlsruhe Institute of Techonology (KIT), Germany and at the University of Wollongong (UOW), Australia. Information of all of these sites can be found in the third article presented in this dissertation.

2.2 FOURIER TRANSFORM SPECTROMETRY: INSTRUMENT AND GENERAL CONCEPTS

Most atmospheric molecules interact with electromagnetic radiation in the infrared spectral region, which makes infrared remote sensing an important tool for atmospheric research. This thesis work is based on the ground-based FTIR experiment. Generally, the experiment uses the direct solar radiation. However, measurements with

1 MUlti-platform remote Sensing of Isotopologues for investigating the Cycle of Atmospheric water, Schneider et al. [39]

less sensitivity using the moon as the light source have been performed (Notholt et al. [24], Notholt and Lehmann [23], Wood et al. [51]), but are not used in this dissertation.

The solar absorption spectra is measured with a Fourier Transform Infrared spectrometer

The ground-based FTIR experiment consists in a high precise solar tracker that captures the direct solar light beam and couples it into a high resolution Fourier Transform spectrometer. The high precision solar tracker is controlled by a combination of astronomical calculations and a solar quadrant sensor, or more recently by a digital camera (Gisi et al. [10]), for active tracker control. The FTIR instrument is based on the two-beam interferometer originally designed by Michelson in 1891. The Michelson interferometer is a device that can divide a beam of radiation into two paths and then recombine the two beams after a path difference has been introduced. A condition is thereby created under which interference between the beams can occur. The variation of intensity of the beam emerging from the interferometer is measured as a function of path difference by a detector. The path difference, also known as optical path difference (OPD), is measured with a monochromatic laser (normally a helium neon laser). The observed intensity fluctuation is an interferogram which is converted by a Fourier transformation into a spectrum. A very detailed description of Fourier transform spectrometry can be found in the textbook of Davis et al. [5].

Currently at IARC we use a Bruker IFS 120/5 HR instrument that records direct solar spectra in the mid- and near- infrared spectral region, using a set of different apertures, filters and detectors. A general view of the FTIR system is shown in Figure 1. The mid-infrared measurements are made between 740 and 4250 cm^{-1}, corresponding to $13.5 - 2.4\,\mu m$, with a spectral resolution of 0.005 cm^{-1}, defined as $0.9/OPD_{max}$, being the OPD_{max} the maximum OPD (180 cm). The near-infrared measurements are made between 3800 and 15500 cm^{-1}, corresponding to $2.6 - 0.65\,\mu m$, with a resolution of 0.02 cm^{-1} (OPD_{max} of 45 cm). In the mid-infrared spectral region a potassium chloride (KBr) beamsplitter and either of two liquid-nitrogen-cooled semiconductor detectors are used for the record of the interferogram. The photovoltaic indium antimonide (InSb) detector or the photoconductive mercury-cadmiun-telluride (HgCdTe), MCT detector. These detectors are sensitive to radiation from $1850 - 9600$ cm^{-1} ($5.4 - 1.1\,\mu m$) and $680 - 6000\,cm^{-1}$ ($14.7 - 1.7\,\mu m$), respectively, and are typically used in conjunction with narrow-bandpass filters and different apertures (current settings at IARC are listed in Table 1). In the near-infrared spectral region a calcium fluoride (CaF_2) beamsplitter and an Indium Gallium Arsenide (InGaAs) (3800-12000 cm^{-1}) or a Silicon (Si) (9500-30000 cm^{-1}) photodiode detectors are used at room temperature for the record of the interferograms. As aforementioned, the first spectrometer at the IARC was the Bruker IFS 120M which was operated between 1999 and 2005. This instrument only measured in the mid-

Table 1: Current measurement settings applied for the acquisition of the IARC FTIR spectra, accordingly to the NDACC and TCCON recommendations.

Filter No.	Entrance aperture (mm)	Spectral range (cm^{-1})	Detector	Resolution (cm^{-1})
1	0.8	$3950 - 4300$	InSb	0.005
2	1.0	$2700 - 3500$	InSb	0.005
3	0.8	$2420 - 3080$	InSb	0.005
4	1.0	$1950 - 2700$	InSb	0.005
5	1.0	$1800 - 2200$	InSb	0.005
6	1.5	$700 - 1400$	MCT	0.005
7	1.5	$3950 - 11000$	InGaAs	0.02

infrared spectral region, at slightly higher resolution (OPD_{max} of 250 cm), but showed a poorer signal-to-noise ratio and, consequently, a lower sensitivity.

The wavelength dependent sensitivity of the detector and the efficiency of the beamsplitter affects the measured broadband signal. This dependence can be cancelled out by performing an absolute calibration, whereby the instrumental sensitivity is determined by a measurement with a black body cavity emitting Planck radiation of known temperature. However, for standard trace gas retrievals relatively narrow spectral windows are used. Then, an absolute calibration is not required, since high resolution solar absorption spectra are self-calibrating in the sense that the absorption signature is referenced to the surrounding continuum. At the IARC the spectra measured in the mid-infrared region are calibrated using a black body source at 1273 K and in the near-infrared at about 3000 K.

Recording of one spectrum requires between some seconds to a few of tens minutes, depending on the spectral resolution and quality needed. For instance, one scan can be performed in 30 seconds, but normally several scans are co-added in order to increase the signal-to-noise ratio. Therefore, the acquisition of one spectrum can last several minutes.

A constant solar input is required to obtain a correct spectrum. If the intensity of the incoming solar radiation varies during the acquisition of an interferogram, which occurs when there are clouds in the path between the FTIR instrument and the Sun, the resulting spectrum will be distorted. This is due to the fact that the continuum level and the higher-resolution spectral structure will have a different gain signals. Although this distortion may be subtle, it can significantly alter the retrievals. Therefore, observations are only performed under homogeneous sky conditions (generally clear sky conditions). However, in the near-infrared spectral region the detectors are supported by electronics that allow for solar intensity variations during data acquisition. And therefore, these variations can be corrected using the method described by Keppel-Aleks et al. [18], resulting in higher-

quality spectra and less data loss during partly cloudy conditions. This correction does not work under thick clouds.

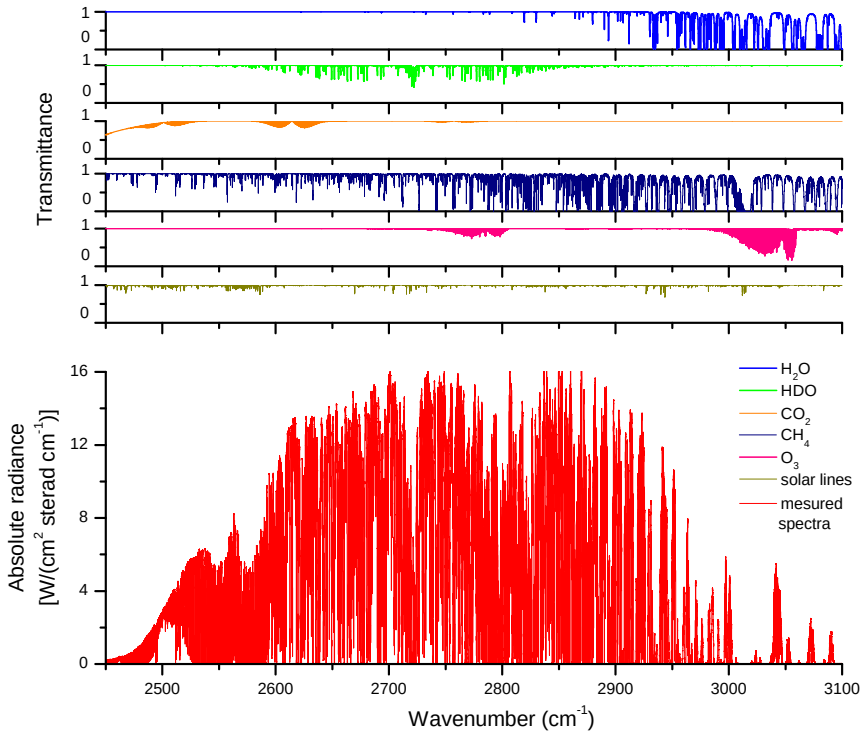

Figure 2: Transmittance of some main absorbers (see legend), solar features (grey line) and solar absorption spectrum measured by the IARC ground-based FTIR spectrometer (red lines).

Solar absorption spectra contain information about the absorbing gases present in the atmosphere (line positions), the amounts of each gas present (line depths/areas) and some information about the altitude distribution of each gas (line shapes). Figure 2 shows a calibrated solar absorption spectrum measured with settings according to filter 3 (see Table 1) on the 20 July, 2013 at the Izaña Observatory (lowermost plot). The upper plots show the absorptions lines of the most relevant absorbers in this spectral region (Meier et al. [21]) plus solar features (observed spectrum from the ATMOS mission, Farmer [6]). This narrow-band filter covers multiple absorbers and gives an impression of the huge amount of information present in these high resolution spectra. Making a zoom to the plot, individual absorption lines of different absorbers are discernible (Figure 3).

The characteristic absorption features seen in Figure 3 are caused by molecules absorbing radiation at frequencies that correspond to the allowed transitions between different vibrational and rotational states. As a consequence of Heisenberg's uncertainty principle, absorption lines are never infinitely narrow. The shorter the lifetime, the larger the uncertainty in a state's energy and the broader the ab-

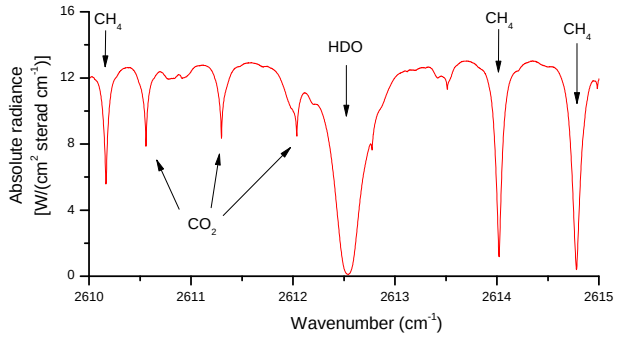

Figure 3: Zoom of Figure 2 for the spectral region $2610 - 2615$ cm^{-1}. The main absorption features are displayed.

sorption or emission line (as the energy uncertainty manifests itself as an uncertainty in the frequency of the line). There are mainly three effects responsible for the broadening of spectral lines:

- *Natural broadening* owing to the finite natural lifetime of a molecule in an excited state. For vibrational-rotational states is usually very small ($< 10^{-6}$ cm^{-1}) and therefore can be ignored in most practical situations.

- *Collision broadening*, also known as *pressure broadening*, occurs when the collisions of atoms, ions or gas molecules shorten the lifetime of states. In gases it is proportional to pressure. This means that absorption lines from spectra taken through the whole atmosphere will have different shapes depending upon the vertical distribution of the absorbing gas in the atmosphere. Pressure broadening leads to a Lorentzian line shape contribution at a given wavenumber υ.

- *Doppler broadening* occurs because molecules travelling with different velocities with respect to the light source absorb at different wavelengths (Doppler effect). Doppler broadening produces a Gaussian line shape due to the Gaussian distribution of molecular velocities.

Pressure broadening dominates in the troposphere, but its effects drop off rapidly with altitude as the pressure drops. Doppler broadening is temperature dependent, but its variation through the atmosphere is much smaller than pressure broadening. Stratospheric gas lines are primarily Doppler broadened. The two types of broadening become equally significant at around 30 km (for $\upsilon \approx 1000$ cm^{-1}). The convolution of Lorentzian and Gaussian line shapes produces a Voigt line shape. This variation of the shape and width of the absorbing gas lines with respect to the pressure means that spectra of atmospheric gases contain information about the altitude of the absorbing

gas as well as the total number of absorbing molecules in the path. Therefore, the high resolution FTIR spectra disclose not only the total column amount of the absorber, but also contain some information about its vertical distribution. The higher the spectral resolution, the larger the amount of information about the absorbers vertical distribution (Paton-Walsh [27]).

In order to deduce correct information from the FTIR measurements, an accurate knowledge of the instrumental line shape (ILS) is crucial to characterize the instrumental performance. If for example, the actual ILS is left undetermined and simply assumed to be perfect, a substantial systematic error might be introduced. A poorly-aligned spectrometer may have an additional loss of modulation efficiency compared with that of an ideal instrument. The ILS of an ideal instrument is affected only by modulation loss that is due to the self-apodization of the interferometer, accepting a finite field of view, and is symmetric. A modulation loss broadens the ILS, and a phase error makes the ILS asymmetric. This simple description allows the characterization of the two main features of any imperfect ILS, its width and degree of asymmetry. Periodic independent ILS measurements using low-pressure gas cell have to be performed. The low-pressure gas inside the cell is chosen such that its absorption lines are preferably narrower than any spectral details observed in the atmospheric spectra. Typically a cell of HBr or N_2O gas is considered within NDACC and of HCl or N_2O within TCCON. At IARC the ILS is retrieved from N_2O absorption measurements using a 20 cm cell at a pressure of 10 Pa within NDACC and a 25 cm cell at a pressure of 5.03 hPa within TCCON. In the atmospheric FTIR community the ILS is determined using the LINEFIT code, as described in Hase et al. [15]. The loss of modulation efficiency and the phase error is described by twenty parameters at equidistant positions along the interferogram connected by an adjustable smoothness constraint. The actual ILS obtained by LINEFIT is then applied in the atmospheric retrievals.

2.3 EVALUATION OF THE SPECTRA

2.3.1 *Retrieval Code*

From one single spectrum many different atmospheric infrared absorbers can be retrieved. However, the inversion of just one single absorber requires a complete dedicated retrieval set up. We derive the total column amounts and the VMR profiles from the FTIR spectra using the retrieval code PROFFIT, which implements the line-by-line radiative transfer model PRFFWD. These algorithms have been developed by Dr. Frank Hase at IMK-ASF (KIT, Germany). Details of the codes can be found in Hase et al. [16]. The PRFFWD model applies the parameters of a spectroscopic database (e.g. HITRAN, Rothman

et al. [31]) and includes a ray tracing module in order to precisely simulate how the radiation passes through the atmosphere (Hase and Höpfner [14]).

In the ground-based remote sensing FTIR community other retrieval codes are also applied: e.g. TCCON uses as official code GFIT (Washenfelder et al. [49]) that only allows scaling retrieval, while NDACC uses SFIT2 (Pougatchev et al. [28]), in addition to PROFFIT. Both codes allow scaling and profile retrievals. A scaling retrieval means that the vertical distribution of the absorber gas is scaled according to the apriori assumptions. A profile retrieval uses optimal estimation techniques that allows the concentration profiles to be adjusted. In addition, PROFFIT allows the simultaneously temperature profile inversion and introduces linear and logarithmic scale retrievals. The latter is specially important when retrieving high variable absorbing gases such as H_2O.

The spectra used in this thesis have been analysed with the inversion code PROFFIT

The basic equation for analysing infrared solar absorption spectra is the Lambert Beer's law:

$$I(\lambda) = I_{sun}(\lambda)\exp\left(-\int_{TOA}^{Obs.} \sigma_x\left(\lambda, s(T,p)x(s)ds\right)\right) \tag{1}$$

where $I(\lambda)$ is the measured intensity at wavelength λ, I_{sun} the extraterrestrial solar intensity, $\sigma_x(\lambda, s)$ is the absorption cross section and $x(s)$ the concentration of an absorber x at location s. The integration is performed along the path of the direct sunlight (between the Observer, Obs., and the Top Of the Atmosphere, TOA). The cross section σ_x depends on temperature and pressure.

The measurement $I(\lambda)$ is simulated by the PRFFWD radiative transfer model. For the purpose of numerical handling, the atmospheric state $x(s)$ and the simulated spectrum $I(\lambda)$ are discretized in form of a state vector x and a measurement vector y. The measurement and state vector are related by a vector valued function F, which simulates the atmospheric radiative transfer and the characteristics of the measurement system (spectral resolution, instrumental line shape, etc.): $y = F(x)$.

The retrieval adjusts the amount of the absorbers to obtain the best fit between the measured and simulated spectra. This is an underdetermined problem, i.e. there are many different atmospheric states (x) that produce almost identical spectra (y). A unique solution cannot be obtained but we can estimate the most probably solution for a given measurement. This optimal estimation approach combines the measurement information with apriori knowledge and provides the most probable solution minimising the following cost function.

$$[y - F(x,p)]^T S_\epsilon^{-1}[y - F(x,p)] + [x - x_a]^T S_a^{-1}[x - x_a] \tag{2}$$

Here the first term is a measure for the difference between the measured spectrum (y) and the spectrum simulated for a given atmo-

spheric state (x), whereby the actual measurement noise level is considered (S_ϵ is the noise covariance). The second term is the regularisation term. It constrains the atmospheric solution state (x) towards an apriori state (x_a), whereby the kind and the strength of the constraint are defined by the matrix (S_a). The constrained solution is reached at the minimum of the cost function Eq. 2.

Since the equations involved in atmospheric radiative transfer are non-linear, the cost function, Eq. 2, is minimised iteratively by a Gauss-Newton method. The solution for the (i+1)*th* iteration is:

$$x_{i+1} = x_a + S_a K_i^T (K_i S_a K_i^T + S_\epsilon)^{-1} [y - F(x_i) + K_i(x_i - x_a)] \quad (3)$$

where K is the Jacobian matrix which samples the derivatives $\partial y/\partial x$ (changes in the spectral fluxes y for changes in the vertical distribution of the absorber x). These regularisation and iteration methods are standard in the field of remote sensing. An extensive treatment of this topic is given in the textbook of Rodgers [29].

VERTICAL RESOLUTION When retrieving vertical profiles, it is important to document the vertical resolution and sensitivity that can be achieved with the remote sensing system. The vertical information contained in the FTIR profile is characterized by the averaging kernel matrix A. It samples the derivatives $\partial\hat{x}/\partial x$ (changes in the retrieved concentration $\hat{x}$ for changes in the actual atmospheric concentration x), describing the smoothing of the real vertical distribution of the absorber by the remote sensing measurement process:

The vertical information contained in the FTIR profile is characterized by the averaging kernel matrix A

$$\hat{x} - x_a = A(x - x_a) \quad (4)$$

Providing these kernels is rather important since they document what is actually measured by the remote sensing system. This matrix depends on the retrieved parameters, the quality of the measurement (the signal-to-noise ratio), the spectral resolution, the solar geometry, the choice of spectral microwindows, and the apriori covariance matrix S_a. The rows of A are generally peaked functions, their full width at half maximum (FWHM) is a measure of the vertical resolution of the retrieval at a given altitude. The so-called sensitivity of the retrievals to the measurements at altitude z is calculated as the sum of the elements of the corresponding averaging kernel (sum along the rows of A), $\sum_j A_{zj}$. It indicates, at each altitude, the fraction of the retrieval that comes from the measurement rather than from the apriori information. A value close to zero at a certain altitude indicates that the retrieved profile at that altitude is nearly independent of the real profile and is therefore approaching the apriori profile. The columns of A give the response of the retrieval to a δ-function perturbation in the state vector. The perturbation should be small enough that the response is linear in the size of the perturbation, but large enough that rounding errors are unimportant. The trace of the averaging kernel

matrix can be interpreted as the degree of freedom of signal (DOFS) of the measurement. It quantifies the amount of information introduced by the measurement and can be considered as the number of independent layer retrieved. The higher the value, the more information is obtained from the measurement.

2.3.2 *Error Analysis*

The error analysis applied to any inverse method shows how a retrieval is related to the true state of the atmosphere and how various sources of errors are propagated into the final product. The error calculations presented in our study apply the error estimation capability incorporated in the PROFFIT retrieval code. The error analysis is based on the analytic error estimation approach of Rodgers [29], where the error given by the difference between the retrieved and the real state, $(\hat{x} - x)$, is linearised about a mean profile x_a (the applied apriori profile), the estimated model parameters $\hat{p}$, and the measurement noise ϵ:

$$(\hat{x} - x) = (\hat{A} - I)(x - x_a) + \hat{G}\hat{K}_p(p - \hat{p}) + \hat{G}\epsilon \tag{5}$$

Here, the circumflex indicates an estimated quantity. I is the identity matrix, $\hat{A}$ is the averaging kernel matrix, $\hat{G}$ the gain matrix ($G = (K^T {S_\epsilon}^{-1} K + {S_a}^{-1})^{-1} K^T {S_\epsilon}^{-1}$), and $\hat{K}_p$ a sensitivity matrix to input parameters (instrumental line shape, spectroscopic parameters, etc). Note that $\hat{p}$ is the best estimate of the model parameters, that differs from the true value p, which is the values that the atmosphere and the instrument know about. The gain matrix $\hat{G}$ samples the derivatives $\partial\hat{x}/\partial y$ (changes in the retrieved atmospheric state $\hat{x}$ for changes at the spectral bin y).

Equation 5 identifies the three classes of errors. The first term on the right hand side, are the errors due to the inherent finite vertical resolution and the limited sensitivity of the observing system (*smoothing error*). The second term are the errors due to uncertainties in the input parameters applied in the inversion procedure, and the third term are the errors due to measurement noise (with an assumed Gaussian noise with $\sigma = \epsilon$).

For the error analysis we assume the following uncertainty sources: measurement noise, ILS (modulation efficiency and phase error), baseline (offset and amplitude), line of sight (solar tracker misalignment), solar lines (intensity and spectral position), spectroscopic line parameters (intensity strength and pressure broadening), temperature and humidity.

2.4 INTERCOMPARISON BETWEEN REMOTE SENSING AND IN-SITU MEASUREMENT TECHNIQUES

The FTIR products require precise documentation of their quality in order to be used as a reference measurement. This documentation is often done by theoretical studies, as mentioned in the previous Section 2.3.2. These calculations give a good overview of the achievable data quality, however, they depend on the assumed error sources. Therefore, a quality assessment should be completed by a comparison to independent measurements of similar or better quality. At IARC, the FTIR H_2O profiles are usually compare to measurements obtained with radiosondes (e.g. Schneider et al. [36]), the FTIR O_3 profiles to Electro Chemical Cell (ECC) or Brewer measurements (e.g. García et al. [8], Schneider et al. [35]), and the FTIR CO_2 and CH_4 column-averaged amounts to surface in-situ measurements (e.g. Sepúlveda et al. [40, 41]).

In the studies presented here, we empirically validate our FTIR H_2O profiles against radiosondes and our retrieved tropospheric column-averaged CH_4 mole fractions against surface in-situ CH_4 GAW measurements.

We use coincident Vaisala RS92 radionsondes to perform the H_2O intercomparison as suggested by (Schneider et al. [36]). The temperature and radiation dependence of the RS92 is corrected (Vömel et al. [47]) and the estimated precision is about 5% for precipitable water vapour and for the lower and middle tropospheric VMR (Miloshevich et al. [22]). In the upper troposphere and for very dry conditions, it is poorer (about $10-20\%$). The FTIR H_2O profiles show a rather vertically poorly-resolved resolution, when comparing to those radiosondes data (resolution of about 20 m). Hence, for an adequate comparison, we have to adjust the vertical resolution of the high-resolved radiosondes data to the poor-resolved FTIR data, by convoluting the RS92 profiles (x_{RS92}) with the FTIR averaging kernels A

$$\hat{x}_{RS92} = A(x_{RS92} - x_a) + x_a \tag{6}$$

The result is a smoothed RS92 profile ($\hat{x}_{RS92}$) with the same vertical resolution as the FTIR profile.

The FTIR measurements are representative of the background signals, thereby the surface in-situ GAW CH_4 data should be filtered to assure comparable conditions, i.e. in-situ regional-scale signals. Different filters have been applied depending on the GAW specific site conditions (time, wind speed, combining information from close stations...). At the GAW stations used in this thesis work, the surface in-situ CH_4 mixing ratios are measured using gas chromatography GC-FID technique or by optical techniques like cavity ring-down spectroscopy (CDRS) or in-situ FTIR analysers. Details on these techniques can be found in Gómez-Peláez and Ramos [11], Winderlich et al. [50], and Griffith et al. [13], respectively.

3

RESULTS AND DISCUSSION

This section presents the findings of this dissertation. Thereby, we summarize the main results and discussion of the three peer-reviewed articles presented for the thesis.

3.1 ARTICLE 1

REMOTE SENSING OF WATER VAPOUR PROFILES IN THE FRAMEWORK OF THE TOTAL CARBON COLUMN OBSERVING NETWORK (TCCON): In this article we demonstrate that TCCON spectra allow to distinguish lower from middle/upper tropospheric water vapour concentrations. We apply an optimal estimation retrieval approach on logarithmic scale to obtain the vertical distribution of H_2O. We perform an error analysis and investigate the vertical information gain for different spectral resolutions. And finally, we empirically validate our H_2O profile FTIR product with data obtained from Vaisala RS92 radiosondes.

TCCON spectra allow distinguishing lower from middle/upper tropospheric water vapour concentrations

The optimal estimation of atmospheric water vapour amounts from ground-based FTIR spectra is far from being a typical atmospheric inversion problem and, due to its large vertical gradient and variability, standard retrieval methods are not appropriate. In this study we apply the inversion strategy as explained in Schneider et al., [34] and Schneider et al. [38] and references therein, using the retrieval code PROFFIT [1]. We have selected the spectral H_2O signatures from six spectral microwindows between $4564 - 4702$ cm^{-1}. These spectral windows contain weak absorption signatures of CO_2, N_2 and CH_4. All these absorbers are jointly fitted. Our forward model applies the HITRAN 2008 (Rothman et al. [31]) spectroscopic line parameters in order to obtain the simulated spectrum. The temperature profiles are taken from the National Centers for Environmental Prediction (NCEP) reanalysis temperature. The apriori information is taken from a large ensembe of Vaisala RS92 radiosonde measurements.

The error estimation method is performed for different spectral resolutions assuming the error sources described in Section 2.3.2. The error estimations reveal that the uncertainties in the ILS, the applied temperatures, and the spectroscopy parameters are the leading error sources. When the temperature is simultaneous fitted with the water vapour lines, the temperature error is reduced. The smoothing error is the most important H_2O total column random error. Water vapour is

1 Please note that we do not use the standard TCCON procedure (scaling retrieval of an apriori profile)

a extremely variable atmospheric trace gas. The FTIR remote sensing system is not equally sensitive at all atmospheric altitude levels and consequently the highly varying vertical water vapour distributions cause significant random errors in the retrieved column abundances.

The smoothing error is the most important H_2O total column random error

We investigate the effect of the spectral resolution on the vertical resolution of the remote sensing system. For this purpose, we have measured spectra with different spectral resolution (0.004 cm^{-1}, 0.02 cm^{-1}, 0.1 cm^{-1}, and 0.5 cm^{-1}). The higher the spectral resolution the longer the time for acquiring a spectra. We conclude that the TCCON spectra (spectral resolution of 0.02 cm^{-1} and spectra acquisition time of 1-2 minutes) achieves a good compromise between vertical resolution and measurement frequency. For TCCON spectra the lower tropospheric water vapour concentration can still be well distinguished from middle/upper tropospheric concentrations (DOFS value of 2.3) and the measurement acquisition time is reduced from 8 minutes for typical NDACC spectra (recorded with a spectral resolution of 0.004 cm^{-1}) to 2 minutes. At resolution lower than 0.02 cm^{-1} the measurement acquisition time is further reduce but also the sensitivity. Then, the profiling capability of the system is limited.

The radiosonde measurements offer a good opportunity for validating the FTIR profiles but for an adequate comparison they have to be degraded to the vertical resolution of the FTIR profiles (we do it accordingly to Schneider et al. [36]). Figure 4 shows coincident measurements for Vaisala RS92 and FTIR H_2O concentrations presented as percentage difference to the apriori climatologic profile. The FTIR data is for TCCON resolution (0.02 cm^{-1}). Two days with different H_2O concentrations are plotted for January 2009, 24 and 25. Both, the FTIR and smoothed RS92 profiles detect very similar differences to the apriori profile, which documents the good quality of the FTIR data. Figure 4 also depicts the profiles produced by an retrieval setup that only allows for a scaling of the apriori profile (e.g. TCCON official retrieval strategy; green dashed line). If the actual profile slope is significantly different from the apriori profile slope the scaled profile and the optimally estimated profile differ significantly (see right pannel). The spectral residuals produced by the scaling retrievals are much larger than the residuals produced by the profile optimal estimation retrieval. This documents that the TCCON spectra contain a lot of information about the vertical distribution of the absorber and an optimal estimation retrieval approach is more reliable.

TCCON measurements can also be used to investigate variations on the tropospheric water vapour distribution on different time scales ranging from few minutes (typical acquisition time) up to several days.

Figure 5 shows the evolution of the lower and middle/upper tropospheric H_2O concentrations (it shows the difference to the climatologic mean). The lower troposphere (black squares) presents large

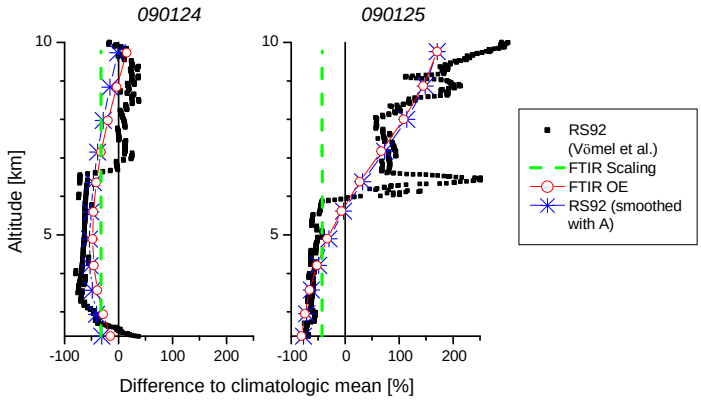

Figure 4: Examples for coincident Vaisala RS92 and FTIR H_2O measurements (scaling and optimal estimation (OE) approach) for spectra taking at TCCON resolution. Presented as percentage difference to a subtropical climatologic profile. A denotes averaging kernel.

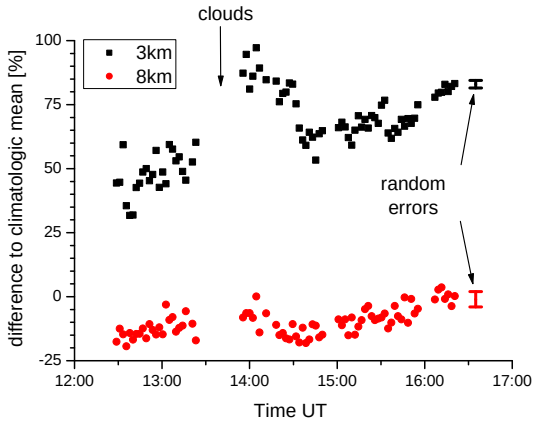

Figure 5: Evolution of the lower (black squares) and middle/upper (red dots) water vapour concentrations on the 19 May 2010.

short term variability after noon time that can be explained due to increased turbulence during the morning hours when the landmass heats faster than the overlying airmass, thereby producing an instable atmospheric layering. This variability is larger than the estimated random error (black error bar in Fig. 5). At the end of the day the situation is different, the landmass cools faster than the overlying airmass, thereby causing high vertical stability. In the upper troposphere (red circles) the diurnal evolution is rather smooth. The water vapour concentrations are rather constant during the whole day. Due to the long-term strategy of the network and the high measurement frequency, the TCCON water vapour profile data offer novel opportunities for estimating the water vapour variability at different time scales and altitudes.

3.2 ARTICLE 2

LONG-TERM VALIDATION OF TROPOSPHERIC COLUMN-AVERAGED CH_4 MOLE FRACTIONS OBTAINED BY MID-INFRARED GROUND-BASED FTIR SPECTROMETRY: In this article we investigate the total column-averaged dry air mole fractions of methane (totXCH4) obtained from a profile scaling and a profile retrieval, and apply two approaches for deriving the tropospheric column-averaged dry air mole fractions: i) we use the FTIR hydrogen fluoride (HF) total column amounts as an estimator for the stratospheric CH_4 contribution and correct the totXCH4 data of a profile scaling retrieval accordingly. We call this product troXCH4$_{post}$. This method has been proposed by Washenfelder et al. [48] for near infrared retrievals and we test it for retrievals in the mid-infrared. ii) We directly determine the tropospheric column-averaged dry air mole fractions of methane from retrieved CH_4 profiles. We call this product troXCH4$_{retr}$. We compare the different FTIR CH_4 data to surface in-situ CH_4 GAW data (CH_{4GAW}). We document the robustness of our suggested approach for obtaining total and tropospheric column-averaged CH_4 concentrations. Our study is done for the mid-infrared NDACC spectra and for the subtropical site of Izaña.

For our CH_4 retrieval we use a set of 4 microwindows (between 2614 and 2904 cm^{-1}) containing strong, unsaturated, and isolated CH_4 lines. We consider spectroscopic signatures of 7 interfering species (H_2O, CO_2, O_3, N_2O, NO_2, HCl, and OCS) and apply spectroscopic parameters from HITRAN 2008 (with 2009 updates, Rothman et al. [31]). As apriori profiles of the interfering species, we apply the climatological entries from WACCM (The Whole Atmosphere Community Climate Model). We use the NCEP analysis for the temperature and pressure input profiles. We examine two different CH_4 fitting procedures: i) we scale the CH_4 WACCM apriori profile and ii) we retrieve CH_4 profiles, whereby a Tikhonov-Phillips method on a logarithmic scale is applied (Schneider et al. [34]).

The totXCH4 is calculated dividing the CH_4 total column by the dry pressure column (DPC) above Izaña. The DPC is calculated converting the ground atmospheric pressure to column air concentration. Similar to Washenfelder et al. [48], we calculate the troXCH4$_{post}$ from the CH_4 total column after correcting the variation in both surface pressure and stratospheric contribution. On the other hand, we calculate the troXCH4$_{retr}$ averaging the retrieved CH_4 VMR profile between Izaña ground level and an altitude of 6.5 km.

Our tropospheric CH_4 is directly calculated from a profile retrieval

The error analysis reveals that the scaling retrieval produces totXCH4 and troXCH4$_{post}$ with precision of 0.51% and 0.61%, respectively. It is important to note that the troXCH4$_{post}$ error calculations do not consider the differences between the CH_4 and HF averaging kernels, thus the actual error is likely larger. The smoothing error is by far

the leading random error and determines the precision of totXCH4. By applying a profiling retrieval, we can reduce the smoothing error, which theoretically improves the precision of totXCH4 to 0.41%. The troXCH4$_{retr}$ has an estimated precision of 0.91%.

We compare different time scale variabilities. When comparing in daily basis the different FTIR CH_4 data with the surface in-situ CH_4 GAW data we obtain that:

- For totXCH4, obtained from scaling and profiling retrieval, there is no significant correlation and a relative difference about 5%.
- For troXCH4$_{post}$ the correlation coefficient is rather low and it does not significantly change when we apply a set of different b-values (the b-value is the assumed slope between HF and stratospheric CH_4 amounts). The relative difference is about 2%, i.e., significantly smaller than for totXCH4.
- For troXCH4$_{retr}$ we get a reasonable correlation (correlation coefficient of 0.60) and a relative difference about 0.13%. This comparison demonstrates that we can retrieve tropospheric CH_4 concentrations directly from the NDACC spectra.

In addition, we assess whether the profiling retrieval can correctly detect the CH_4 variation in the UTLS. We observe that the troXCH4$_{retr}$ time series shows the upwards shift of the tropopause altitude during the summer months and can validate this signal by the HF observations. Vice versa to CH_4 the HF concentrations are very small in the troposphere and start to increase significantly as function of altitude in the stratosphere. The total column of HF is a good indicator for the tropopause altitude and thus, it should be anticorrelated with the CH_4 UTLS concentrations. Indeed, we obtain a strong anticorrelation ($R = -0.81$) between the HF total amounts and the CH_4 mixing ratio at 21 km (altitude that is very representative for the UTLS region). This confirms the good quality of our CH_4 profile retrieval.

In addition, we compare the annual cycle of the different CH_4 FTIR products with the GAW data. For this purpose, we de-trend the CH_4 time series (see Figure 6). We observe that totXCH4 does not reproduce the tropospheric surface in-situ CH_4 variability. The totXCH4 annual variability is dominated by the annual variability of the tropopause height, which is lowest by the end of winter and continuously increases during summer. The totXCH4 cycle obtained from the scaling retrieval (shown as open green triangles in Figure 6) differs from the totXCH4 cycle obtained from the profile retrieval (solid orange triangles).

The troXCH4$_{retr}$ cycle is the more consistent with the GAW in-situ cycle

The troXCH4$_{post}$ cycle (open blue stars) behaves similar to the totXCH4 cycle and thus, the HF correction method as applied in this study does not adequately account for the stratospheric contribution. Finally, the troXCH4$_{retr}$ cycle (solid red stars) is more consistent with

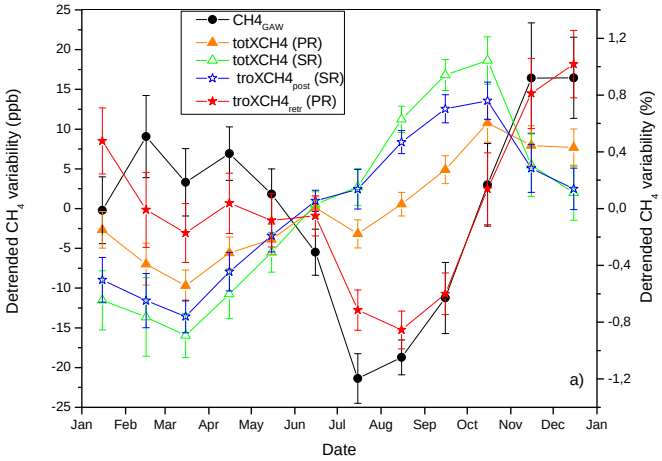

Figure 6: The multi-annual mean annual cycles of different CH_4 datasets. (SR) denotes scaling retrieval and (PR) profile retrieval. The error bars correspond to the standard error of the mean [2 x STD/sqrt(N)].

the GAW in-situ cycle (dark circles). The amplitudes and phases of both cycles are very similar, thereby confirming that the directly retrieved tropospheric column-averaged XCH_4 values are a very good proxy for the free tropospheric CH_4 concentrations.

Finally, the interannual trend of the different FTIR products agree similarly well with the GAW data.

3.3 ARTICLE 3

TROPOSPHERIC CH_4 SIGNALS AS OBSERVED BY NDACC FTIR AT GLOBALLY DISTRIBUTED SITES AND COMPARISON TO GAW SURFACE IN-SITU MEASUREMENTS: Article 2 only works with data from the subtropical site of Izaña. For article 3 we extend that study to a set of nine globally distributed NDACC sites (listed in Table 2) and focus on the quality of the lower free tropospheric CH_4 FTIR data. We compare this tropospheric CH_4 data with surface in-situ CH_4 measurements from the GAW network (stations listed in Table 2). We document that our tropospheric CH_4 data are largely independent on the local small-scale signals of the boundary layer, and only weakly dependent on UTLS CH_4 variations. In order to achieve the weak dependency on the UTLS, we use an aposteriori correction method. The study shows that there is a reasonable consistency between the tropospheric CH_4 data produced for the different NDACC FTIR sites.

We extend the last study to a set of nine globally distributed NDACC sites

We apply exactly the same retrieval setup for all the NDACC FTIR stations, improving the retrieval strategy of Sepúlveda et al. [41] (article 2). We slightly change our microwindow selection to further re-

Table 2: Pairing of NDACC FTIR and surface in-situ GAW stations.

FTIR NDACC site	Location	GAW site	Location
Eureka	80.1°N, 86.4°W	Alert	82.45°N, 62.52°W
Ny-Ålesund	78.9°N, 11.9°W	Ny-Ålesund	78.9°N, 11.9°W
Kiruna	67.8°N, 20.4°E	Pallas-Sammaltunturi	67.97°N, 24.12°E
Bremen	53.1°N, 8.9°E	Mace Head	53.33°N, 9.90°W
Karlsruhe	49.1°N, 8.9°E	Schauinsland	47.92°N, 7.92°E
Izaña	28.3°N, 16.5°E	Izaña	28.3°N, 16.5°E
Wollongong	34.4°S, 150.9°E	Cape Grim	40.68°S, 144.68°E
Lauder	45.1°S, 169.7°E	Lauder	45.1°S, 169.7°E
Arrival Heights	77.8°S, 166.7°E	Arrival Heights	77.8°S, 166.7°E

duce the impact of H_2O. We again apply the HITRAN 2008 spectroscopy (with 2009 updates, Rothman et al. [31]) for all the interferences species, except for CH_4, for which we use a new preliminary linelist parameters provided by D. Dubravica and F. Hase (private communication, December 2012). Similar to the previous study: we perform the inversion of the CH_4 profiles on a logarithmic scale applying a Tikhonov–Phillips ad-hoc constraint; the apriori knowledge is taken from the WACCM model and we use the NCEP analysis as the temperature and pressure input profiles.

FTIR measurements contain information about the vertical distribution from the surface up to the middle stratosphere. We obtain typical DOFS values close to or above 2.5, indicative of the number of independent layers present in the retrieved profile. The left panel of Figure 7 shows lower/middle tropospheric row averaging kernels as red lines and kernels at and above the UTLS as blue lines. However, the averaging kernels indicate contributions of the UTLS to the retrieved tropospheric CH_4 (negative values between 12 and 25 km for the red tropospheric kernels). This means that the stratospheric CH_4 variations might significantly affect the retrieved tropospheric CH_4 signals, especially since in the UTLS the typical CH_4 variation (caused by tropopause altitude shifts) is larger than the small tropospheric CH_4 variation. These cross-dependencies are the leading error source in our retrieval, but can be significantly reduced by an aposteriori correction method. This consists in a simple matrix multiplication and can be easily applied to any CH_4 profile retrieval whenever the retrieved CH_4 state is provided together with the corresponding averaging kernel. The details of this correction method can be found in section 2.3.3 of this third article (in Chapter 7). The right panel of Figure 7 depicts the same as the left panel but for the modified averaging kernel. We see that for the aposteriori corrected row kernel (green lines) there is much less cross talk from the UTLS than for un-

corrected/original kernel (red lines, left panel). At the same time, the sensitivity with respect to the lower troposphere is not modified.

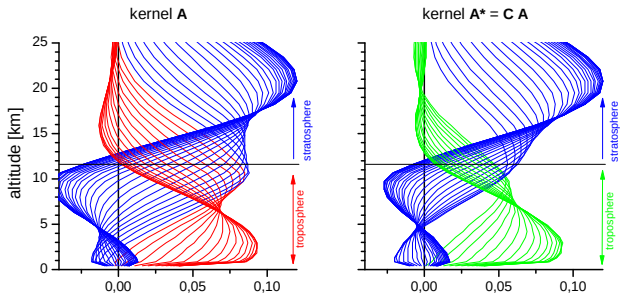

Figure 7: Row averaging kernels of the CH_4 product for a typical observation. Left panel: original kernels A (red: tropospheric kernels, blue: UTLS kernels). Right panel: kernels A^* obtained after applying the aposteriori method (green: tropospheric kernels, blue: UTLS kernels). The typical altitude where the UTLS starts is indicated by the horizontal black line (11.5 km).

The smoothing error is calculated by separating the signals into the three rather independent atmospheric CH_4 signals: the small-scale boundary layer signal ($S_{sm,bl}$), the regional-scale tropospheric signal ($S_{sm,tro}$), and the UTLS signal ($S_{sm,utls}$). We see that, when the aposteriori correction method is not applied, the FTIR can well resolve the tropospheric background CH_4 signals with a precision of 0.4-1.2% between the surface and 6 km altitude. However, the cross dependency on the UTLS variability, caused by shifts in the tropopause altitude, adds an uncertainty of up to 1.5% to the lower tropospheric CH_4 product. This error is the more important, the lower the tropopause (it is more important for the polar than for the subtropical sites) and it can occasionally exceed 2%, which is on the same order as the tropospheric CH_4 variations. The contribution from the stratospheric CH_4 signal is clearly the leading smoothing error.

When we apply the correction method the smoothing error caused by the stratospheric variability is significantly reduced in the troposphere if compared to the uncorrected state. We get for all stations (except for Arrival Heights) total smoothing errors that are smaller than 1%. We conclude that to obtain precise tropospheric CH_4 product, it is important to apply the aposteriori correction.

We empirically validate our retrieved tropospheric CH_4 by comparison with surface in-situ CH_4 data obtained from GAW stations located close to the NDACC FTIR sites. We pair the stations as shown in Table 2. In order to get the regional-scale CH_4 signal we apply site specific filters (e.g. filtering by time, wind speed,...). For the Schauinsland Central Europe GAW station, this kind of filter does not rea-

sonably eliminate all the expected local small-scale signals. For this reason, we introduce a new filter method that combines the surface in-situ CH_4 data measured at two Central European sites (Schauinsland and Jungfraujoch). We define the Schauinsland CH_4 background signal as the signal that remains after requiring common variability in the Schauinsland and Jungfraujoch data. This filter effectively eliminate the local small-scale signals, thereby allowing the reconstruction of regional-scale in-situ signals.

We perform daily comparison between the FTIR and GAW data only for Izaña and Karlsruhe. For the rest of stations we compare monthly data. This is due to the fact that there are either no measurements available on daily basis or the distance between FTIR and GAW stations is considerable. We analyse the FTIR and in-situ time series on different time scales: day-to-day variability (only for Izaña and Karlsruhe), intra-annual variability (annual cycle) and inter-annual variability (long term). We find a good consistency for the correlations for all the different time scales.

GAW and NDACC FTIR instruments consistently detect different time scales CH_4 variations

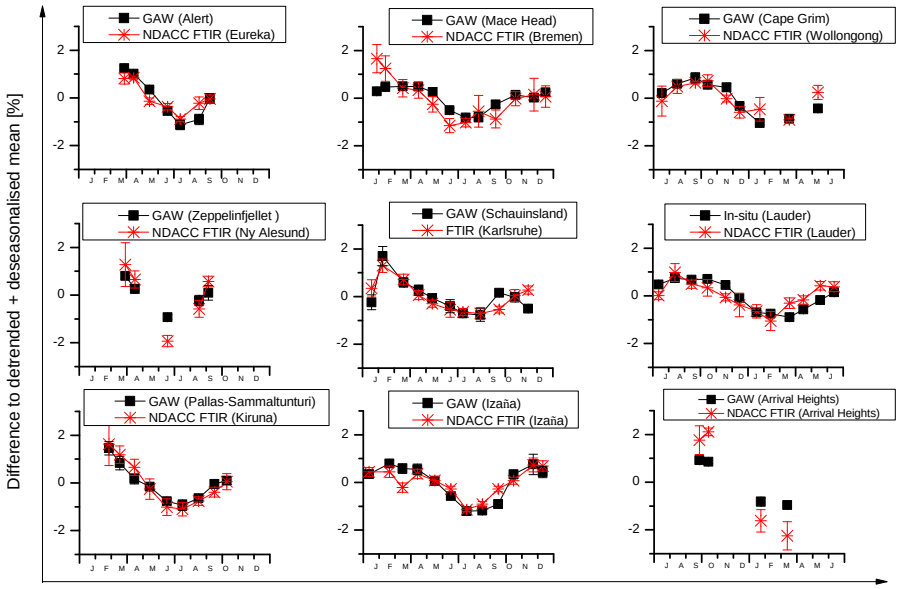

Figure 8: Tropospheric CH_4 annual cycle obtained by NDACC FTIR (red stars) and in-situ GAW (black squares) stations.

We show that both remote sensing and in-situ data observe very similar lower tropospheric regional-scale CH_4 signals. But they show a systematic difference of about 2% likely due to uncertainties in the applied spectroscopy parameters of CH_4. This documents that the GAW and NDACC FTIR instruments consistently detect intra-monthly, seasonal, and long-term CH_4 variations. For instance, Fig-

ure 8 shows the annual cycle obtained at the different NDACC FTIR and GAW stations.

Finally, we examine whether the FTIR and GAW data observe similar site specific long-term CH_4 evolution. For this purpose, we look at the de-seasonalised biannual mean data and compare FTIR-WACCM with GAW-WACCM for each station. We remove the WACCM apriori data in order to reduce the influence of the apriori in our retrieved results (note that the apriori is site specific). We observe that both GAW and FTIR data show similar differences with respect to the WACCM climatological mean data. We obtain a correlation coefficient of $R^2 = 0.69$ and calibration factor of 0.98. We think that this is a conservative documentation of the data consistency.

4

SUMMARY AND CONCLUSIONS

Understanding the global carbon cycle and predicting its evolution under future climate scenarios require precise long-term observations of GHG concentrations. Global models use theses observations in combination with atmospheric transport models for estimating the surface fluxes. Currently surface in-situ measurements are very precise but they can be affected by local small-scale processes, which are poorly simulated in the global models. On the other hand, remote sensing measurements can well complement the in-situ data. Among the existing ground-based remote sensing instruments, the FTIR spectrometer has a special status. The ground-based FTIR technique determines total column amounts and VMR profiles of many different atmospheric constituents with high precision. Two globally distributed networks (TCCON and NDACC) using ground-based FTIR techniques are in operation, providing long-term observation of many atmospheric trace gases. In this dissertation, we have optimized the retrieval strategies of two main contributors to the GHG effect: firstly, for the inversion of precise tropospheric H_2O vertical distribution in the framework of TCCON. And secondly, for the inversion of precise total column and tropospheric CH_4 concentrations for NDACC sites. These high-quality FTIR products can be used for satellite validation or as input for inverse modelling. Our studies have been published in three peer-reviewed articles, which are used for the presentation of this dissertation work.

In the first article we document that near-infrared TCCON spectra (at 0.02 cm^{-1} resolution) contain enough information to retrieve H_2O vertical distribution. The TCCON measurements can be used to monitor tropospheric water vapour profiles (measure lower and middle/upper tropospheric H_2O rather independently). We show the good agreement between the H_2O vertical profiles obtained with Vaisala RS92 radiosondes and the FTIR instrument at Izaña. TCCON can provide data at very high measurement frequency (one measurement every 1-2 min). The high-temporal density of the TCCON H_2O profile data will allow an analysis of tropospheric water vapour variability for different altitudes and on different time scales (from several hours to a few minutes).

In the second article our study shows that the high quality mid-infrared NDACC spectra (at 0.005 cm^{-1} resolution) contain significant information about the typical vertical variability of CH_4. For a scaling retrieval we estimate that the smoothing error is the leading error component. The smoothing error of total column-averaged dry air

mole fractions of methane (totXCH4) can be reduced when performing a profile retrieval. We compare our FTIR CH_4 products with surface in-situ measurements ($CH4_{GAW}$), documenting that the annual cycle of totXCH4 rather follows the annual cycle of the tropopause altitude and not the annual cycle of tropospheric CH_4 mole fractions. Our study shows that totXCH4 is no valid proxy for tropospheric CH_4. Furthermore, we investigate two methods for obtaining a tropospheric CH_4 proxy from the FTIR measurements. First, we apply an aposteriori HF correction method applying a scaling retrieval ($troXCH4_{post}$) and second, we directly retrieve tropospheric column-averaged XCH4 amounts from the spectra ($troXCH4_{retr}$). We see that the $troXCH4_{post}$ data do not capture the full amplitude of the tropospheric CH_4 annual cycle, while the $troXCH4_{retr}$ and $CH4_{GAW}$ behaves similarly.

In the third article we extend the previous study, which was limited to the subtropical site of Izaña, to a set of nine globally distributed NDACC FTIR sites covering polar, mid-latitudes, and subtropical regions. We slightly change our previous profiling retrieval in order to minimise potential humidity interferences at the humid sites. We demonstrate that the retrieved lower tropospheric CH_4 mole fractions can be significantly affected by CH_4 variations in the UTLS caused by tropopause altitude shifts. We show that this dependency on UTLS variations can be significantly reduced by an aposteriori correction method. We compare our retrieved tropospheric CH_4 signal to the surface in-situ CH_4 GAW data. To do so, we filter the GAW data to get the regional-scale signal. We show that both the remote sensing and in-situ GAW data observe very similar lower tropospheric regional-scale CH_4 signals. The good agreement is demonstrated for the different time scales that are interesting for CH_4 source/sink research: daily, seasonal, and long-term biannual mean evolution. In addition we demonstrate that both networks observe consistent latitudinal CH_4 gradients. We conclude that long-term NDACC FTIR observations can make valuable contributions when investigating sources and sinks of CH_4.

BIBLIOGRAPHY

[1] P. Bousquet, B. Ringeval, I. Pison, E. J. Dlugokencky, E.-G. Brunke, C. Carouge, F. Chevallier, A. Fortems-Cheiney, C. Frankenberg, D. A. Hauglustaine, P. B. Krummel, R. L. Langenfelds, M. Ramonet, M. Schmidt, L. P. Steele, S. Szopa, C. Yver, N. Viovy, and P. Ciais. Source attribution of the changes in atmospheric methane for 2006–2008. *Atmos. Chem. Phys.*, 11:3689–3700, 2011.

[2] F. Chevallier, F. M. Bréon, and P. J. Rayner. Contribution of the Orbiting Carbon Observatory to the estimation of CO_2 sources and sinks: Theoretical study in a variational data assimilation framework. *J. Geophys. Res.*, 112(D09307):2917–2931, 2007.

[3] P. Ciais, A. J. Dolman, R. Dargaville, L. Barrie, A. Bombelli, J. Butler, P. Canadell, and T. Moriyama. Geocarbon strategy geo secretariat. In *Geneva, FAO, Rome, 48 pp.*, 2010. Available at: `http://www.globalcarbonproject.org/global/pdf/GEO_CARBONSTRATEGY_20101020.pdf`.

[4] C. Clerbaux, M. George, S. Turquety, K. A. Walker, B. Barret, P. Bernath, C. Boone, T. Borsdorff, J. P. Cammas, V. Catoire, M. Coffey, P. F. Coheur, M. Deeter, M. De Mazière, J. Drummond, P. Duchatelet, E. Dupuy, R. de Zafra, F. Eddounia, D. P. Edwards, L. Emmons, B. Funke, J. Gille, D. W. T. Griffith, J. Hannigan, F. Hase, M. Höpfner, N. Jones, A. Kagawa, Y. Kasai, I. Kramer, E. Le Flochmoën, N. J. Livesey, M. López-Puertas, M. Luo, E. Mahieu, D. Murtagh, Ph. Nédélec, A. Pazmino, H. Pumphrey, P. Ricaud, C. P. Rinsland, C. Robert, M. Schneider, C. Senten, G. Stiller, A. Strandberg, K. Strong, R. Sussmann, V. Thouret, J. Urban, and A. Wiacek. CO measurements from the ACE-FTS satellite instrument: data analysis and validation using ground-based, airborne and spaceborne observations. *Atmos. Chem. Phys.*, 8:2569–2594, 2008.

[5] S. P. Davis, M. C. Abrams, and J. W. Brault. *Fourier Transform Spectrometry*. 1st Edition. Academic Press, 2001.

[6] C. B. Farmer. The ATMOS Solar Spectra. *Infrared Solar Physics*, pages 511–521, 1994.

[7] C. Frankenberg, K. Yoshimura, T. Warneke, I. Aben, A. Butz, N. Deutscher, D. Griffith, F. Hase, J. Notholt, M. Schneider, H. Schrejver, and T. Röckmann. Dynamic processes governing

lower-tropospheric HDO/H_2O ratios as observed from space and ground. *Science*, 325:1374–1377, 2009.

[8] O.E. García, M. Schneider, A. Redondas, Y. González, F. Hase, T. Blumenstock, and E. Sepúlveda. Investigating the long-term evolution of subtropical ozone profiles applying ground-based FTIR spectrometry. *Atmos. Meas. Tech.*, 5:2917–2931, 2012.

[9] O.E. García, M. Schneider, F. Hase, T. Blumenstock, E. Sepúlveda, and A. Gómez-Peláez. Validation of the IASI operational CH_4 and N_2O products using ground-based Fourier Transform Spectrometer: Preliminary results at the Izaña Observatory (28°N, 17°W). *Annals of Geophysics.*, Fast Track-1(104401/ag-6326), 2013.

[10] M. Gisi, F. Hase, S. Dohe, and T. Blumenstock. Camtracker: a new camera controlled high precision solar tracker system for FTIR-spectrometers. *Atmos. Meas. Tech.*, 4:47–54, 2011.

[11] A. J. Gómez-Peláez and R. Ramos. Improvements in the carbon dioxide and methane continuous measurement programs at Izaña global GAW station (Spain) during 2007–2009, Report of the 15th WMO/IAEA meeting of experts on carbon dioxide, other greenhouse gases, and related tracer measurement techniques, 7–10 September 2009, Jena, Germany. GAW Report number 194, WMO TD 1553, 2011. Available at `http://www.wmo.int/pages/prog/arep/gaw/gaw-reports.html`.

[12] A. J. Griesfeller, F. Hase, I. Kramer, P. Loës, S. Mikuteit, U. Raffalski, T. Blumenstock, and H. Nakajima. Comparison of ILAS-II and ground-based FTIR measurements of O_3 , HNO_3 , N_2O, and CH_4 over Kiruna, Sweden. *J. Geophys. Res.*, 111(D11S07), 2006.

[13] D. W. T. Griffith, N. M. Deutscher, C. Caldow, G. Kettlewell, M. Riggenbach, and S. Hammer. A fourier transform infrared trace gas and isotope analyser for atmospheric applications. *Atmos. Meas. Tech.*, 5:2481–2498, 2012.

[14] F. Hase and M. Höpfner. Atmospheric raypath modelling for radiative transfer algorithms. *Appl. Optics*, 38:3129–3133, 1999.

[15] F. Hase, T. Blumenstock, and C. Paton-Walsh. Analysis of the instrumental line shape of high-resolution fourier transform IR spectrometers with gas cell measurements and new retrieval software. *Appl. Opt.*, 38:3417–3422, 1999.

[16] F. Hase, J. W. Hanningan, M. T. Coffey, A. Goldman, M. Höpfner, N. B. Jones, C. P. Rinsland, and S. W. Wood. Intercomparison of retrieval codes used for the analysis of high-resolution ground-based FTIR measurements. *J. Quant. Spectrosc. and Rad. Transfer*, 87:25–52, 2004.

[17] Climate Change IPCC. The Physical Science Basis: Contribution of Working Group I to the Fourth Assessment Report of the Intergovernmental Panel on Climate. In *Cambridge University Press, Cambridge, United Kingdom and New York, NY, USA*, 2007.

[18] G. Keppel-Aleks, G. C. Toon, P. O. Wennberg, and N. M. Deutscher. Reducing the impact of source brightness fluctuations on spectra obtained by Fourier-transform spectrometry. *Appl. Opt.*, 46:4774–4779, 2007.

[19] M. J. Kurylo and R. Zander. The NDSC–its status after 10 years of operation. In *Proceedings of XIX Quarennial Ozone Symposium*, pages 167–168, Hokkaido University, Sapporo, Japan, 2000.

[20] A.T.J. De Laat, A. M. S. Gloudemans, H. Schrijver, I. Aben, Y. Nagahama, K. Suzuki, E. Mahieu, N. B. Jones, C. Paton-Walsh, N. M. Deutscher, D. W. T. Griffith, M. De Mazière, R. L. Mittermeier, H. Fast, J. Notholt, M. Palm, T. Hawat, T. Blumenstock, F. Hase, M. Schneider, C. Rinsland, A. V. Dzhola, E. I. Grechko, A. M. Poberovskii, M. V. Makarova, J. Mellqvist, A. Strandberg, R. Sussmann, T. Borsdorff, and M. Rettinger. Validation of five years (2003–2007) of SCIAMACHY CO total column measurements using ground-based spectrometer observations. *Atmos. Meas. Tech.*, 3:1457–1471, 2010.

[21] A. Meier, G.C. Toon, C.P. Rinsland, A. Goldman, and F. Hase. Spectroscopic atlas of atmospheric microwindows in the middle infra-red (2nd edition). In *IRF Technical Report No.48, ISSN 0248-1738*, Kiruna, 2004.

[22] L. M. Miloshevich, H. Vömel, D. N. Whilteman, and T. Leblanc. Accuracy assessment and correction of Vaisala RS92 radiosonde water vapor measurements. *J. Geophys. Res.*, 114(D11305), 2009.

[23] J. Notholt and R. Lehmann. The moon as light source for atmospheric trace gas observations: measurement technique and analysis method. *J. Quant. Spectrosc. and Rad. Transfer*, 76:435–445, 2003.

[24] J. Notholt, R. Neuber, O. Schrems, and T. v. Clarmann. Stratospheric trace gas concentrations in the Arctic polar night derived by FTIR-spectroscopy with the moon as IR light source. *Geophys. Res. Letters.*, 20:2059–2062, 1993.

[25] D. M. O'Brien and P. J. Rayner. Global observations of the carbon budget, 2. CO_2 column from differential absorption of reflected sunlight in the 1.61 band of CO_2. *J. Geophys. Res.*, 107(D18), 2002.

[26] S. C. Olsen and J. T. Randerson. Differences between surface and column atmospheric CO_2 and implications for carbon cycle research. *J. Geophys. Res.*, 109(D02301), 2004.

[27] Clare Paton-Walsh. Remote sensing of atmospheric trace gases by ground-based solar Fourier transform infrared spectroscopy. *In G. Nikolic (Eds.)*, pages 459–478, 2011.

[28] N. S. Pougatchev, B. J. Connor, and C. P. Rinsland. Infrared measurements of the ozone vertical-distribution above Kitt Peak. *J. Geophys. Res.*, 100(D8):16689–16697, 1995.

[29] C.D. Rodgers. *Inverse Methods for Atmospheric Sounding: Theory and Praxis*. World Scientific Publishing Co., Singapore, 2000. ISBN 981-02-2740-X.

[30] J. J. Rodriguez-Franco and E. Cuevas. Characteristics of the subtropical tropopause region based on long-term highly resolved sonde records over Tenerife. *J. Geophys. Res.*, 118(19):10754–10769, 2013.

[31] L. S. Rothman, I. E. Gordon, A. Barbe, D. Chris Benner, P. F. Bernath, M. Birk, V. Boudon, L. R. Brown, A. Campargue, J.-P. Champion, K. Chance, L. H. Coudert, V. Dana, V. M. Devi, S. Fally, J.-M. Flaud, R. R. Gamache, A. Goldmanm, D. Jacquemart, I. Kleiner, N. Lacome, W.J. Lafferty, J.-Y. Mandin, S. T. Massie, S. N. Mikhailenko, C. E. Miller, N. Moazzen-Ahmadi, O. V. Naumenko, A. V. Nikitin, J. Orphal, V. I. Perevalov, A. Predoi-Cross A. Perrin, C. P. Rinsland, M. Rotger, M. Šimečková, M. A. H. Smith, K. Sung, S. A. Tashkun, J. Tennyson, R. A. Toth, A. C. Vandaele, and J. Vander Auwera. The HITRAN 2008 molecular spectroscopic database. *J. Quant. Spectrosc. and Rad. Transfer*, 110:533–572, 2009.

[32] M. Schneider and F. Hase. Technical note: Recipe for monitoring of total ozone with a precision of 1 DU applying mid-infrared solar absorption spectra. *Atmos. Chem. Phys.*, 8:63–71, 2008.

[33] M. Schneider and F. Hase. Optimal estimation of tropospheric H_2O and δD with IASI/METOP. *Atmos. Chem. Phys.*, 11:16107–16146, 2011.

[34] M. Schneider, F. Hase, and T. Blumenstock. Water vapour profiles by ground-based FTIR spectroscopy: study for an optimised retrieval and its validation. *Atmos. Chem. Phys.*, 6:811–830, 2006.

[35] M. Schneider, A. Redondas, F. Hase, C. Guirado, T. Blumenstock, and E. Cuevas. Comparison of ground-based brewer and FTIR total column O_3 monitoring techniques. *Atmos. Chem. Phys.*, 8: 5535–5550, 2008.

[36] M. Schneider, P. M. Romero, F. Hase, T. Blumenstock, E. Cuevas, and R. Ramos. Continuous quality assessment of atmospheric water vapour measurement techniques: FTIR, Cimel, MFRSR, GPS, and Vaisala RS92. *Atmos. Meas. Tech.*, 3:323–338, 2010.

[37] M. Schneider, E. Sepúlveda, O. García, F. Hase, and T. Blumenstock. Remote sensing of water vapour profiles in the framework of the Total Carbon Column Observing Network (TCCON). *Atmos. Mes. Tech.*, 3:1785–1795, 2010.

[38] M. Schneider, G. C. Toon, J.-F. Blavier, F. Hase, and T. Leblanc. H_2O and δD profiles remotely-sensed from ground in different spectral infrared regions. *Atmos. Meas. Tech.*, 3:1599–1613, 2010.

[39] M. Schneider, S. Barthlott, F. Hase, Y. González, K. Yoshimura, O. E. García, E. Sepúlveda, A. Gomez-Pelaez, M. Gisi, R. Kohlhepp, S. Dohe, T. Blumenstock, A. Wiegele, E. Christner, K. Strong, D. Weaver, M. Palm, N. M. Deutscher, T. Warneke, J. Notholt, B. Lejeune, P. Demoulin, N. Jones, D. W. T. Griffith, D. Smale, and J. Robinson. Ground–based remote sensing of tropospheric water vapour isotopologues within the project MUSICA. *Atmos. Meas. Tech.*, 5:3007–3027, 2012.

[40] E. Sepúlveda, M. Schneider, A. Gómez, E. Cuevas, F. Hase, T. Blumenstcok, and J. C. Guerra. Total Carbon Column Observing Network (TCCON) activities at Izaña, Tenerife. *Óptica Pura y Aplicada. Sociedad Española de Óptica*, 45(1):1–4, 2011.

[41] E. Sepúlveda, M. Schneider, F. Hase, O. E. García, A. Gómez-Peláez, S. Dohe, T. Blumenstock, and J. C. Guerra. Long-term validation of total and tropospheric column-averaged CH_4 mole fractions obtained by mid-infrared ground-based FTIR spectrometry. *Atmos. Mes. Tech.*, 5:1425–1441, 2012.

[42] E. Sepúlveda, M. Schneider, F. Hase, S. Barthlott, D. Dubravica, O. E. García, A. Gómez-Peláez, Y. González, J. C. Guerra, M. Gisi, R. Kohlhepp, S. Dohe, T. Blumenstock, K. Strong, D. Weaver, M. Palm, A. Sadeghi, N. M. Deutscher, T. Warneke, J. Notholt, N. Jones, D. W. T. Griffith, D. Smale, G. W. Brailsford, J. Robinson, F. Meinhardt, M. Steinbacher, T. Aalto, and D. Worthy. Tropospheric CH_4 signals as observed by NDACC FTIR at globally distributed sites and comparison to GAW surface in-situ measurements. *Atmos. Mes. Tech. Disc.*, 7:633–701, 2014.

[43] R. W Spencer and W. D. Braswell. How dry is the tropical free troposphere? implications for global warming theory. *Bull. Am. Meteorol. Soc.*, 78:1097–1106, 1997.

[44] R. Sussmann, F. Forster, M. Rettinger, and N. Jones. Strategy for high-accuracy-and-precision retrieval of atmospheric methane from the mid-infrared FTIR network. *Atmos. Meas. Tech.*, 4:1943–1964, 2011.

[45] P. P. Tans, I. Y. Fung, and T. Takahashi. Observational constraints on the global atmospheric CO_2 budget. *Science*, 247:1431–1438, 1990.

[46] C. Viatte, M. Schneider, A. Redondas, F. Hase, M. Eremenko, P. Chelin, J.-M. Flaud, T. Blumenstock, and J. Orphal. Comparison of ground-based FTIR and brewer O_3 total column with data from two different IASI algorithms and from OMI and GOME-2 satellite instruments. *Atmos. Meas. Tech.*, 4:535–546, 2011.

[47] H. Vömel, H. Selkirk, L. Miloshevich, J. Valverde, J. Valdés, E. Kyrö, R. Kivi, W. Stolz, G. Peng, and J. A. Diaz. Radiation dry bias of the Vaisala RS92 humidity sensor. *J. Atmos. Oceanic Technol.*, 24:953–963, 2007.

[48] R. A. Washenfelder, P. O. Wennberg, and G. C. Toon. Tropospheric methane retrieved from ground-based near-IR solar absorption spectra. *Geophys. Res. Lett.*, 30(L017969), 2003.

[49] R. A. Washenfelder, G. C. Toon, and J. F. Blavier. Carbon dioxide column abundances at the wisconsin tall tower site. *J. Geophys. Res.*, 109(D18), 2006.

[50] J. Winderlich, H. Chen, C. Gerbig, T. Seifert, O. Kolle, J. V. Lavri, C. Kaiser A. Höfer, and M. Heimann. Continuous low-maintenance $CO_2/CH_4/H_2O$ measurements at the Zotino Tall Tower Observatory (ZOTTO) in Central Siberia. *Atmos. Meas. Tech.*, 3:1113–1128, 2010.

[51] S. W. Wood, R. L. Batchelor, A. Goldman, C. P. Rinsland, B. J. Connor, F. J. Murcray, T. M. Stephen, and D. N. Heuff. Ground-based nitric acid measurements at Arrival Heights, Antarctica, using solar and lunar Fourier transform infrared observations. *J. Geophys. Res.*, 109(D18307), 2004.

[52] D. Wunch, G. C. Toon, J.-F. L. Blavier, R. Washenfelder, J. Notholt, B. J. Connor, D. W. T. Griffith, V. Sherlock, and P. O. Wennberg. The Total Carbon Column Observing Network. *Phil. Trans. R. Soc. A*, 369(2087-2112), 2011.

Part II

DISSERTATION BY COMPENDIUM OF PUBLICATIONS: ARTICLES

This second part of the manuscript presents the three articles as they have been published in the peer-reviewed Atmospheric Measurement Technique on-line journal. Note that the third article presented in Chapter 7 was submitted recently and is currently under discussion in the Atmospheric Measurement Technique Discussion on-line journal.

5

REMOTE SENSING OF WATER VAPOUR PROFILES IN THE FRAMEWORK OF THE TOTAL CARBON COLUMN OBSERVING NETWORK (TCCON)

Atmos. Meas. Tech., 3, 1785–1795, 2010
www.atmos-meas-tech.net/3/1785/2010/
doi:10.5194/amt-3-1785-2010

Atmospheric Measurement Techniques

Remote sensing of water vapour profiles in the framework of the Total Carbon Column Observing Network (TCCON)

M. Schneider[1,2], **E. Sepúlveda**[3,1], **O. García**[1], **F. Hase**[2], **and T. Blumenstock**[2]

[1]Agencia Estatal de Meteorología (AEMET), CIAI, Santa Cruz de Tenerife, Spain
[2]Karlsruhe Institute of Technology (KIT), IMK-ASF, Karlsruhe, Germany
[3]University of La Laguna, Santa Cruz de Tenerife, Spain

Received: 15 July 2010 – Published in Atmos. Meas. Tech. Discuss.: 31 August 2010
Revised: 19 December 2010 – Accepted: 20 December 2010 – Published: 22 December 2010

Abstract. We show that the near infrared solar absorption spectra recorded in the framework of the Total Carbon Column Observing Network (TCCON) can be used to derive the vertical distribution of tropospheric water vapour. The resolution of the TCCON spectra of 0.02 cm^{-1} is sufficient for retrieving lower and middle/upper tropospheric water vapour concentrations with a vertical resolution of about 3 and 8 km, respectively. We document the good quality of the remotely-sensed profiles by comparisons with coincident in-situ Vaisala RS92 radiosonde measurements. Due to the high measurement frequency, the TCCON water vapour profile data offer novel opportunities for estimating the water vapour variability at different timescales and altitudes.

1 Introduction

During the last years large investments have been undertaken to set up the Total Carbon Column Observing Network (TCCON, www.tccon.caltech.edu, Wunch et al., 2010a) as a quasi-automated monitoring network. A TCCON experiment consists of a high precision solar tracker and a high quality ground-based Fourier Transform Infrared (FTIR) spectrometer (e.g., Geibel et al., 2010). A big shipping container is typically used as housing of the equipment whose overall material costs are about 500 kEUR. In the meanwhile there are about 15 globally-distributed FTIR experiments operating in the framework of the TCCON. The experiments record direct solar spectra in the near-infrared spectral region (4000–9000 cm^{-1}). In this spectral region there are distinct rotational-vibrational bands of the atmospheric trace gases CO_2, CH_4, N_2O, HF, CO, H_2O, and HDO. The TCCON will focus on the measurement of accurate and precise total column abundances of the greenhouse gases CO_2, CH_4, and N_2O (e.g., Yang et al., 2002; Washenfelder et al., 2006; Wunch et al., 2010b). Concerning CO_2 a precision of 0.1–0.2% (0.4–0.8 ppm) is targeted. Achieving such high precision is essential for using the column-averaged data in carbon cycle research (Olsen and Randerson, 2004) however, it is a very challenging task.

In this context there have been large efforts to ensure that the TCCON experiments produce spectra of very high quality: (1) At almost all sites very stable FTIR spectrometer are applied (Bruker IFS 125HR) and the instrumental line shape (ILS) is characterised routinely (Hase et al., 1999). (2) A DC-correction is applied on the interferogram, which avoids artificial baseline offsets caused by intensity fluctuations while scanning (Keppel-Aleks et al., 2007). (3) Detector nonlinearities – which cause baseline offsets – are corrected (Abrams et al., 1994). (4) The sampling accuracy is optimised in order to avoid ghosts (Messerschmidt et al., 2010). (5) A very high quality solar tracking system has been developed (Gisi et al., 2010). It guarantees a very high quality of the measurements, also for low solar elevation angles.

TCCON will provide solar absorption spectra of highest quality, at several globally distributed sites, and for many years, which makes it very attractive for many fields of atmospheric research. Water vapour is a key parameter concerning climate variability and climate feedbacks (Randall et al., 2007; Sherwood et al., 2010) whereby long-term observations of middle/upper tropospheric water vapour are particularly interesting for climate research, since at these altitudes water vapour acts very effectively as greenhouse gas (Spencer and Braswell, 1997). TCCON's demanding quality

Correspondence to: M. Schneider
(matthias.schneider@kit.edu)

requirements and its long-term strategy are very promising for studying the atmospheric water vapour distribution and its interaction with climate change, but it is important to document the quality and characteristics of the water vapour data that can be produced by the TCCON. In addition precise TCCON water vapour retrievals are important for ensuring a high quality of the TCCON's prime target gases (CO_2, CH_4, and N_2O). Since the highly variable water vapour absorption signatures often interfere with signatures of the other TCCON absorbers a precise estimation of the actual atmospheric H_2O distribution for each individual spectra is needed in order to avoid significant interference errors.

Ground-based solar absorption spectra measured in the middle infrared in the framework of the Network for the Detection of Atmospheric Composition Change (NDACC, Kurylo and Zander, 2000, www.acd.ucar.edu/irwg) allow the remote sensing of tropospheric water vapour profiles (Schneider et al., 2006; Schneider and Hase, 2009; Schneider et al., 2010a). More recently, Schneider et al. (2010c) show that the water vapour profiles retrieved from near infrared signatures (4500–4700 cm^{-1}) are also of very good quality. However, the so far applied spectra have been highly-resolved (spectral resolution of 0.0025–0.0075 cm^{-1}), whereas the resolution of the TCCON spectra is limited to 0.02 cm^{-1}. In this paper we use TCCON spectra measured at the Izaña Observatory (Tenerife Island, Spain, 28°18′ N, 16°29′ W at 2370 m a.s.l.) and show that the TCCON spectral resolution is still sufficient to derive tropospheric water vapour profiles. Since a lower resolution spectrum is measured within 1–2 min the TCCON can provide free tropospheric water vapour data with an unprecedented high measurement frequency. In Sect. 2 we briefly describe the measurement principle of the TCCON and the generalities of evaluating high resolution solar absorption spectra and the setup of the water vapour profile retrieval. Sections 3–5 characterise and validate the profiles and Sect. 6 demonstrates the unique measurement frequency of the TCCON water vapour profiles. The paper ends with a summary (Sect. 7).

2 A TCCON experiment and the principles of ground-based infrared remote sensing

Figure 1 shows the two main components of a TCCON experiment: a precise solar tracker (left photograph) that captures the direct solar light beam and a high resolution FTIR spectrometer (right photograph). For TCCON the FTIR spectrometer measures in the 4000–9000 cm^{-1} region with a resolution of 0.02 cm^{-1} (i.e., maximum optical path difference, OPD, of 45 cm). This corresponds to a resolution power $\lambda/\Delta\lambda$ at 5000 cm^{-1} of approx. 2.5×10^5. Recording of one spectrum requires between 30 seconds and a few minutes, depending on the quality needed: one scan can be performed in 3 s, but often several scans are co-added in order to increase the signal to noise ratio. Together with the AC-signal, the DC-signal of the interferogram is recorded. This allows correcting for inhomogeneous sky conditions, like cirrus cloud cover (Keppel-Aleks et al., 2007). No observations can be performed for a sky covered with optically thick clouds.

Fig. 1. The TCCON experiment at the Izaña Atmospheric Research Centre. The solar tracker (left photograph) is situated at the top of the experimental housing. It collects the direct solar beam and reflects it into the housing of the FTIR spectrometer (right photograph) where it is coupled into the spectrometer (circular light spot on the right part of the photograph).

The basic equation for analysing near infrared solar absorption spectra is Lambert Beer's law:

$$I(\lambda) = I_{\text{sun}}(\lambda)\exp(-\int_{\text{TOA}}^{\text{Obs.}} \sigma_x(\lambda, s(T,p))x(s)ds) \quad (1)$$

Here $I(\lambda)$ is the measured intensity at wavelength λ, I_{sun} the solar intensity, $\sigma_x(\lambda, s)$ is the absorption cross section and $x(s)$ the concentration of an absorber x at location s. The integration is performed along the path of the direct sunlight (from the top of the atmosphere (TOA) to the observer). The cross section σ_x depends on temperature and pressure. The measurement $I(\lambda)$ is simulated by a precise line-by-line radiative transfer model, which includes a ray tracing module (e.g., Hase and Höpfner, 1999) in order to determine how the solar light passes through the different atmospheric layers.

By means of the discretisation we can describe the vertical distribution of the absorber in form of a vector $\boldsymbol{x}(z)$ (amount of the absorber x at level z). If we also describe the simulated spectrum, $I(\lambda)$, in form of a vector $\boldsymbol{y}$ containing the radiances in the different spectral bins, we can define a forward relation, F, that connects the solar absorption spectrum ($\boldsymbol{y}$) to the vertical distribution of the absorber ($\boldsymbol{x}$), to parameters describing the atmospheric state ($\boldsymbol{p}_{\text{atmos}}$), and to parameters describing the measurement system ($\boldsymbol{p}_{\text{exp}}$):

$$\boldsymbol{y} = \boldsymbol{F}(\boldsymbol{x}, \boldsymbol{p}_{\text{atmos}}, \boldsymbol{p}_{\text{exp}}) \quad (2)$$

$\boldsymbol{F}$ is a vector valued function which simulates the atmospheric radiative transfer and the characteristics of the measurement system (spectral resolution, instrumental line shape, etc.). The retrieval consists in adjusting the amount of the absorber so that simulated and measured spectrum agree. This is a non-linear problem (see Eq. 1) and the

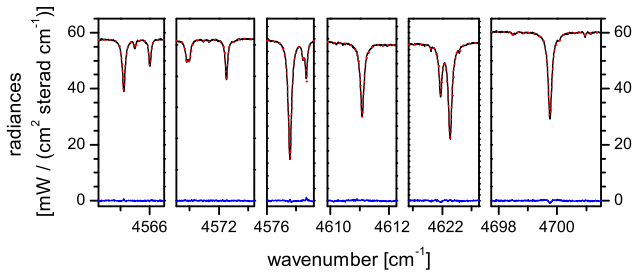

Fig. 2. The used spectral microwindows with H_2O signatures. The shown measurement was taken on the 31st of March 2010, at a solar elevation of 43.4°, and for a total water vapour column amount of 4.7 mm. Black line: measured spectrum; Red line: simulated spectrum; Blue line: residuals (difference between measurement and simulation).

solution is obtained by iterative calculations. For each iteration the derivatives $\partial y/\partial x$ determine the changes in the spectral fluxes $\boldsymbol{y}$ for changes in the vertical distribution of the absorber $\boldsymbol{x}$. These derivatives are sampled in a Jacobian matrix $\mathbf{K}$:

$$\boldsymbol{\partial y} = \mathbf{K}\boldsymbol{\partial x} \tag{3}$$

Inverting $\mathbf{K}$ of Eq. 3 would allow an iterative calculation of the sought variables $\boldsymbol{x}$, but the problem is under-determined, i.e., the columns of $\mathbf{K}$ are not linearly independent and there are many different solutions that are in acceptable agreement with the measurement. We cannot derive a unique solution but we can estimate the most probable solution for the given measurement. This optimal estimation (OE) approach combines the measurement information with a priori knowledge and provides the most probable solution by minimising the following cost function:

$$[\boldsymbol{y}-\boldsymbol{F}(\boldsymbol{x})]^T \mathbf{S}_\epsilon{}^{-1}[\boldsymbol{y}-\boldsymbol{F}(\boldsymbol{x})]+[\boldsymbol{x}-\boldsymbol{x}_a]^T \mathbf{S_a}^{-1}[\boldsymbol{x}-\boldsymbol{x}_a] \tag{4}$$

Where $\mathbf{S}_\epsilon$ is the noise covariance, $\boldsymbol{x_a}$ and $\mathbf{S_a}$ are the a-priori known mean distribution and the covariance of the distribution of the absorber, respectively. The a priori water vapour information is deduced from daily Vaisala RS92 radiosondes, which have been launched since 2005 just about 15 km southeast of the Izaña Observatory. For more details about OE approaches please refer to the textbook of C. D. Rodgers (Rodgers, 2000).

The optimal estimation of atmospheric water vapour amounts from ground-based FTIR spectra is far from being a typical atmospheric inversion problem and, due to its large vertical gradient and variability, standard retrieval methods are not appropriate. Only very recently the ground-based infrared remote sensing of water vapour profiles has become feasible. Among others, it requires the inversion to be performed on a logarithmic scale (Schneider et al., 2006) and the application of a speed dependent Voigt line shape model (Schneider et al., 2011, and references therein). We use the code PROFFIT (Hase et al., 2004), which comprises all the retrieval options that are required for ground-based water vapour profile analyses (for a review please refer to Schneider and Hase, 2009).

For the near infrared water vapour retrieval we fit the spectral microwindows as depicted in Fig. 2. In addition to the water vapour lines these spectral windows contain weak absorption signatures of CO_2, N_2O, and CH_4. All these absorbers are jointly fitted. For our spectral line-by-line simulations we apply the HITRAN 2008 (Rothman et al., 2009) spectroscopic line parameters which we adjusted for a speed-dependent Voigt line shape model (Schneider et al., 2011). As temperature profile we apply the National Centers for Environmental Prediction (NCEP) 12:00 UT reanalysis temperatures.

3 Water vapour profile error analyses

Our assumed uncertainty sources are given in Table 1. Major efforts have been undertaken for constraining the instrumental uncertainties of a TCCON experiment (Abrams et al., 1994; Hase et al., 1999; Keppel-Aleks et al., 2007; Messerschmidt et al., 2010; Gisi et al., 2010). As remaining instrumental uncertainties we assume a measurement noise and baseline offset of 0.1% (noise-to-signal and offset-to-signal, respectively), a modulation efficiency of 5% per 100 cm optical path difference (OPD), a phase error of 0.01 rad, and a line of sight (LOS) uncertainty of 1′.

In addition there are uncertainties in the applied 12:00 UT NCEP reanalysis temperature profiles and the spectroscopic line parameters. We assume uncorrelated temperature uncertainty of 2 K for the lower troposphere (below 5km) as well as 2 K for the upper troposphere (above 5 km). These uncertainties might be caused by errors in the NCEP data or by diurnal cycles (the applied NCEP data is for 12:00 UT, whereas Izaña's FTIR measurements are performed between 10 and 18:00 UT). As uncertainties in the line strength (S) and pressure broadening parameter (γ_{air}) we assume 1 % and for the strength of the speed-dependence (Γ_2/Γ_0, Wagner and Birk, 2009; Schneider et al., 2011) we assume 5%. Please note that uncertainties in the spectroscopic parameters – although being systematic – can produce random errors, since the effect of the errors depends on the sensitivity of the remote sensing system which, for example, differs for dry and wet atmospheric conditions.

The error estimation method is the same as described in Schneider et al. (2010c), which should be consulted for more details. In Figs. 3 and 4 we depict the estimated random and systematic errors for the retrieved profiles. We perform the estimations for very high resolution spectra (spectral resolution of 0.004 cm^{-1} typically used in NDACC) and for spectra with TCCON resolution (0.02 cm^{-1}). Uncertainties in the ILS, the applied temperatures, and the spectroscopic parameters are the leading error sources. In addition to the

Table 1. Assumed experimental and temperature random uncertainty.

source	uncertainty
measurement noise	0.1 %
baseline offset	0.1 %
modulation eff.	5 % (per 100 cm OPD)
phase error	0.01 rad
Line of sight (LOS)	$1'$
LT temperature	2 K
UT temperature	2 K
line strength, S	+1 %
pres. broad. coef., γ_{air}	+1 %
SDV strength, Γ_2/Γ_0	+5 %

Table 2. Estimated random errors of the retrieved H_2O column abundances for different spectral resolutions: 0.004 cm^{-1} (typical for NDACC) and 0.02 cm^{-1} (typical for TCCON).

source	Res: 0.004 cm^{-1}	Res: 0.02 cm^{-1}
spectroscopy	0.01 %	< 0.01 %
measurement noise	0.08 %	0.09 %
ILS	0.04 %	0.03 %
temperature (T-fit)	0.05 %	0.08 %
temperature (no T-fit)	0.16 %	0.14 %
baseline offset	0.14 %	0.14 %
LOS (@80° SZA)	0.17 %	0.17 %
smoothing	0.57 %	0.68 %

optimal estimation of an absorber profile PROFFIT can estimate temperature profiles. We get the additional temperature information by fitting two spectral microwindows with CO_2 lines (at 4720–4735 cm^{-1}) simultaneously with the water vapour lines shown in Fig. 2. The simultaneous temperature fit significantly reduces the temperature error (compare solid and dotted cyan lines of Fig. 3). The temperature retrieval is mandatory when analysing very high resolution spectra and when aiming on middle/upper tropospheric water vapour concentrations (see also Schneider et al., 2006).

The systematic profile errors are dominated by uncertainties in the parameters that describe the line shape. Uncertainties in the air broadening parameter (γ_{air}) are mainly responsible for lower/middle tropospheric errors, whereas an uncertainty in the strength of the speed-dependence (Γ_2/Γ_0) mainly affects the middle/upper troposphere (Schneider et al., 2011).

Table 2 collects the estimated random error for the retrieved H_2O total column abundances. When using the assumptions of Table 1 and performing a simultaneous temperature retrieval only baseline offsets and LOS uncertainties produce errors that are larger than 0.1 %. We also list the so-called smoothing error, which is due to the limited vertical resolution of a remote sensing system. Water vapour is

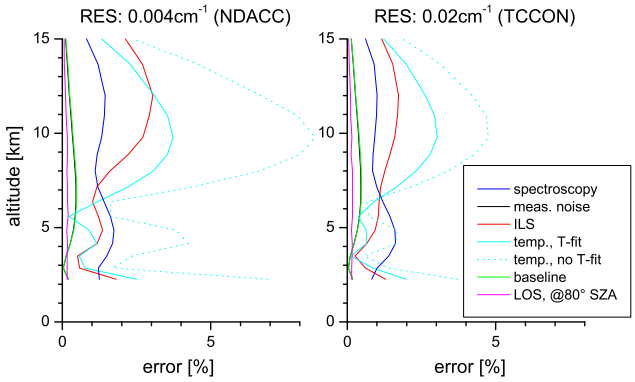

Fig. 3. Estimated H_2O random profile errors for the profile retrievals of spectra with typical NDACC and TCCON spectral resolution (0.004 and 0.02 cm^{-1}, respectively). Blue: spectroscopic parameters; Black: measurement noise; Red: ILS; Cyan: temperature profile; Green: baseline offset; Magenta: line of sight.

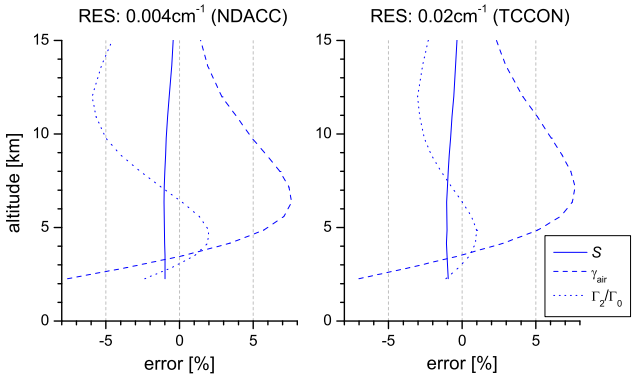

Fig. 4. Same as Fig. 3 but for systematic profile errors. Solid line: line strength (S) uncertainty; Dashed line: pressure broadening coefficient (γ_{air}) uncertainty; Dotted line: speed-dependence strength (Γ_2/Γ_0) uncertainty.

a extremely variable atmospheric trace gas. Often there are sharp filaments of increased water vapour amounts followed by layers with reduced amounts. The FTIR remote sensing system is not equally sensitive at all atmospheric altitude levels and consequently the highly varying vertical water vapour distributions cause significant random errors in the retrieved column abundances: the smoothing errors.

The smoothing error is larger for the lower resolution TCCON spectra than for the very high resolution NDACC spectra. On the other hand we observe that the retrievals applying very high resolution NDACC spectra have a slightly larger error sensitivity in the middle/upper troposphere than the retrievals applying TCCON spectra (see Figs. 3 and 4). This is due to the fact the retrievals based on the very high resolution spectra are more sensitive to the actual water vapour distribution but at the same time they are also more sensitive to the uncertainty source.

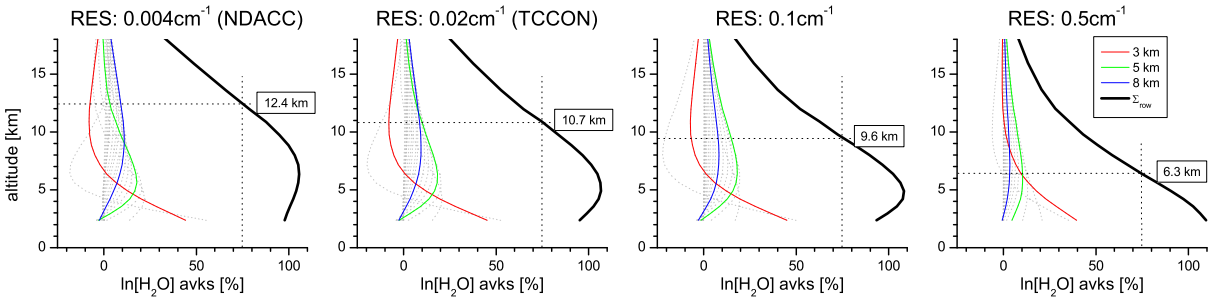

Fig. 5. Averaging kernels for ln[H_2O] for different spectral resolution. From the left to the right: 0.004 cm^{-1}, 0.02 cm^{-1} (resolution of TCCON spectra), 0.1 cm^{-1}, and 0.5 cm^{-1}. Grey lines: kernels for all atmospheric model grid levels; Black, red, and green lines: kernels for the 3, 5, and 8 km grid level (representative for the lower, middle, and upper troposphere), respectively; Thick black line: Sensitivity (sum along the row of the averaging kernel matrix). Indicated is also the altitude where the sensitivity falls below 75%.

It is important to note that ground-based FTIR measurements need clear sky conditions. No measurements can be performed when there is a optically thick cloud cover. This introduces a significant clear sky dry bias in the FTIR data (Schneider et al., 2010a), which has to be considered when interpreting the data.

4 Vertical resolution versus spectral resolution

Atmospheric profiles remotely-sensed by ground-based infrared spectrometry offer – compared to in-situ measurements – a limited vertical resolution. The vertical structures that are detectable are documented by the averaging kernels. Figure 5 depicts typical sets of averaging kernels for water vapour profile retrievals when applying the near infrared microwindows of Fig. 2.

In order to assess the effect of spectral resolution on the vertical resolution of the remote sensing system we measured spectra with different spectral resolution (0.004 cm^{-1}, 0.02 cm^{-1}, 0.1 cm^{-1}, and 0.5 cm^{-1}) during 20 min on a stable day and for typical conditions (stable typical and water vapour content, solar elevation angles about 35°, typical aerosol loading, etc.).

The averaging kernels for 3, 5, and 8 km (representative for the lower, middle and upper troposphere) are highlighted by red, blue and green colors, respectively. The sum along the rows of the averaging kernel matrix documents the sensitivity of the remote sensing system. It is depicted as thick black line. For a very high spectral resolution (typical for NDACC measurements) we can detect 3 km thick layers in the lower troposphere, 6 km layers in the middle troposphere, and 10 km layers in the upper troposphere (the layer thickness is defined as the full width at half maximum of the kernels). Then the sensitivity is almost optimal (close to unity) throughout the whole troposphere, which means that the FTIR system is well able to detect the atmospheric variability between the surface and an altitude of about 12.4 km, where still 75% of the real atmospheric variability can be detected by the remote sensing system. Measuring a high resolution NDACC spectra takes about 8 min.

If we reduce the spectral resolution to 0.02 cm^{-1} – which is the resolution of TCCON spectra – the middle and upper tropospheric averaging kernels become broader, but on the other hand the measurement time reduces to 2 min. With TCCON spectra lower tropospheric water vapour concentrations can still be well distinguished from middle/upper tropospheric concentrations and we can measure a profile each 2 min. However, then the range with a sensitivity of at least 75% is limited to altitudes below 10.7 km.

For a spectral resolution of 0.1 cm^{-1} the measurement time but also the sensitivity range get further reduced, but we still can distinguish water vapour variations that occur above 5 km altitude from variation close to the surface. If we reduce the spectral resolution to 0.5 cm^{-1} a measurement takes just a few seconds, but then the system is not well able to separate water vapour variations that occur at different altitudes and it is only satisfactorily sensitive below an altitude of 6.3 km.

The averaging kernels depend on the actual atmospheric water vapour content (level of saturation of the applied water vapour lines). However, we use lines that are typically unsaturated. Even for observations performed at sea level the averaging kernels are similar to the kernels depicted in Fig. 5. As an approximation one can consider the different observer altitudes by vertically shifting the kernels (see also Fig. 1 of Schneider and Hase, 2009).

Ground-based solar absorption spectra contain information about the vertical distribution of the absorber mainly due to the pressure broadening effect (lines are the broader the higher the pressure at the absorbers location). The broadening coefficients are typically 0.04–0.08 cm^{-1} atm^{-1}. In the stratosphere, e.g., at 25 km, the pressure is about 0.025 atm and the frequency of the absorptions that take place in the stratosphere are very well defined. In order to detect the pressure broadening effect in the stratosphere very highly-resolved spectra – like those measured within the NDACC (typical resolution of 0.004 cm^{-1}) – are mandatory. In the

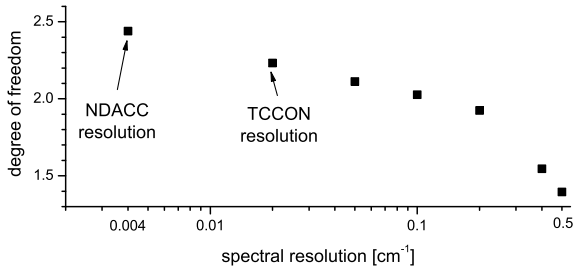

Fig. 6. Degree of freedom of the measurement (dof value) versus spectral resolution.

troposphere the pressure is more than an order of magnitude higher (e.g., it is still about 0.2 atm at 12 km). For a retrieval of tropospheric profiles a spectral resolution of $0.02\,cm^{-1}$ (or even $0.1\,cm^{-1}$, see Fig. 5) is obviously sufficient. Naturally, a very high spectral resolution is also advantageous when estimating tropospheric profiles. The higher the spectral resolution the larger the amount of information about the absorbers vertical tropospheric distribution. For this reason the smoothing error is the smaller the higher the resolution of the applied spectra (see Table 2).

The degree of freedom of the measurement (dof value) is a measure of the amount of information that is introduced by the measurement. Figure 6 shows how the dof value depends on the spectral resolution. It is about 2.5 for high resolution spectra, 2.3 for TCCON spectra, and about 2 for $0.1\,cm^{-1}$ spectral resolution, which seems to be the limit for identifying two independent atmospheric layers. For a poorer spectral resolution the dof value is below 2 and the profiling capability of the system is limited. The TCCON resolution is a good compromise enabling both, good vertical resolution and high measurement frequency.

Please note that the near infrared spectra allow a retrieval of H_2O profiles but not of HDO profiles. Above $3000\,cm^{-1}$ the signatures of the latter are rather weak. HDO/H_2O profiles, which are very useful for investigating the atmospheric water cycle (e.g., Worden et al., 2007; Frankenberg et al., 2009; Schneider et al., 2010b), can only be remotely-sensed from ground applying NDACC's mid-infrared spectra but not TCCON's near infrared spectra.

5 Empirical validation

In this Section we empirically prove TCCON's water vapour profiling capability, whereby we take Izaña's TCCON measurements as an example. First, we document that the measured water vapour absorption signatures contain significant information about the vertical distribution of tropospheric water vapour. And second, we compare the retrieved water vapour profiles to all in-situ Vaisala RS92 radiosonde profiles measured in coincidence.

5.1 Absorption signatures and vertical distribution of H_2O

At Tenerife Island radiosondes (Vaisala RS92) are launched twice per day (11:15 and 23:15 UT). The launch site is just about 15 km southeast of the Observatory on the coastline. The radiosonde measurements offer a good opportunity for documenting the FTIR's H_2O profiling capability (e.g. Schneider et al., 2010a). Figure 7 shows some examples for the agreement between radiosonde and FTIR profiles measured in coincidence. The small black squares show the RS92 profiles after correction of temperature effects and radiation bias (Vömel et al., 2007). These in-situ profiles offer a very high vertical resolution. In contrast, the remote sensing technique only allows resolving rather rough vertical structures (see averaging kernels of Fig. 5). For an adequate comparison we have to degrade the RS92 profiles to the vertical resolution of the FTIR profiles (e.g., Schneider et al., 2010a). The blue stars in Fig. 7 depict the RS92 profiles with the vertical resolution adjusted to the the FTIR profiles and the red circles depict the optimally estimated FTIR profiles. The profiles are shown as relative difference to the climatologic profile that is applied as the a priori. Any difference to the 0% line is produced by the FTIR measurement. For the coincidences shown in Fig. 7, FTIR and smoothed RS92 profiles detect very similar differences to the a priori profile, which documents the good quality of the FTIR data.

In addition Fig. 7 depicts the profiles produced by an retrieval setup that only allows for a scaling of the a priori profile (thick green dashed line). This retrieval approach postulates that the absorption signatures contain information about the total column abundances of the absorber but not of its vertical distribution. Naturally, if the actual atmosphere contains vertical water vapour structures which are similar to the a priori situation (slope of the actual profile is similar to the slope of the a priori profile) the scaled profile and the optimally estimated profile are similar. This is the case on the days 090124 and 100609. However, if the actual profile slope is significantly different from the a priori profile slope (days 090125 and 100611) the scaled profile and the optimally estimated profile differ significantly.

Figure 8 shows the residuals between measured and simulated spectra for the four exemplary measurements presented in Fig. 7. Here we take the 4609.9–4612.25 cm^{-1} spectral window as example. If the actual vertical H_2O structures significantly differ from the climatologic mean situation (day 090125 and 100611) the spectral residuals produced by the scaling retrievals are much larger than the residuals produced by the profile optimal estimation retrieval. On day 090125 the scaling approach produces a spectral residual of 0.53% (expressed as the root-mean-squares value: rms). We observe that the synthetic spectra does not well simulate the measured absorption signature. To the contrary the rms value corresponding to the profile optimal estimation approach is only 0.21%. For this approach the simulated and the measured

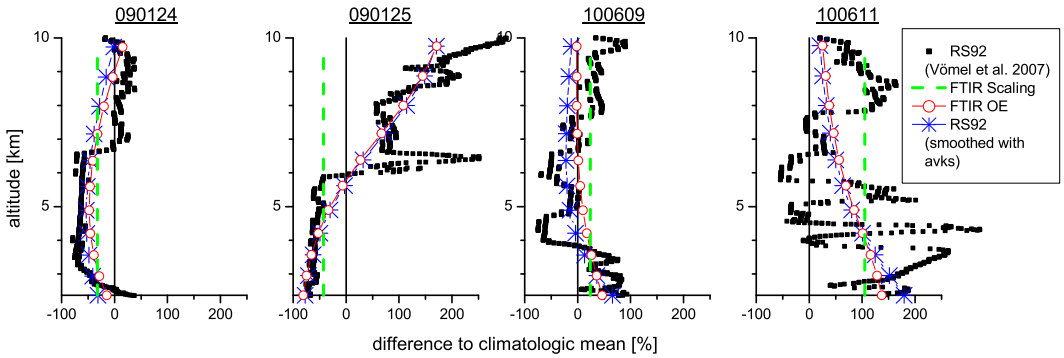

Fig. 7. Examples for coincident Vaisala RS92 and FTIR H_2O measurements (scaling and OE approach). Presented as percentage difference to a subtropical climatologic profile. Black squares: RS92 data corrected by the Vömel et al. (2007) method; Green dashed line: FTIR scaling approach; Red circles: FTIR OE approach; Blue stars: RS92 smoothed with FTIR averaging kernels.

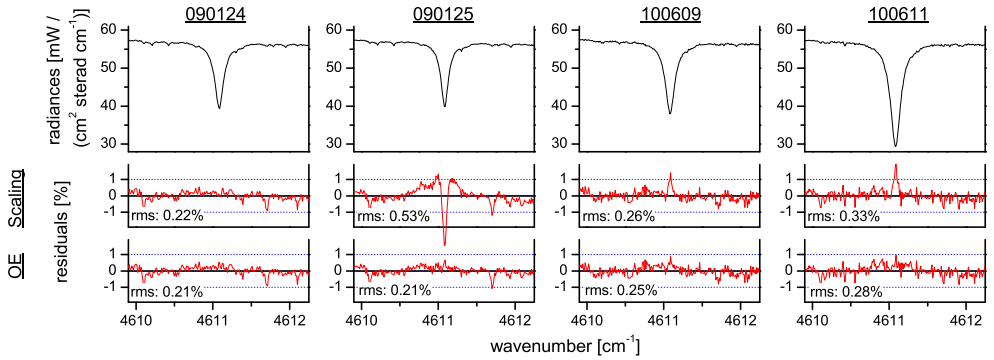

Fig. 8. Measured spectra and residuals of the 4609.9–4612.25 cm^{-1} spectral window corresponding to the four examples of Fig. 7. Top panels: measured spectra; Middle panels: residuals for scaling approach; Bottom panel: residuals for OE approach. The root-mean-squares (rms) values of the residuals are given in each panel.

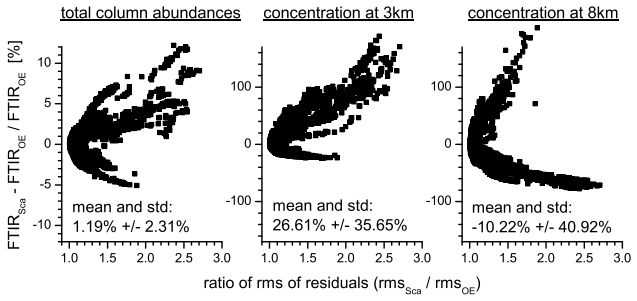

Fig. 9. Difference between H_2O total column amounts and lower and middle/upper tropospheric concentrations obtained by the FTIR scaling (Sca) and profile optimal estimation (OE) approach versus the rms value of the respective residuals.

spectra are in very good agreement. The increased spectral residuals produced by the scaling retrieval documents that the spectra contain a lot of information about the vertical distribution of the absorber.

Figure 9 expands the findings of Figs. 7 and 8 to the more than 3000 Izaña near-infrared spectra that have been measured since June 2008 (when we started recording AC and DC signals in the near-infrared). The Figure shows a comparison of the H_2O data retrieved by the scaling and the optimal estimation approach versus the ratio of the respective spectral residuals. The vertical distribution of water vapour is highly-variable and we observe that a situation like on day 091025 or 100611 is rather frequent: for about 50% of all measurements the scaling retrieval produces residuals that are at least by 20% larger than the residuals produced by the optimal estimation approach. The increased residuals of the scaling retrievals document that the TCCON spectra contain significant information about the vertical distribution of tropospheric water vapour. Figure 9 documents that the high variability of the vertical distribution of water vapour is well reflected in the water vapour absorption signatures and that the FTIR system is well able to distinguish lower from middle/upper tropospheric water vapour amounts.

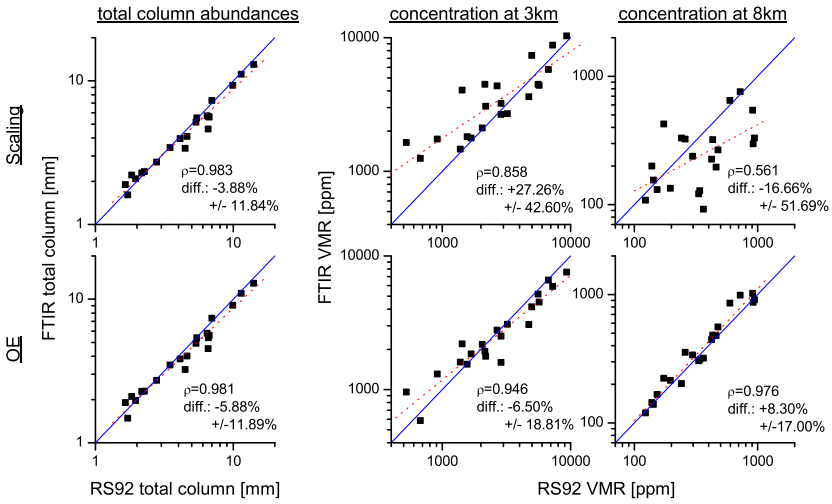

Fig. 10. Correlation between column amounts and volume mixing ratios obtained from coincident Vaisala RS92 and FTIR H_2O measurements (Upper panels for scaling and bottom panels for OE approach). From left to right: total column abundances, volume mixing ratios at 3 km and 8 km. Blue solid lines: diagonals; Red dotted lines: linear regression lines.

5.2 Correlation between coincident FTIR and RS92 measurements

Between June 2008 and August 2010, there are 21 very close coincidences between the Vaisala RS92 and FTIR near-infrared measurements (including the four situations shown in Fig. 7). As close coincidence we define the situation that the radiosonde measures at 3 km within 10 min of the FTIR near-infrared measurement (which takes about 2 min). Figure 10 shows correlations between the water vapour data measured by the RS92 and the FTIR system: the upper panels for the scaling retrieval and the bottom panels for the profile optimal estimation retrieval. The left panels depict total column abundances, the central panels concentrations at 3 km and the right panels concentrations at 8 km (whereby RS92 data have been smoothed with the FTIR kernels obtained from the profile optimal estimation retrieval).

Naturally the data produced by the scaling approach do not well correlate with the RS92 profile. On the other hand, the optimal estimation approach produces middle/upper tropospheric H_2O concentrations which very nicely agree with the RS92 concentrations (see bottom right panel: correlation coefficient ρ of 0.976 at 8 km). In the lower troposphere (see bottom middle panel) the correlation is weaker (ρ of 0.946 at 3 km), since both experiments detect very likely a different lower tropospheric airmass: the RS92 is launched from the coastline, 15 km southeast of the observatory. When reaching the altitude of the FTIR instrument (2370 m a.s.l.) it is floating in the free troposphere at a significant distance from any landmass. In contrast the water vapour amounts detected by the FTIR instrument will certainly be affected by the landmass (turbulent processes, latent heat transfer, etc.). Therefore, lower tropospheric and total column H_2O abundances detected by the RS92 and the FTIR are hardly comparable.

For more extensive FTIR-RS92 inter-comparison studies at different sites and applying different spectral signatures please refer to Schneider et al. (2010a) and Schneider et al. (2010c).

6 Time scale analysis

Spectra with a resolution of 0.02 cm^{-1} are measured in less than 2 min. TCCON can provide a uniquely dense set of solar absorption spectra. Applying the optimal estimation approach we can use the TCCON measurements for investigating variations in the tropospheric water vapour distribution on different timescales ranging from a few minutes up to several days. Figure 11 shows an example of a diurnal evolution of lower and upper tropospheric H_2O concentration as obtained from TCCON measurements at Izaña. Shown is the difference to the climatologic mean ($\frac{\hat{x}-x_a}{x_a}$, whereby $\hat{x}$ represents the retrieved water vapour concentrations and x_a the a priori climatologic mean). On this day we measured about 90 near infrared spectra between 12:30 and 16:30 UT. The black and red error bars on the right side of the plot indicate the total random errors as estimated in Sect. 3.

Concerning the lower troposphere at 3 km we observe rather large short-term variability between 12:30 and 14:30 UT. This variability is much larger than the estimated random error (compare the black error bar with the short timescale scatter of the black squares before 14:30 UT). This variability is due to increased turbulence during the morning hours when the landmass heats faster than the overlying airmass, thereby producing an instable atmospheric layering. The vertical instabilities efficiently increase the water vapour amounts and adiabatically cool the lower/middle

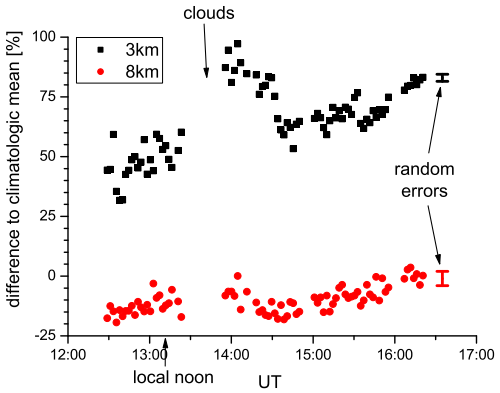

Fig. 11. Evolution of lower (black squares) and middle/upper (red dots) water vapour concentrations between 12:30 and 16:30 UT on the 19 May 2010. The error bars indicate total random errors as estimated for the respective altitudes (see right panel of Fig. 3).

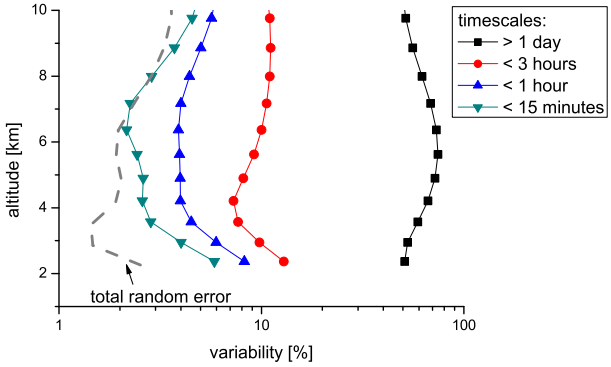

Fig. 12. Water vapour variability for the different timescales as indicated in the legend. The dotted grey line indicates the estimated total random error (see right panel of Fig. 3).

troposphere. As a consequence between 13:30 and 14:00 UT the lower/middle troposphere above Izaña gets saturated and the water partly condensates to cloud droplets. The situation is different at the end of the day. Then the landmass cools faster than the overlying airmass thereby causing high vertical stability. After 15:30 UT the low short-term variability can fully be explained by the estimated random error.

In the upper troposphere the diurnal evolution is rather smooth. There the water vapour concentrations are rather constant during the whole day. The observed short-term variability can fully be explained by the random error (compare scatter of red dots with red error bar).

We find that such increased lower tropospheric short-term variability is a typical situation. Figure 12 plots profiles of the tropospheric water vapour variability on different timescales as obtained from TCCON measurements. The study bases on measurements taken at Izaña on 57 different days between June 2008 and August 2010. On 15 of these days we measured continuously near-infrared spectra for at least 2 h allowing 50–100 individual profile retrievals for each of these days. We define the variability as the 1σ standard deviation of the difference to the a priori value. We observe that most variability occurs on timescales that are larger than 1 day. However, even on very short timescales lower tropospheric variabilities cannot be neglected. Within 15 min only, lower tropospheric water vapour already varies by 6%, which is clearly larger than the estimated measurement uncertainty (dotted grey line). The significant variability on rather short timescales justifies the strict coincidence criterion applied for the comparison shown in Figs. 7 and 10. The short timescale variability also points to small-scale structures in the horizontal water vapour fields of the lower troposphere. The significant small-scale and short timescale variability converts the inter-comparison of lower tropospheric water vapour measurement techniques into a difficult task. It is strongly recommendable that the different techniques measure at exactly the same time and at the same place. Detecting a slightly different airmass can introduce significant uncertainties in the inter-comparison study.

The situation is a bit less critical in the middle/upper troposphere, where a variability of larger than 6% is only observed for timescales larger than 1 h. It seems that the middle/upper troposphere is more stable and changes are smoother in time as well as in space.

It should be noted that the lower tropospheric water vapour structure can also be observed at very high temporal resolution using ground-based atmospheric emission measurements in the infrared and microwave region (Smith et al., 1999; Güldner and Spänkuch, 2001). However, to our knowledge and concerning middle/upper tropospheric water vapour only TCCON can provide a temporally dense data set with good quality.

7 Conclusions

TCCON is a rather new and expensive network of high quality ground-based FTIR systems. There has been a lot of effort for guaranteeing an ultimate quality of the measured spectra. TCCON's high quality standards as well as its long-term strategy are very attractive for many fields of atmospheric research, in particular for climate change research. Understanding the atmospheric water vapour distribution is very important for understanding Earth's climate. We show that the TCCON measurements can be used to monitor tropospheric water vapour profiles with a vertical resolution of 3 and 8 km in the lower and middle/upper troposphere, respectively. As long as one does not aim for an ultimate sensitivity in the upper troposphere it is not necessary to record additional spectra with higher resolution. The TCCON resolution is sufficient and can provide data at a very high measurement frequency (one measurement every 1–2 min).

The density of the TCCON H_2O profile data will allow an analysis of tropospheric water vapour variability for different altitudes and on different timescales ranging from several hours to a few minutes. This is important for assessing the validity and limits of water vapour profile inter-comparison studies. Furthermore, it might allow novel studies of short timescale processes thereby leading to an improved parameterisation and thus model representation of turbulence, convection, or lateral mixing processes.

Acknowledgements. M. Schneider was supported by the Deutsche Forschungsgemeinschaft via the project RISOTO (Geschäftszeichen SCHN 1126/1-1 and 1-2) and since May 2010 he has enjoyed a Ramón y Cajal grant from the Spanish Ministry of Science and Innovation. E. Sepúlveda receives a predoctoral fellowship from the Spanish Ministry of Education. The establishment of TCCON was generously supported by grants from NASA's terrestrial carbon cycle program and from the OCO project office. We are grateful to the Goddard Space Flight Center for providing the temperature and pressure profiles of the National Centers for Environmental Prediction via the automailer system.

Edited by: B. Funke

References

Abrams, M. C., Toon, G. C., and Schindler, R. A. : Practical example of the correction of Fourier-transform spectra for detector nonlinearity, Appl. Optics, 33(27), 6307–6314, doi:10.1364/AO.33.006307, 1994.

Frankenberg, C., Yoshimura, K., Warneke, T., Aben, I., Butz, A., Deutscher, N., Griffith, D., Hase, F., Notholt, J., Schneider, M., Schrejver, H., and Röckmann, T.: Dynamic processes governing lower-tropospheric HDO/H_2O ratios as observed from space and ground, Science, doi:10.1126/science.1173791, 325, 1374–1377, 2009.

Geibel, M. C., Gerbig, C., and Feist, D. G.: A new fully automated FTIR system for total column measurements of greenhouse gases, Atmos. Meas. Tech., 3, 1363–1375, doi:10.5194/amt-3-1363-2010, 2010.

Gisi, M., Hase, F., Dohe, S., and Blumenstock, T.: Camtracker: a new camera controlled high precision solar tracker system for FTIR-spectrometers, Atmos. Meas. Tech. Discuss., 3, 4865–4887, doi:10.5194/amtd-3-4865-2010, 2010.

Güldner, J. and Spänkuch, D.: Remote sensing of the thermodynamic state of the atmospheric boundary layer by ground-based microwave radiometry, J. Atmos. Ocean. Technol., 18, 925–933, 2001.

Hase, F., Blumenstock, T., and Paton-Walsh, C.: Analysis of the instrumental line shape of high-resolution Fourier transform IR spectrometers with gas cell measurements and new retrieval software, Appl. Opt., 38, 3417–3422, 1999.

Hase, F. and Höpfner, M.: Atmospheric raypath modelling for radiative transfer algorithms, Appl. Opt., 38, 3129–3133, 1999.

Hase, F., Hannigan, J. W., Coffey, M. T., Goldman, A., Höpfner, M., Jones, N. B., Rinsland, C. P., and Wood, S. W.: Intercomparison of retrieval codes used for the analysis of high-resolution, ground-based FTIR measurements, J. Quant. Spectrosc. Ra., 87, 25–52, 2004.

Keppel-Aleks, G., Toon, G. C., Wennberg, P. O., and Deutscher, N. M.: Reducing the impact of source brightness fluctuations on spectra obtained by Fourier-transform spectrometry, Appl. Opt., 46, 4774–4779, 2007.

Kurylo, M. J. and Zander, R.: The NDSC – Its status after 10 years of operation, Proceedings of XIX Quadrennial Ozone Symposium, Hokkaido University, Sapporo, Japan, 167–168, 2000.

Messerschmidt, J., Macatangay, R., Notholt, J., Petri, C., Warneke, T., and Weinzierl, C.: Side by side measurements of CO_2 by ground-based Fourier transform spectrometry (FTS), Tellus B, 62, 749–758, 2010.

Olsen, S. C., and Randerson, J. T.: Differences between surface and column atmospheric CO_2 and implications for carbon cycle research, J. Geophys. Res., 109, D02301, doi:10.1029/2003JD003968, 2004.

Randall, D. A., Wood, R. A., Bony, S., Colman, R., Fichefet, T., Fyfe, J., Kattsov, V., Pitman, A., Shukla, J., Srinivasan, J., Stouffer, R. J., Sumi, A., and Taylor, K. E.: Climate Models and Their Evaluation, in: Climate Change 2007: The Physical Science Basis, Contribution of Working Group I to the Fourth Assessment Report of the Intergovernmental Panel on Climate Change, edited by: Solomon, S., Qin, D., Manning, M., Chen, Z., Marquis, M., Averyt, K. B., Tignor, M., and Miller, H. L., Cambridge University Press, Cambridge, United Kingdom and New York, NY, USA, 2007.

Rodgers, C. D.: Inverse Methods for Atmospheric Sounding: Theory and Praxis, World Scientific Publishing Co., Singapore, ISBN 981-02-2740-X, 2000.

Rothman, L. S., Gordon, I. E., Barbe, A., Chris Benner, D., Bernath, P. F., Birk, M., Boudon, V., Brown, L. R., Campargue, A., Champion, J.-P., Chance, K., Coudert, L. H., Dana, V., Devi, V. M., Fally, S., Flaud, J.-M., Gamache, R. R., Goldman, A. Jacquemart, D., Kleiner, I., Lacome, N., Lafferty, W. J., Mandin, J.-Y., Massie, S. T., Mikhailenko, S. N., Miller, C. E., Moazzen-Ahmadi, N., Naumenko, O. V., Nikitin, A. V., Orphal, J., Perevalov, V. I., Perrin, A., Predoi-Cross, A., Rinsland, C. P., Rotger, M., Simecková, M., Smith, M. A. H., Sung, K., Tashkun, S. A., Tennyson, J., Toth, R. A., Vandaele, A. C., and Vander-Auwera, J.: The HITRAN 2008 molecular spectroscopic database, J. Quant. Spectrosc. Radiat. Transfer, 110, 533–572, doi:10.1016/j.jqsrt.2009.02.013, 2009.

Schneider, M., Hase, F., and Blumenstock, T.: Water vapour profiles by ground-based FTIR spectroscopy: study for an optimised retrieval and its validation, Atmos. Chem. Phys., 6, 811–830, doi:10.5194/acp-6-811-2006, 2006.

Schneider, M. and Hase, F.: Ground-based FTIR water vapour profile analyses, Atmos. Meas. Tech., 2, 609–619, doi:10.5194/amt-2-609-2009, 2009.

Schneider, M., Romero, P. M., Hase, F., Blumenstock, T., Cuevas, E., and Ramos, R.: Continuous quality assessment of atmospheric water vapour measurement techniques: FTIR, Cimel, MFRSR, GPS, and Vaisala RS92, Atmos. Meas. Tech., 3, 323–338, doi:10.5194/amt-3-323-2010, 2010a.

Schneider, M., Yoshimura, K., Hase, F., and Blumenstock, T.: The ground-based FTIR network's potential for investigating the atmospheric water cycle, Atmos. Chem. Phys., 10, 3427–3442, doi:10.5194/acp-10-3427-2010, 2010b.

Schneider, M., Toon, G. C., Blavier, J.-F., Hase, F., and Leblanc, T.: H_2O and δD profiles remotely-sensed from ground in different spectral infrared regions, Atmos. Meas. Tech., 3, 1599–1613, doi:10.5194/amt-3-1599-2010, 2010c.

Schneider, M., Hase, F., Blavier, J.-F., Toon, G. C., and Leblanc, T.: An empirical study on the importance of a speed-dependent Voigt line shape model for tropospheric water vapor profile remote sensing, J. Quant. Spectrosc. Radiat. Transfer, 112, 465–474, doi:10.1016/j.jqsrt.2010.09.008, 2011.

Sherwood, S. C., Ingram, W., Tsushima, Y., Satoh, M., Roberts, M., Vidale, P. L., and O'Gorman, P. A.: Relative humidity changes in a warmer climate, J. Geophys. Res., 115, D09104, doi:10.1029/2009JD012585, 2010.

Smith, W. L., Feltz, W. F., Knuteson, R. O., Revercomb, H. E., Woolf, H. M., and Howell, H. B.: The Retrieval of Planetary Boundary Layer Structure Using Ground-Based Infrared Spectral Radiance Measurements, J. Atmos. Ocean. Technol., 16, 323–333, 1999.

Spencer, R. W. and Braswell, W. D.: How Dry is the Tropical Free Troposphere?, Implications for Global Warming Theory, B. Am. Meteor. Soc., 78, 1097–1106, 1997.

Vömel, H., Selkirk, H., Miloshevich, L., Valverde, J., Valdés, J., Kyrö, E., Kivi, R., Stolz, W., Peng, G., and Diaz, J. A.: Radiation dry bias of the Vaisala RS92 humidity sensor, J. Atmos. Oceanic Technol., 24, 953–963, 2007.

Wagner G. and Birk, M.: Water spectroscopy in the 1 µm region – a case study for collisional narrowing, 64th International Meeting on Molecular Spectroscopy, Columbus, Ohio, USA, 22–26 June, 2009.

Washenfelder, R. A., Toon, G. C., Blavier, J.-F., Yang, Z., Allen, N. T., Wennberg, P. O., Vay, S. A., Matross, D. M., and Daube, B. C.: Carbon dioxide column abundances at the Wisconsin Tall Tower site, J. Geophys. Res., 111, D22305, doi:10.1029/2006JD007154, 2006.

Worden, J. R., Noone, D., Bowman, K., Beer, R., Eldering, A., Fisher, B., Gunson, M., Goldman, A., Herman, R., Kulawik, S. S., Lampel, M., Osterman, G., Rinsland, C., Rodgers, C., Sander, S., Shephard, M., Webster, C. R., and Worden, H.: Importance of rain evaporation and continental convection in the tropical water cycle, Nature, 445, 528–532, doi:10.1038/nature05508, 2007.

Wunch, D., Toon, G. C., Blavier, J.-F., Washenfelder, R., Notholt, J., Connor, B. J., Griffith, D. W. T., Sherlock, V., and Wennberg, P. O.: The Total Carbon Column Observing Network (TCCON), Philos. T. R. Soc. A, accepted, 2010a.

Wunch, D., Toon, G. C., Wennberg, P. O., Wofsy, S. C., Stephens, B. B., Fischer, M. L., Uchino, O., Abshire, J. B., Bernath, P., Biraud, S. C., Blavier, J.-F. L., Boone, C., Bowman, K. P., Browell, E. V., Campos, T., Connor, B. J., Daube, B. C., Deutscher, N. M., Diao, M., Elkins, J. W., Gerbig, C., Gottlieb, E., Griffith, D. W. T., Hurst, D. F., Jimnez, R., Keppel-Aleks, G., Kort, E. A., Macatangay, R., Machida, T., Matsueda, H., Moore, F., Morino, I., Park, S., Robinson, J., Roehl, C. M., Sawa, Y., Sherlock, V., Sweeney, C., Tanaka, T., and Zondlo, M. A.: Calibration of the Total Carbon Column Observing Network using aircraft profile data, Atmos. Meas. Tech., 3, 1351–1362, doi:10.5194/amt-3-1351-2010, 2010b.

Yang, Z., Toon, G. C., Margolis, J. S., and Wennberg, P. O.: Atmospheric CO_2 retrieved from ground-based near IR solar spectra, Geophys. Res. Lett., 29, 1339, doi:10.1029/2001GL014537, 2002.

6

LONG-TERM VALIDATION OF TROPOSPHERIC COLUMN-AVERAGED CH_4 MOLE FRACTIONS OBTAINED BY MID-INFRARED GROUND-BASED FTIR SPECTROMETRY

Atmos. Meas. Tech., 5, 1425–1441, 2012
www.atmos-meas-tech.net/5/1425/2012/
doi:10.5194/amt-5-1425-2012

Atmospheric Measurement Techniques

Long-term validation of tropospheric column-averaged CH_4 mole fractions obtained by mid-infrared ground-based FTIR spectrometry

E. Sepúlveda[1,2], M. Schneider[2,3], F. Hase[3], O. E. García[2], A. Gomez-Pelaez[2], S. Dohe[3], T. Blumenstock[3], and J. C. Guerra[1]

[1]La Laguna University, Physics Department, Tenerife, Spain
[2]Izaña Atmospheric Research Center, Agencia Estatal de Meteorología (AEMET), Spain
[3]Institute for Meteorology and Climate Research (IMK-ASF), Karlsruhe Institute of Technology, Germany

Correspondence to: E. Sepúlveda (esepulvedah@aemet.es)

Received: 26 December 2011 – Published in Atmos. Meas. Tech. Discuss.: 13 February 2012
Revised: 25 May 2012 – Accepted: 29 May 2012 – Published: 26 June 2012

Abstract. At the Izaña Atmospheric Research Center, high-resolution mid-infrared solar absorption spectra have been recorded for more than 12 yr using Fourier Transform InfraRed (FTIR) spectrometers. We use the spectral fitting algorithm PROFFIT to retrieve long-term time series of methane (CH_4) from the measured spectra. We investigate the total column-averaged dry air mole fractions of methane ($totXCH_4$) obtained from a profile scaling and a profile retrieval, and apply two approaches for deriving the tropospheric column-averaged dry air mole fractions: firstly, we use the FTIR hydrogen fluoride (HF) total column amounts as an estimator for the stratospheric CH_4 contribution and a posteriori correct the $totXCH_4$ data of a profile scaling retrieval accordingly ($troXCH_{4_{post}}$); secondly, we directly determine the tropospheric column-averaged dry air mole fractions of methane ($troXCH_{4_{retr}}$) from retrieved CH_4 profiles. Our theoretical estimation indicates that the scaling retrieval leads to $totXCH_4$ amounts that are subject to a large smoothing error, which can be widely avoided by applying a profile retrieval (for the latter we estimate an overall precision of 0.41 %).

We compare the different FTIR CH_4 data to Izaña's Global Atmospheric Watch (GAW) surface in-situ CH_4 data ($CH_{4_{GAW}}$), which in the case of the Izaña Atmospheric Research Center high mountain observatory are very representative for the free tropospheric CH_4 amounts. Concerning $totXCH_4$, the agreement between the FTIR data product and the in-situ measurement is rather poor documenting that $totXCH_4$ is not a valid free tropospheric CH_4 proxy, as it is significantly affected by the varying stratospheric CH_4 contribution and it rather follows the variation in the tropopause altitude. The a posteriori correction method as applied here only removes a part of this stratospheric CH_4 contribution. In contrast the profile retrieval allows for a direct estimation of the tropospheric column-averaged CH_4 amounts. Results of the profile retrieval analysis correlate well with the $CH_{4_{GAW}}$ data (correlation coefficient of 0.60, FTIR-GAW scatter of 0.97 %), and both data sets show very similar annual cycles and trend behaviour for the 2001–2010 time period. Furthermore, we find a very good absolute agreement between the $troXCH_{4_{retr}}$ and $CH_{4_{GAW}}$ (mid-infrared FTIR/GAW scaling factor of 0.9987) suggesting that mid-infrared FTIR data can be well combined with the surface in-situ GAW data.

Our study strongly supports the value of mid-infrared ground-based FTIR CH_4 profile retrievals as well as the robustness of the approach for achieving total and tropospheric column-averaged XCH_4 data of high quality.

1 Introduction

Methane (CH_4) is the second most important anthropogenic greenhouse gas (GHG), after carbon dioxide (CO_2). While CH_4 is 200 times less abundant than CO_2, it is about 20 times more efficient than CO_2 to trap outgoing long wave radiation, on a 50 yr timescale. The change in the CH_4 mixing ratio

since pre-industrial times (1750) to 2005 (from 715 to 1774 ppb) gives a radiative forcing (RF) of $+0.48 \pm 0.05\,W\,m^{-2}$, ranking CH_4 as the second highest RF of the GHGs after CO_2 (RF of CO_2 in 2005, $1.66 \pm 0.17\,W\,m^{-2}$; IPCC, 2007). In 2009 CH_4 global atmospheric concentrations have reached more than 1780 ppb for column-averaged mole fractions on global average in 2009 (Frankenberg et al., 2011). At surface stations higher annual average values are registered (e.g. 1830 ppb at the Izaña's Global Atmospheric Watch (GAW) station in 2009, Gomez-Pelaez et al., 2010.

CH_4 plays an important role in atmospheric chemistry, affecting the oxidizing capacity of the atmosphere and acting as a precursor of tropospheric ozone (O_3). The main sources producing methane are considered to be biogenic CH_4 formation that occurs in natural wetlands, water-flooded rice paddies, landfills, stomachs of ruminant animals, incomplete burning of biomass, oceans and vegetation. Further sources are released from melting permafrost and from shallow hydrates on the continental shelf (Dlugokencky et al., 2009). Thermogenic formation is the main process for generation of natural gas deposits over geological time scales. Parts of this inventory are released into the atmosphere due to fossil fuel extraction, processing, transportation and distribution (Keppler et al., 2006; Frankenberg et al., 2005). The main sink of atmospheric CH_4 is the reaction with hydroxyl radical OH. The destruction of CH_4 by OH in the troposphere represents about 90 % of CH_4 loss in the atmosphere. The rest of the sink is due to an uptake of CH_4 by soils, reaction with Cl in the marine boundary layer, and due to transport into the stratosphere where it is decomposed by reactions with OH, O (^{1}D) and Cl (Bousquet et al., 2011).

Prediction of the evolution of GHGs in the atmosphere requires an understanding of their sources and sinks. Therefore, inverse modelling techniques applying atmospheric concentration measurement monitored at global surface networks are used (Bousquet et al., 2011). The in-situ surface measurements show very high precision and absolute accuracy (approx. 0.1 %), but they are strongly affected by local processes like small-scale turbulences or nearby sources or sinks. It is very difficult for the inverse models to capture these small-scale processes. In this context, vertically averaging the concentrations can be helpful. For instance, Olsen and Randerson (2004) document that total column-averaged observations of GHGs are significantly less affected by small-scale processes, but still conserve valuable GHG source/sink information. However, total column-averaged data are affected by the stratospheric contribution, the correct modelling of which is a significant error source when investigating the GHG cycling between the atmosphere, the biosphere, and the ocean.

Ground-based high spectral resolution FTIR measurements allow a precise determination of the atmospheric abundances (total column amounts and vertical profiles) of many constituents, including GHGs. The ground-based FTIR total column data are essential for the validation of GHGs measured from space by current and future satellite sensors (e.g. SCIAMACHY, GOSAT, OCO-2). Furthermore, by means of the ground-based FTIR vertical profile data, one can calculate tropospheric column-averaged mixing ratios. These ratios would neither be affected by small-scale near-surface processes nor by stratospheric contributions. If provided with high accuracy and precision, the tropospheric column-averaged mixing ratios would be a very useful data product for investigating the GHG cycling between the atmosphere, the biosphere, and the ocean.

In this work we present, discuss, and validate different ground-based FTIR CH_4 products derived from mid-infrared spectral region: the total column-averaged volume mixing ratio (totXCH_4), and two tropospheric column-averaged volume mixing ratios (troXCH_4): a first derived by a posteriori correction method using HF as indicator for the stratospheric contribution (similar to Washenfelder et al., 2003), and a second directly retrieved from the measured spectra.

In the following Sect. 2, we describe the CH_4 program at the Izaña Atmospheric Research Center: the GAW in-situ and FTIR activities. In Sect. 3 we present the FTIR technique and the FTIR CH_4 products. We describe the data analysis method and document the characteristics of the FTIR data (sensitivity and uncertainty). In Sect. 4 the different FTIR CH_4 products are compared to the GAW surface CH_4 measurements. In Sect. 5 we comment on the comparability of retrievals in the mid- and near- infrared spectral region, and Sect. 6 summarizes our study.

2 CH_4 program at the Izaña Atmospheric Research Center

2.1 Site description

Izaña is a subtropical high mountain observatory located on the Canary Island of Tenerife, 300 km from the African west coast at 28°18′ N, 16°29′ W at 2370 m a.s.l. It is part of the Meteorological State Agency of Spain (Spanish acronym: AEMET), and it is run by the Izaña Atmospheric Research Center. It is a global station of the WMO (World Meteorological Organisation) network of GAW (Global Atmospheric Watch) stations and has a comprehensive measurement program of a large variety of different atmospheric constituents. More detailed information can be found on the official webpage of the Izaña Atmospheric Research Center: http://www.izana.org.

The Izaña Observatory is usually located above a strong subtropical temperature inversion layer (generally well established between 500 and 1500 m a.s.l.). While during daytime the strong diurnal insolation generates a slight upslope flow of air originating from below the inversion layer (from a woodland that surrounds the station at a lower altitude), during nighttime the Izaña Observatory is very representative of the free troposphere (or at least of the lower levels of the free troposphere; see Fig. 1).

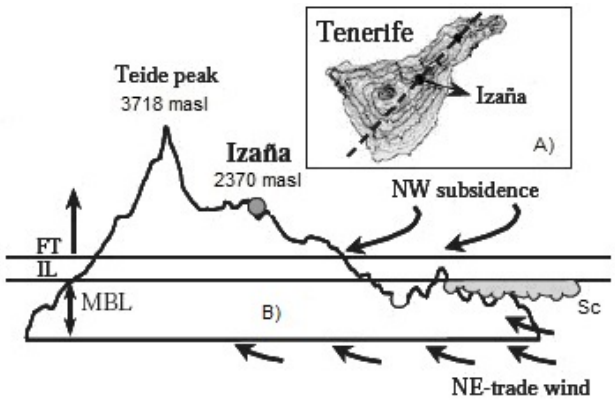

Fig. 1. (A) Location of Izaña in Tenerife Island, **(B)** transect of Tenerife Island – along the dotted line in **(A)** – showing the vertical stratification: MBL: marine boundary layer, IL: inversion layer, FT: free troposphere, Sc: stratocumulus.

2.2 In-situ measurement program

Continuous surface in-situ measurements of atmospheric CO_2 and CH_4 have been carried out at Izaña station since 1984. Furthermore, CO concentrations have been measured since 1998 and N_2O and SF_6 since 2007.

CH_4 mole fraction is measured using a DANI 3800 gas chromatograph. The carrier gas is synthetic air. Ambient air is cooled to −70 °C to partially remove water vapour content before flowing towards the sample loop (10 ml size). Sample loop temperature is not regulated. A self-developed software integrator provides the area and height of the CH_4 peak in the chromatogram. See Gomez-Pelaez and Ramos (2011), and references therein, for more details about the measurements and technique. The most recent World Calibration Centre (WCC-Empa) system and performance audit for CH_4 at Izaña was carried in 2009 and documents the good quality of the Izaña CH_4 in-situ data (Zellweger et al., 2009). This good data quality is also confirmed by the continuous comparison to NOAA data obtained from simultaneously collected weekly flask samples (Gomez-Pelaez et al., 2012).

2.3 FTIR measurement program

Ground-based FTIR activities started at Izaña Observatory in the late 1990s in the framework of a collaboration between AEMET and KIT (Karlsruhe Institute of Technology, Germany). In 1999 KIT scientists installed a Bruker IFS 120M instrument at Izaña. In early 2005 KIT substituted this spectrometer by a Bruker IFS 125HR. During March–April of 2005, both instruments were running side-by-side. The Izaña FTIR experiment is involved in two global networks: since 1999 it has contributed to the Network for the Detection of Atmospheric Composition Change (NDACC, http://www.ndacc.org) and since 2007 to the Total Carbon Column Observing Network (TCCON, http://www.tccon.caltech.edu). For NDACC, solar absorption spectra are measured in the mid-infrared spectral region (740–4250 cm^{-1}, corresponding to 13.5–2.4 µm) and for TCCON in the near- infrared spectral region (3500–14 000 cm^{-1}, corresponding to 2.9–0.7 µm). The applied high-resolution FTIR spectrometer allows for a detailed observation of the pressure broadening effect, i.e. the absorption line width of an atmospheric absorber depends on the pressure (and thus altitude) where the absorption takes place. Therefore, one can retrieve concentration profiles of the atmospheric absorbers in addition to total column abundances. The Instrumental Line Shape (ILS) also affects the observed line shape, and in particular for the profile retrievals a continuous monitoring of the ILS is important. At Izaña we determine the ILS about every 2 months by low-pressure gas cell (HBr and N_2O) measurements and the LINEFIT software (LINEFIT code, Hase et al., 1999). The respective LINEFIT results are then applied in the atmospheric retrievals.

CH_4 has absorption lines in both the mid-infrared and near-infrared spectral regions. In this study we present CH_4 retrieved only from NDACC mid-infrared spectra.

3 Ground-based FTIR technique and CH_4 products

3.1 General setup of a ground-based FTIR analysis

Ground-based NDACC FTIR systems measure solar absorption spectra, under clear sky conditions, applying a high-resolution Fourier Transform Spectrometer (typical resolution of 0.005 cm^{-1}; maximum optical path difference, OPD_{max} of 180 cm). The measured spectra are simulated by a precise line-by-line radiative transfer model that applies the parameters of a spectroscopic database (e.g. HITRAN, Rothman et al., 2009). The basic equation for analyzing the solar absorption is the Lambert Beer's law:

$$I(\lambda) = I_{\text{sun}}(\lambda) \cdot \exp\left(-\int_{\text{TOA}}^{\text{Obs}} \sigma_x(\lambda, s(T,p)) \cdot x(s)\,\mathrm{d}s\right) \quad (1)$$

where $I(\lambda)$ is the measured intensity at wavelength λ, I_{sun} the extraterrestrial solar intensity, $\sigma_x(\lambda, s)$ is the absorption cross section and $x(s)$ the concentration of an absorber x at location s. The integration is performed along the path of the direct sunlight (between the Observer, Obs, and the Top Of the Atmosphere, TOA). At higher wavenumbers (above 1500 cm^{-1}), atmospheric self-emission can be neglected as compared to direct solar radiances.

For the purpose of numerical handling, the atmospheric state $x(s)$ and the simulated spectrum $I(\lambda)$ are discretized in form of a state vector $\boldsymbol{x}$ and a measurement vector $\boldsymbol{y}$. The measurement and state vector are related by a vector valued function $\boldsymbol{F}$, which simulates the atmospheric radiative transfer and the characteristics of the measurement system (spectral resolution, instrumental line shape, etc.): $\boldsymbol{y} = \boldsymbol{F}(\boldsymbol{x})$.

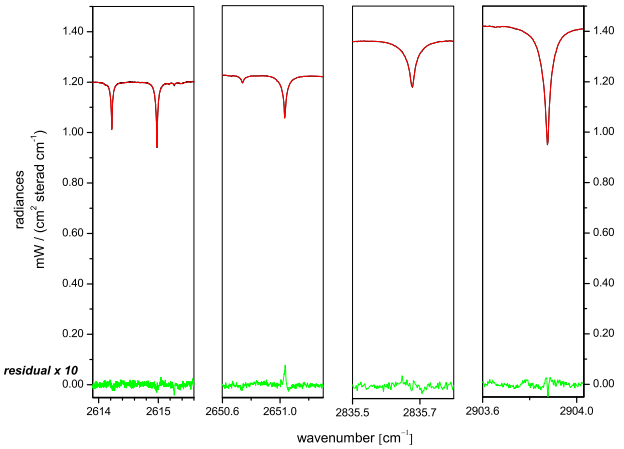

Fig. 2. The four applied spectral microwindows: measured spectrum (black), simulated spectrum (red), and residuals multiplied by a factor of 10 (green).

The derivatives $\partial \boldsymbol{y}/\partial \boldsymbol{x}$ determine the changes in the modelled spectral fluxes $\boldsymbol{y}$ for changes in the vertical distribution of the absorber $\boldsymbol{x}$. These derivatives are collected in a Jacobian matrix $\mathbf{K}$:$\partial \boldsymbol{y} = \mathbf{K}\partial \boldsymbol{x}$. Direct inversion of this last equation would allow an iterative calculation of the sought variables $\boldsymbol{x}$. However, the problem is generally ill-determined, i.e. the columns of $\mathbf{K}$ are not linearly independent and there are many solutions that are in acceptable agreement with the measurement. Thus, the solution has to be properly constrained. An extensive treatment of this topic is given in the textbook of C. D. Rodgers (Rodgers, 2000). We apply the retrieval code PROFFIT and the included radiative transfer code PROFFWD to accomplish our analysis (Hase et al., 2004).

3.2 The CH_4 retrieval strategy

Currently, the establishment of an improved NDACC CH_4 retrieval guideline is under discussion. The objective is an NDACC CH_4 product that approaches the high precision requirements of TCCON (a few per mil). At some stations NDACC measurements have been performed since the early 1990s, and high quality NDACC CH_4 data could well complement the TCCON time series, which are limited to the last few years.

Our CH_4 retrieval strategy is a modification of the current official NDACC retrieval guideline and includes a set of 4 microwindows containing strong, unsaturated, and isolated CH_4 lines (see Fig. 2 and Table 1). Besides CH_4 we have considered spectroscopic signatures of 7 interfering species. For the target species (CH_4) and the interfering species (CO_2, O_3, N_2O, NO_2 and HCl), we have applied spectroscopic parameters from HITRAN 2008 (Rothman et al., 2009), while for H_2O and OCS we have applied the recent HITRAN 2009 update.

As a-priori profiles of the interfering species, we apply the climatological entries from WACCM (The Whole Atmosphere Community Climate Model) provided by NCAR (National Centre for Atmospheric Research, J. Hannigan, personal communication, 2009). For the minor interfering species (O_3, N_2O, HCl and OCS), we simply simulate the spectral signatures according to the WACCM concentrations. For the major absorbers (CO_2 and NO_2), we scale the WACCM profiles during the CH_4 retrieval process and the H_2O interferences are accounted for by a two step strategy: first, we perform a dedicated H_2O retrieval (Schneider et al., 2010a) and then we scale the retrieved daily mean H_2O profile in the subsequent CH_4 retrieval process. Thereby, we minimise the interferences due to H_2O and HDO. Such interferences have been investigated in recent studies applying different sets of microwindows at both high and low altitude sites (Sussmann et al., 2011; Hase, 2011). Izaña is a rather dry high-altitude site, so the H_2O interference problem is less severe than for low latitude sites at sea-level. We expect that our results are transferable to at least other high altitude or polar sites of the NDACC.

Furthermore, we fit the continuum background slope and the residual ILS asymmetry. We use the NCEP analysis (National Centers for Environmental Prediction) at 12:00 UT as the temperature and pressure input profiles.

We examine two different CH_4 fitting procedures. A first consists in scaling the CH_4 WACCM a-priori profile (in the following referred to as scaling retrieval, SR), and a second retrieves CH_4 profiles (profile retrieval, PR), whereby a Tikhonov-Phillips method on a logarithmic scale is applied (Hase, 2000; Hase et al., 2004; Schneider et al., 2006).

3.3 The FTIR CH_4 products

3.3.1 Total column-averaged CH_4 dry air mole fraction (totXCH_4)

The totXCH_4 is calculated dividing the CH_4 total column by the dry pressure column (DPC) above Izaña. The DPC is calculated converting the ground pressure to column air concentration:

$$\mathrm{DPC} = \frac{P_\mathrm{s}}{m_\mathrm{dryair} \cdot g\,(\varphi)} - \frac{m_{\mathrm{H_2O}}}{m_\mathrm{dryair}} \times \mathrm{H_2O_{col}} \qquad (2)$$

being P_s the surface pressure at Izaña ground level, m_dryair the molecular mass of the dry air ($\sim$28.96 g mol^{-1}), $m_{\mathrm{H_2O}}$ the molecular mass of the water vapour ($\sim$18 g mol^{-1}), $\mathrm{H_2O_{col}}$ the water vapour total column amount (retrieved with a dedicated H_2O retrieval, Schneider, et al., 2010b), and $g(\varphi)$ the latitude-dependent surface acceleration due to gravity. The ground pressure was acquired with a Setra System (precision of $\pm$0.3 hPa).

Table 1. Spectral microwindows (MW) chosen for the CH_4 retrieval shown in this study.

	Spectral microwindows (cm^{-1})
MW1	2613.7000–2615.4000
MW2	2650.6000–2651.3000
MW3	2835.5000–2835.8000
MW4	2903.6000–2904.0250

3.3.2 A posteriori-corrected total column-averaged CH_4 dry air mole fraction (troXCH$_{4_{post}}$)

Similar to Washenfelder et al. (2003), we calculate the troXCH$_{4_{post}}$ from the CH_4 total column after correcting the variation in both surface pressure and stratospheric contribution:

$$\text{troXCH}_{4_{\text{post}}} = \frac{\text{CH}_{4_{\text{col}}} - b \cdot \text{HF}_{\text{col}}}{\text{DPC}} \quad (3)$$

where $CH_{4_{col}}$ is the CH_4 total column from the scaling retrieval, HF_{col} is the HF total column, and b is the stratospheric slope equilibrium relationship between the CH_4 and HF columns. In Appendix A we describe and discuss different approaches for calculating the b-value in the context of the method presented by Washenfelder et al. (2003).

In Eq. (3) we apply a de-trended HF total column time series retrieved from the FTIR measurements at Izaña. The HF trend and annual cycle were calculated by fitting the following function to the HF daily mean time series:

$$f(t) = a_1 + a_2 t + \sum_{j=1}^{2} \left[d_j \cos(k_j t) + e_j \sin(k_j t) \right] \quad (4)$$

where t is the time in days, a_1 is a constant value, a_2 is the parameter of the linear trend, and d_j and e_j are the parameters of the annual cycle ($k_j = 2\pi j/T$ with $T = 365.25$ days).

Subtracting $a_2 t$ from the HF time series yields the de-trended HF time series. Alternatively, we can divide the HF time series by the term ($a_1 + a_2 t$), which yields a normalised and de-trended HF time series. The normalisation has the advantage that we can apply a normalised b-value, which does not change with a trend in HF (see discussion in Appendix A). Both the de-trended and normalised HF time series keep the variability caused by changes of the tropopause altitude (as long as there is no linear trend in the tropopause altitude), but are not affected by the anthropogenic HF increase. HF is believed to originate in the middle atmosphere solely from the photodissociation of man-made chlorofluorocarbons (CFCs) and hydrochlorofluorocarbons (HCFCs). The de-trending is performed in order to reduce the influence of the chemical variability of HF in the calculations. But it must be said that the whole HF chemical variability cannot be removed by de-trending. Finally, the variable fluorine partitioning between HF and COF_2 introduces additional uncertainty into the HF post-correction approach.

Table 2. Assumed random and systematic uncertainties. It is assumed that 80 % of the values listed in the table below correspond to random uncertainties and 20 % to systematic uncertainties (except for spectroscopy that is assumed to be 100 % systematic).

Source	Uncertainty
Baseline/continuum (offset and channelling)	0.1 %
Instrumental lines shape (modulation efficiency and phase error)	1 % and 0.01 rad
Line of sight	0.001 rad
Solar lines (intensity and spectral scale)	1 % and 1.0×10^{-6}
Temperature	1.0 K (trop)/2.0 K (strat)
Spectroscopy (intensity strength and pressure broadening – γ air)	2 % and 5 %

3.3.3 Directly retrieved tropospheric column-averaged CH_4 dry air mole fraction (troXCH$_{4_{retr}}$)

The retrieval code PROFFIT is able to perform profile inversion and we can directly retrieve tropospheric CH_4 concentration profiles from the measured spectra. We use the retrieved concentration profiles to obtain a tropospheric column-averaged CH_4 mole fraction directly from the measured spectra (troXCH$_{4_{retr}}$). Therefore, we average the retrieved CH_4 volume mixing ratios between Izaña ground level and an altitude of 6.5 km. The values retrieved at these altitudes are very sensitive to free tropospheric CH_4 and are not affected by stratospheric CH_4 (see also next Sect. 3.4.2).

3.4 Characteristics of the FTIR CH_4 data

3.4.1 Error estimation

The error calculations presented here apply the error estimation capability incorporated in the PROFFIT retrieval algorithm. This computationally efficient implementation allows performing a reasonably complete estimate of the total error budget for each individual measurement. It is based on the analytic error estimation approach of Rodgers (2000). We assume the uncertainty sources as listed in Table 2. To avoid a too optimistic systematic error budget, both a statistical as well as a systematical contribution are allowed for each error source. We assume that 80 % of the uncertainties are random and 20 % systematic, respectively. Exceptions are the spectroscopic line parameter uncertainty (line strength and pressure broadening), which is assumed to be purely systematic, and the error due to spectral measurement noise, which is assumed to be purely statistical.

The estimated random and systematic errors for the scaling retrieval are listed in Table 3. While the uncertainty in the spectroscopic parameter determines the systematic error, the baseline/continuum uncertainty is dominating the random error sources listed in Table 2.

Table 3. Errors for each parameter for the scaling retrieval for CH_4 total column.

	Statistic error (%)	Systematic error (%)
Baseline/continuum	0.23	6×10^{-3}
Instrumental lines shape	0.03	7×10^{-3}
Line of sight	0.06	7×10^{-3}
Solar lines	0.02	4×10^{-3}
Temperature	0.11	0.03
Measurement noise	0.08	
Smoothing error	0.43	
Spectroscopy		3.59
Total error	0.51	3.59

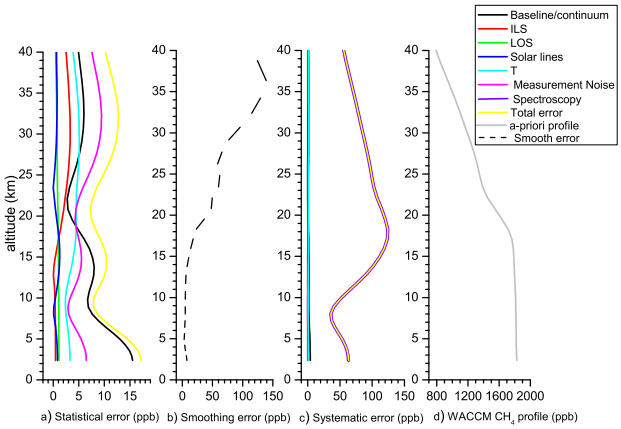

Fig. 3. Estimated errors for the profiling retrieval (PR): **(a)** statistical (random) errors of parameters listed in Table 2, **(b)** smoothing error, **(c)** systematic errors, and **(d)** climatologic CH_4 profile simulated by the WACCM model that is used as the a-priori profile. The different colours are for the different uncertainty sources as explained in the legend. The yellow line represents the total errors, and the grey line is the WACCM profile.

In addition to these parameter errors, we have to consider errors caused by the variability in the CH_4 profile shape. Generally, the shape of the actual atmospheric CH_4 will differ from the shape of the scaled WACCM CH_4 profile. This gives rise to so-called smoothing error, which can be calculated as $(\mathbf{I}-\mathbf{A})\,\mathbf{S}_a(\mathbf{I}-\mathbf{A})^T$. Here, $\mathbf{I}$ is a unity matrix, $\mathbf{A}$ is the averaging kernel, and $\mathbf{S}_a$ the assumed a priori covariance of atmospheric CH_4. Here, we use a $\mathbf{S}_a$ matrix that is obtained from the WACCM simulations. We find that the smoothing error is by far the leading random error and thus determines the precision of $totXCH_4$ produced by the scaling retrieval. When considering the smoothing error, we estimate an overall precision of about 0.51 %.

The estimated random and systematic errors for the profile retrieval are shown in Fig. 3a–c respectively. Figure 3d shows the WACCM a priori CH_4 profile in order to have a reference. We observe that in the troposphere the random errors are dominated by instrumental specific uncertainty sources: the baseline offset uncertainty and the measurement noise. The total estimated random error due to parameter uncertainties is depicted as yellow line in Fig. 3a. It is about 17 ppb (0.9 % with respect to the WACCM profile) in the lower troposphere and about 10 ppb (0.7 %) in the UT/LS region. In the stratosphere the smoothing error becomes the leading random error component.

Concerning systematic errors, spectroscopic parameters are the dominating uncertainty sources. The estimated total systematic error is depicted as yellow line in Fig. 3c. It is about 65 ppb (3.6 %) and 100 ppb (7.1 %) for the lower troposphere and the UT/LS region, respectively.

Table 4 collects the total systematic and random errors for our total XCH_4 product ($totXCH_4$) and the a posteriori-calculated tropospheric XCH_4 ($troXCH_{4_{post}}$) as obtained from the scaling retrieval (SR). Furthermore, it shows the errors for the directly retrieved tropospheric XCH_4 ($troXCH_{4_{retr}}$) and $totXCH_4$ obtained from the profile retrieval (PR). For these calculations, we assume the following uncertainties: 0.3 hPa for the surface pressure, 2.7 % for the HF column (Schneider et al., 2005), 1 % for the H_2O column (Schneider et al., 2010a), and 10 % for the b-value.

Theoretically, the scaling retrieval produces total column-averaged CH_4 ($totXCH_4$) and a posteriori-corrected tropospheric column-averaged CH_4 ($troXCH_{4_{post}}$) with a precision of 0.51 % and 0.61 %, respectively (square root of the square sum of the smoothing error, measurement noise and the statistical error). By applying a profiling retrieval, we can significantly reduce the smoothing error, which theoretically improves the precision of $totXCH_4$ to 0.41 %. The directly retrieved tropospheric column-averaged CH_4 ($troXCH_{4_{retr}}$) has an estimated precision of 0.91 %. Please note that the precision estimate for the a posteriori- calculated tropospheric XCH_4 ($troXCH_{4_{post}}$) is very likely too optimistic since we assume an uncertainty of the b-value applied in Eq. (3) of only 10 %, whereas the model-deduced HF-CH_4 correlation might be afflicted with a larger uncertainty.

3.4.2 Characteristics of the retrieved CH_4 profiles

When retrieving vertical profiles, it is important to document the vertical resolution that can be achieved with the remote sensing system. The vertical information contained in the FTIR profile is characterized by the averaging kernel matrix ($\mathbf{A}$). This matrix depends on the retrieved parameters, the quality of the measurement (the signal to noise ratio), the spectral resolution, the solar zenith angle, etc. The averaging kernel matrix describes the smoothing of the real vertical distribution of the absorber by the FTIR measurements process. Figure 4 shows the rows of a typical averaging kernel matrix of our CH_4 retrieval. The row kernels indicate the altitude regions that mainly contribute to the retrieved state. The first atmospheric levels (from Izaña ground level up to 6.5 km) are highlighted by red colour showing that, for the

Table 4. Total errors estimated for typical measurement conditions (16 June 2010).

		Typical value	Smoothing error		Statistic error		Systematic error	
		ppb	%	ppb	%	ppb	%	ppb
SR	$totXCH_4$	1743	0.43	7.50	0.27	4.71	3.50	61.01
SR*	$troXCH_{4_{post}}$	1810	0.43	7.78	0.43	7.87	3.38	61.26
PR	$totXCH_4$	1743	0.06	1.05	0.41	7.15	2.23	38.87
PR	$troXCH_{4_{retr}}$	1812	0.20	3.62	0.89	15.95	3.26	59.07

SR: scale retrieval; PR: profile retrieval; SR*: applying HF correction using the CH_4 total column from SR.

Table 5. Statistics of the daily mean comparisons between the side-by-side measuring instruments 120M and 125HR.

		N	*R*	MRD (%)	STD (%)	SF ± SEM
SR	$totXCH_4$	17	0.91	−0.17	0.28	0.9983 ± 0.0014
SR*	$troXCH_{4_{post}}$	17	0.73	−0.14	0.27	0.9986 ± 0.0014
PR	$totXCH_4$	17	0.73	−0.10	0.30	0.9990 ± 0.0015
PR	$troXCH_{4_{retr}}$	17	0.83	0.06	0.51	1.0006 ± 0.0025

N: number of data points; *R*: correlation coefficient; MRD: mean relative difference (120M – 125HR)/125HR; STD: standard deviation; SF: scaling factor (120M/125HR); SEM: standard error of the mean of the scaling factor = 2 × STD/sqrt(*N*); SR: scale retrieval; PR: profile retrieval; SR*: applying HF correction using the CH_4 total column from SR.

CH_4 mole fractions retrieved at these altitudes, there is no significant contribution from the stratosphere. The respective mixing ratios are very representative of the free troposphere, and we calculate our $troXCH_{4_{retr}}$ as the average of the mole fractions at these altitudes. With the green colour, we highlight the row kernel for an altitude of 21 km. We observe that the mole fractions values retrieved at 21 km well reflect the upper troposphere/lower stratosphere (UT/LS) region.

The trace of the averaging kernel matrix can be interpreted as the degree of freedom (DOF) of the measurement. The higher the value, the more information is obtained from the measurement. A typical DOF value obtained for our CH_4 retrieval is 2.5.

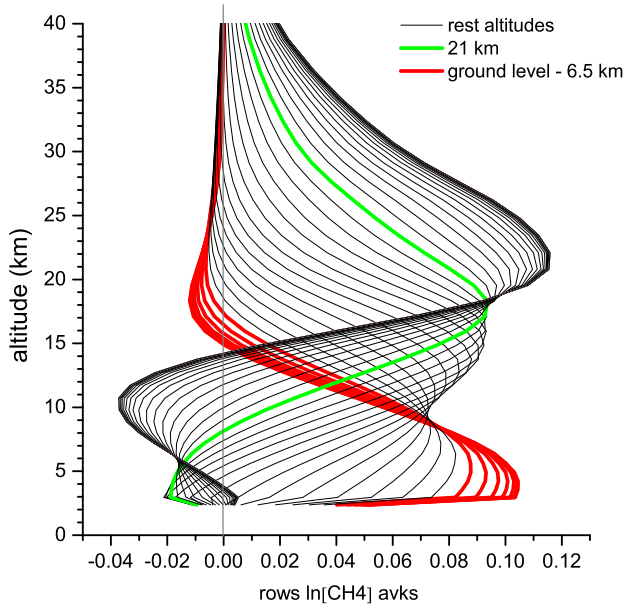

Fig. 4. Typical row averaging kernels for profiling retrieval (PR): red lines show the kernels between Izaña ground level and 6.5 km, while the green line shows the kernel corresponding to an altitude of 21 km.

4 Empirical validation

4.1 Intercomparison between the Bruker spectrometers IFS 120M and IFS 125HR

The Bruker spectrometers IFS 120M and IFS 125HR were operated side-by-side during March–April of 2005. On 17 days both instruments measured in coincidence and we can use these periods for empirically documenting the errors caused by instrument specific random uncertainties. In case of the profile retrieval, such instrument-specific random uncertainties (baseline offset and measurement noise) dominate the total random error and we can use the side-by-side instrument intercomparison as an empirical validation of the overall precision. Table 5 shows statistics of the intercomparison of the different CH_4 products obtained from the scaling and the profile retrieval. Concerning the profile retrieval (marked as PR), we find scatter values of 0.3 % for $totXCH_4$ and 0.5 % for $troXCH_{4_{retr}}$, thereby empirically documenting the good precision of these data. Concerning the scaling retrieval (marked as SR), the scatter values are even smaller; however, it is important to note that in this case the smoothing error cancels out, since it is very similar for both instruments.

4.2 FTIR versus surface in-situ GAW data

As already mentioned in Sect. 2.1, the in-situ nighttime data are very representative of free troposphere background conditions. Therefore, we compare the average of two consecutive in-situ nighttime means with the mean of the FTIR data obtained during the enclosed day. We limit this study to the 2001–2010 period, since in 1999–2000 we find an inconsistency in the surface pressure data. Due to this inconsistency,

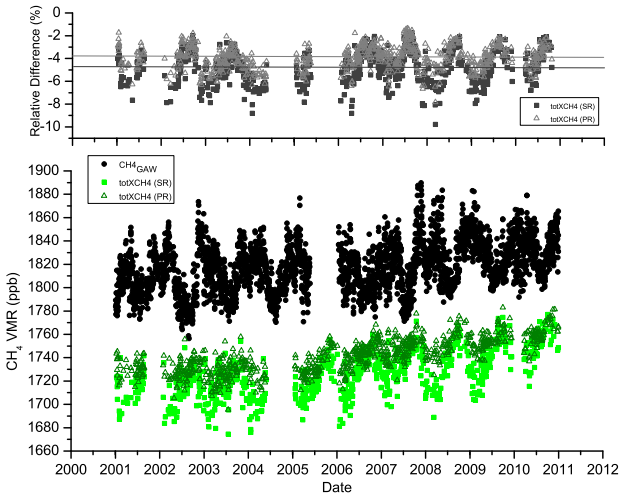

Fig. 5. $CH_{4_{GAW}}$ in-situ (black circles) and $totXCH_4$ FTIR data obtained from scaling (squares) and profiling (triangles) retrieval, respectively. Bottom panel: 2001–2010 time series for all available data; top panel: time series of the difference expressed as (FTIR − GAW)/GAW for the scaling (squares) and profiling (triangles) retrieval, respectively. The solid lines represent the mean relative difference for the scaling and profiling retrieval, respectively.

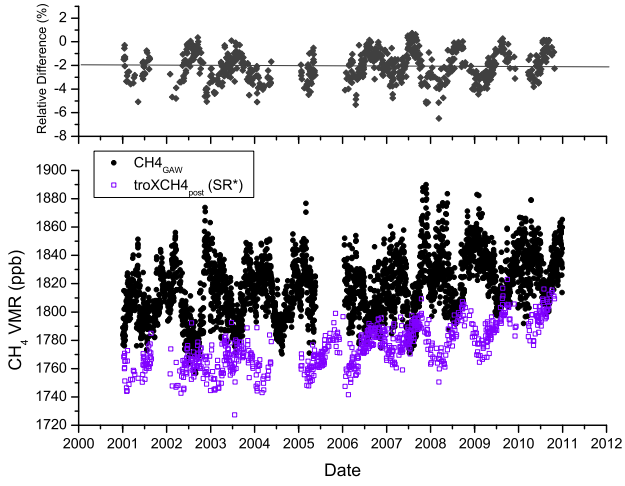

Fig. 6. Same as Fig. 5, but for the a posteriori-corrected tropospheric XCH_4 calculated from the total CH_4 column obtained from the scaling retrieval and applying the HF correction ($troXCH_{4_{post}}$, violet empty squares).

we are not able to calculate consistent DPC values for the 1999–2000 period (for more details see Appendix B).

The lower panel of Fig. 5 shows the daily means for $totXCH_4$ (dark green open triangles for the profiling retrieval, PR, and green solid squares for the scaling retrieval, SR) and GAW CH_4 in-situ values (black points). The upper panel depicts the relative difference between FTIR and GAW data ((FTIR − GAW)/GAW, grey open triangles for PR and dark grey solid squares for SR). For the scaling retrieval, we find a mean and standard deviation of the difference of $-4.69\,\% \pm 1.42\,\%$. The FTIR/GAW scaling factor is 0.9531. We find no significant correlation between the FTIR and GAW data (Correlation coefficient $R = 0.09$). In order to reduce the scatter caused by comparing different air masses (we compare nighttime with daytime data), we perform an additional comparison of monthly mean data (graphic not shown). There, the difference between the FTIR and GAW data is $-5.05\,\% \pm 1.28\,\%$, and the scaling factor 0.9495. Using monthly averages instead of daily mean data does not significantly reduce scatter and the bias between the two data sets. For the profiling retrieval, we find a better agreement: mean and scatter of $-3.90\,\% \pm 1.06\,\%$ and $-4.17\,\% \pm 0.92\,\%$ for daily and monthly mean differences, respectively. The FTIR/GAW scaling factor is 0.9610 (daily mean). The results of this daily and monthly mean intercomparison between the GAW data and the FTIR products are collected in Tables 6 and 7.

The lower panel of Fig. 6 shows daily means GAW data (black circles) and the $troXCH_{4_{post}}$ data (violet open squares) obtained by applying the b-value determined from the HF and CH_4 climatology of ACE-FTS ($b = -743$; see Appendix A). In the upper panel, the relative FTIR-GAW difference is shown. We obtain a mean difference and scatter of $-2.01\,\% \pm 1.24\,\%$ (FTIR/GAW scaling factor of 0.9799). The correlation plot provides a rather low correlation coefficient of 0.22 (see Table 6). For the monthly mean comparison, there is no significant change: correlation coefficient (0.15) and the relative FTIR-GAW scatter decrease to 1.19 % (see Table 7). In addition, we calculate the $troXCH_{4_{post}}$ data by applying a set of different b-values obtained by different approaches. We find that the different $troXCH_{4_{post}}$ calculations do not significantly affect the level of agreement with the GAW data (for a detailed discussion please refer to Appendix A).

Table 6. Statistics of the daily mean comparisons between the FTIR products ($totXCH_4$, $troXCH_{4_{post}}$, and $troXCH_{4_{retr}}$) and the GAW data for the period 2001–2010.

	FTIR product	N	R	MRD (%)	STD (%)	SF ± SEM
SR	$totXCH_4$	709	0.09	−4.69	1.42	0.9531 ± 0.0011
SR*	$troXCH_{4_{post}}$	709	0.22	−2.01	1.24	0.9799 ± 0.0009
PR	$totXCH_4$	709	0.39	−3.90	1.06	0.9610 ± 0.0008
PR	$troXCH_{4_{retr}}$	709	0.60	−0.13	0.97	0.9987 ± 0.0007

N: number of data points; R: correlation coefficient; MRD: mean relative difference (FTIR − GAW)/GAW; STD: standard deviation; SF: scaling factor (FTIR/GAW); SEM: standard error of the mean of the scaling factor = 2 × STD/sqrt(N); SR: scale retrieval; PR: profile retrieval; SR*: applying HF correction using the CH_4 total column from SR.

The NDACC mid-infrared spectra contain sufficient information to retrieve a CH_4 concentration profile with the characteristics that are described by the averaging kernels of Fig. 4. Theoretically, we should be able to distinguish tropospheric from stratospheric CH_4. Figure 7 shows a time series of the CH_4 profiles retrieved from the FTIR measurements

Table 7. Same as Table 6 but for monthly means.

	FTIR product	N	R	MRD (%)	STD (%)	SF ± SEM
SR	$totXCH_4$	98	0.09	−5.05	1.28	0.9495 ± 0.0026
SR*	$troXCH_{4_{post}}$	98	0.15	−2.22	1.19	0.9778 ± 0.0024
PR	$totXCH_4$	98	0.40	−4.17	0.92	0.9583 ± 0.0019
PR	$troXCH_{4_{retr}}$	98	0.69	−0.32	0.69	0.9968 ± 0.0014

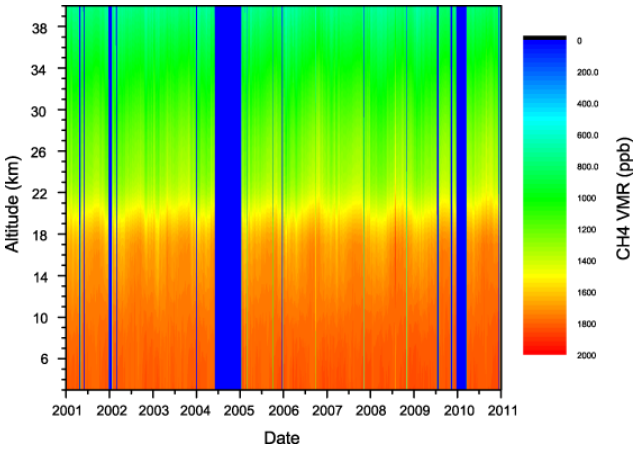

Fig. 7. Retrieved CH_4 profile time series for the period 2001–2010.

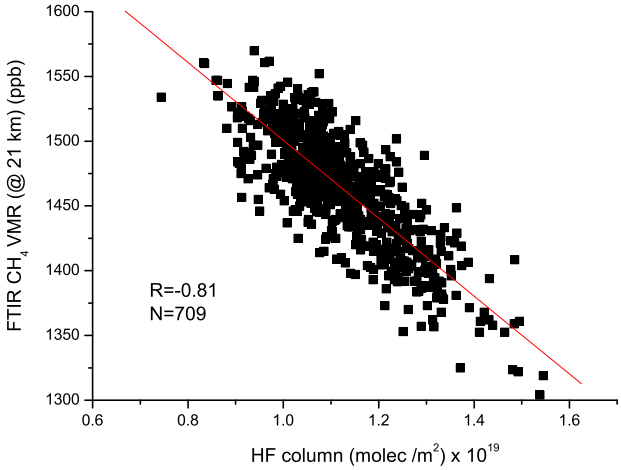

Fig. 8. Correlation plot of the retrieved total HF column versus CH_4 VMR in the UT/LS region (at 21 km). The red line shows the linear regression line.

between 2001 and 2010. CH_4 concentrations are high in the troposphere and significantly decrease in the stratosphere where CH_4 is effectively destroyed by reaction with OH, Cl, and O(^{1}D). In the CH_4 profile time series, we can clearly observe the upward shift of the UT/LS region during the summer months: in winter above 18 km, the CH_4 concentrations are typically smaller than 1600 ppb, whereas in summer 1600 ppb are still achieved at an altitude of 20 km. Vice versa to CH_4, the HF concentrations are very small in the troposphere and start to increase significantly as function of altitude in the stratosphere (HF is produced in the stratosphere by photolysis of CFCs). Similar to CH_4 in the UT/LS region, the total column of HF is a good indicator for the stratospheric contribution. Indeed, we observe a strong anti-correlation between the HF amounts and the CH_4 mixing ratio at 21 km (altitude that is very representative for the UT/LS region; see Sect. 3.4.2). This strong anti-correlation ($R = -0.81$, see Fig. 8) confirms the good quality of the CH_4 concentration retrieved for the UT/LS region.

The lower panel of Fig. 9 depicts the $troXCH_{4_{retr}}$ time series (red stars) and in black circles the daily means GAW data. The upper panel depicts the respective relative FTIR-GAW difference. We get a mean and scatter of $-0.13\,\% \pm 0.97\,\%$ and a correlation coefficient of 0.60. For the monthly mean comparison, the correlation further improves (coefficient of 0.69) and the relative FTIR-GAW scatter decreases to 0.69 % (see Tables 6 and 7). The good correlation between the GAW data and the tropospheric FTIR CH_4 concentrations, on the one hand, and the strong anti-correlation between the HF columns and the UT/LS FTIR CH_4 concentrations document the good quality of the retrieved CH_4 profiles. The NDACC FTIR systems allow measuring tropospheric CH_4 independently from stratospheric CH_4. Furthermore, the FTIR/GAW scaling factor for $troXCH_{4_{retr}}$ is very close to unity (it is 0.9987, see Table 6) indicating that the applied CH_4 HITRAN 2008 line strength parameters are in good absolute agreement to the GAW CH_4 measurements. The $troXCH_{4_{retr}}$ and the GAW datasets are consistent and could be used in a synergetic manner in flux inversion models.

Figure 10 shows the $troXCH_{4_{retr}}/<SF>$ versus $CH_{4_{GAW}}$ (being <SF> the mean scaling factor between $troXCH_{4_{retr}}$ and $CH_{4_{GAW}}$). We observe that the slope of the linear regression line is smaller than unity: the fitted linear function goes from 20 ppb above the diagonal to 20 ppb below the diagonal. This is in agreement with the column sensitivity of the FTIR retrieval being smaller than 1.0 in the lower part of the troposphere (∼0.8; graphic not shown), i.e. the FTIR system does not capture the whole CH_4 variation. However, Fig. 10 might also suggest that the $troXCH_{4_{retr}}$ and the GAW datasets are not fully equivalent, because the former applies for the tropospheric column, whereas the latter applies only for the lower part of the free troposphere. The CH_4 variability might be larger in the lower part of the free troposphere than in the upper part of the free troposphere.

4.3 Interannual trend

We analyzed the CH_4 interannual trend for the FTIR and surface in-situ values. For estimating the interannual trend, we calculate yearly mean data. However, since sampling is not uniform and there might be years with more measurements than usual during a certain season, we have to subtract the

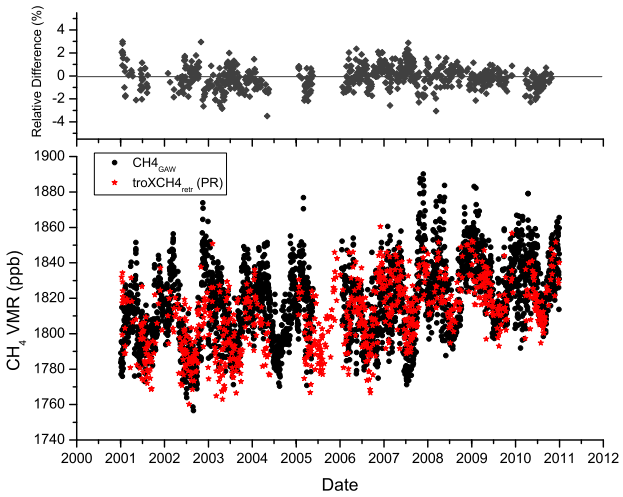

Fig. 9. Same as Fig. 5, but for the directly retrieved tropospheric XCH_4 ($troXCH_{4_{retr}}$, red stars) from the profile retrieval.

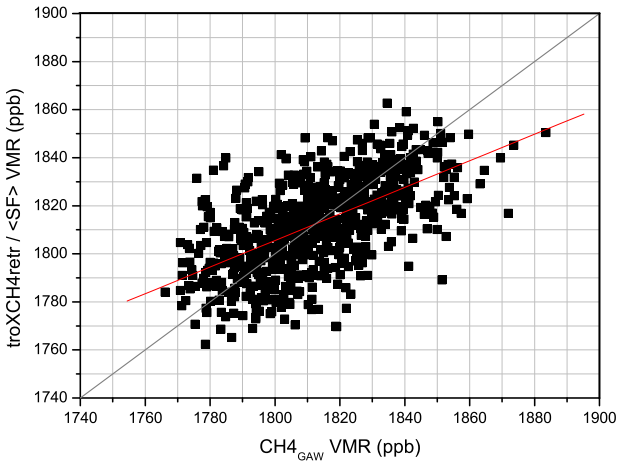

Fig. 10. $CH_{4_{GAW}}$ in-situ versus $troXCH_{4_{retr}}$/<SF> correlation plot. <SF> is the mean scaling factor between both quantities. The red line shows the linear regression line, while the grey one shows the diagonal as a reference.

annual cycle (de-seasonalise the time series). We estimate the annual cycle by fitting the following function to the time series:

$$f(t) = a_1 + a_2 t + \sum_{i=1}^{4} [b_i \cos(w_i t) + c_i \sin(w_i t)] + \sum_{j=1}^{2} [d_j \cos(k_j t) + e_j \sin(k_j t)] \quad (5)$$

where t is the time in days; a_1, a_2, b_i and c_i are the parameters of the interannual trend and d_j and e_j are the parameters of the annual cycle, all of them to be determined; $w_i = 2\pi i/N$ with N equal to the number of days in the considered period and $k_j = 2\pi j/T$ with $T = 365.25$ days. The de-seasonalised time series can then be used to calculate the yearly mean time series. The yearly mean time series of $CH_{4_{GAW}}$ and of the different FTIR products are shown in Fig. 11: in Fig. 11a for $totXCH_4$ from the scaling retrieval (SR) and the profiling retrieval (PR) and in Fig. 11b for the $troXCH_4$ products. Beside $troXCH_{4_{post}}$ and $troXCH_{4_{retr}}$, we show here $troXCH_{4_{retr\_gbm}}$, which is the same as $troXCH_{4_{retr}}$ but applying the spectral microwindows, retrieval settings and line lists recommended by Sussmann et al. (2011). For all datasets we observe that before 2005 the CH_4 concentrations remained stable and after 2005 there has been a continuous CH_4 increase. Although a detailed discussion of this trend is beyond the scope of this paper, we would like to mention that our results are in excellent agreement with those of Dlugokencky et al. (2009) and Rigby et al. (2008).

In order to assess how the yearly mean time series of the different FTIR products agree with the corresponding GAW time series, we calculate the random mean square between the yearly mean GAW data and the yearly mean FTIR data. The results are collected in Table 8. The different FTIR products agree similarly well with the GAW data.

In Table 9 we collect the change in mean CH_4 VMR between the 2001–2003 and the 2008–2010 period. The GAW concentrations ($CH_{4_{GAW}}$) changed by about 20 ppb. This change is slightly overestimated by all the FTIR data products. However, this overestimation is not significant. It is within the 1σ uncertainty range. We find that the directly retrieved tropospheric column-averaged CH_4 shows the best agreement with the GAW dataset.

4.4 De-trended CH_4 annual cycle

We compare the annual CH_4 cycles of the GAW data and of the different FTIR CH_4 products. Therefore, we de-trend the CH_4 time series. This de-trending is performed by removing the interannual trends as depicted in Fig. 11. Figure 12 shows the de-trended monthly means calculated for the 2001–2010 period: black circles for the GAW data, green solid squares and dark green open triangles for $totXCH_4$ obtained from the scaling and profiling retrieval, respectively (see Fig. 12a), violet open squares for $troXCH_{4_{post}}$, red stars for $troXCH_{4_{retr}}$, and dark yellow open stars for $troXCH_{4_{retr\_gbm}}$. All the annual cycles have been centered to zero.

We observe that $totXCH_4$ does not reproduce the tropospheric surface in-situ CH_4 variability. It is obvious that $totXCH_4$ is not a good proxy for the tropospheric seasonal CH_4 variability. Instead, the $totXCH_4$ annual variability is dominated by the annual variability of the tropopause height, which is lowest by the end of winter and continuously increases during summer. The $totXCH_4$ cycle obtained from the scaling retrieval differs significantly from the $totXCH_4$ cycle obtained from the profile retrieval. This implies that the smoothing error – which is very important for a scaling

Table 8. Root mean square (RMS) between the annual means (2001–2010 period) of GAW and the FTIR data (see Fig. 10).

	$CH_{4_{GAW}}$-*a*				
a	$totXCH_4$ (SR)	$totXCH_4$ (PR)	$troXCH_{4_{post}}$ (SR*)	$troXCH_{4_{retr}}$ (PR)	$troXCH_{4_{retr\_gbm}}$ (PR)
RMS [ppb]	5.15	4.52	4.54	4.81	7.51

SR: scale retrieval; PR: profile retrieval; SR*: applying HF correction using the CH_4 total column from SR.

Table 9. Difference between the mean CH_4 VMR in 2001–2003 and in 2008–2010 with its associated $1\,\sigma$ uncertainty.

Dataset	$CH_{4_{GAW}}$	$totXCH_4$ (SR)	$totXCH_4$ (PR)	$troXCH_{4_{post}}$ (SR*)	$troXCH_{4_{retr}}$ (PR)	$troXCH_{4_{retr\_gbm}}$ (PR)
Difference [ppb]	19.65 $\pm$5.00	26.46 $\pm$9.19	25.61 $\pm$4.74	26.97 $\pm$7.71	22.79 $\pm$5.12	26.79 $\pm$4.91

SR: scale retrieval; PR: profile retrieval; SR*: applying HF correction using the CH_4 total column from SR.

retrieval with fixed first guess profile shape – depends on the season.

As with the $totXCH_4$ cycle, the $troXCH_{4_{post}}$ cycle does not capture the minimum during summer and the maximum in the early winter. Instead, it follows more or less the annual cycle of the tropopause altitude. We observe that the a posteriori correction method as applied here does not adequately account for the stratospheric contribution.

By comparison, the $troXCH_{4_{retr}}$ cycle is more consistent with the GAW in-situ cycle. The amplitudes and phases of both cycles are very similar, thereby confirming that the directly retrieved tropospheric column-averaged XCH_4 values are a very good proxy for the free tropospheric CH_4 concentrations.

We find that the $troXCH_{4_{retr\_gbm}}$ cycle does not reconstruct the GAW in-situ cycle as well as does $troXCH_{4_{retr}}$. The $troXCH_{4_{retr\_gbm}}$ retrieval was optimised for retrievals of total column-averaged XCH_4 from a range of sites and water vapour amounts, not tropospheric column-averaged XCH_4. The difference is presumed to be due to different treatment of water vapour and the use of different line lists for CH_4.

5 Remark on non-transferability to the near-infrared spectra

In our work we investigate CH_4 retrievals by applying the NDACC high- resolution mid-infrared solar absorption spectra (typical spectral resolution is $0.005\,cm^{-1}$). We find that the HF correction method based on a simple scaling retrieval of a climatologic CH_4 profile does not work sufficiently well when applying the high-resolution mid-infrared NDACC spectra. In Appendix A we document that the problem is not the b-value but the limited precision of the CH_4 total column amount that is achieved by a simple scaling retrieval. In addition to NDACC, the ground-based FTIR network TCCON has been established during the last few years. Within TCCON, spectra are measured in the near-infrared spectral region at a spectral resolution of $0.02\,cm^{-1}$. It is important to remark that our results about the HF correction method found for the mid-infrared spectra cannot be transferred in a straightforward manner to the near-infrared TCCON retrievals. There are some important differences:

1. In the high-resolution mid-infrared NDACC spectra, we can well observe the pressure broadening effect, i.e. these spectra contain a lot of information about the vertical distribution of the CH_4 molecules. As a consequence for NDACC, a CH_4 profile retrieval is more feasible. A simple scaling retrieval will produce less precise CH_4 total column amounts. The situation is different for the near-infrared TCCON spectra. There, the CH_4 signatures are less sensitive to the vertical distribution of CH_4. First, in the near-infrared spectra, the Doppler core is more important than in the mid-infrared spectra (pressure broadening is more difficult to observe), and second, the spectral resolution of TCCON spectra is significantly lower than the one of the NDACC spectra. Consequently, in the near-infrared TCCON, a profile retrieval may have only small or negligible benefit and a scaling retrieval may produce equally precise and accurate column amounts.

2. The TCCON near-infrared observations have the great advantage that the observed air mass can be monitored by analyzing O_2 absorption signatures. Since atmospheric O_2 amounts are very stable, one can use the CH_4/O_2 ratio as a measure of the column-averaged CH_4 amount. Thereby, the measurement is a relative measurement and TCCON CH_4 columns are theoretically very precise.

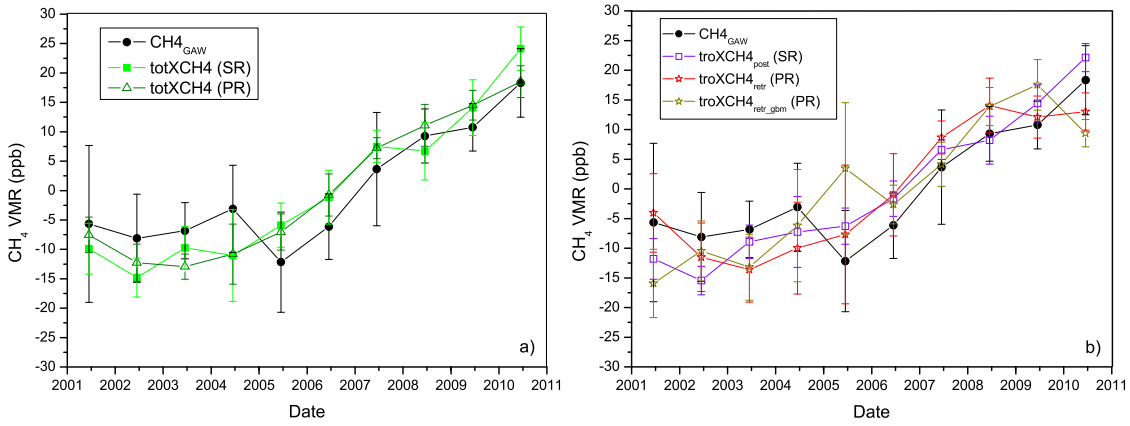

Fig. 11. Annual mean for the $CH_{4_{GAW}}$ in-situ (black dots) and the different FTIR products considering coincident data and centered at zero. **(a)** total XCH_4 products: green squares for $totXCH_4$ from SR, and green dark open triangles for $totXCH_4$ from PR; **(b)** tropospheric XCH_4 products: violet open squares for $troXCH_{4_{post}}$, red stars for $troXCH_{4_{retr}}$, and open dark yellow stars for $troXCH_{4_{retr\_gbm}}$. The error bars correspond to the standard error of the mean [2 × STD/sqrt(N)].

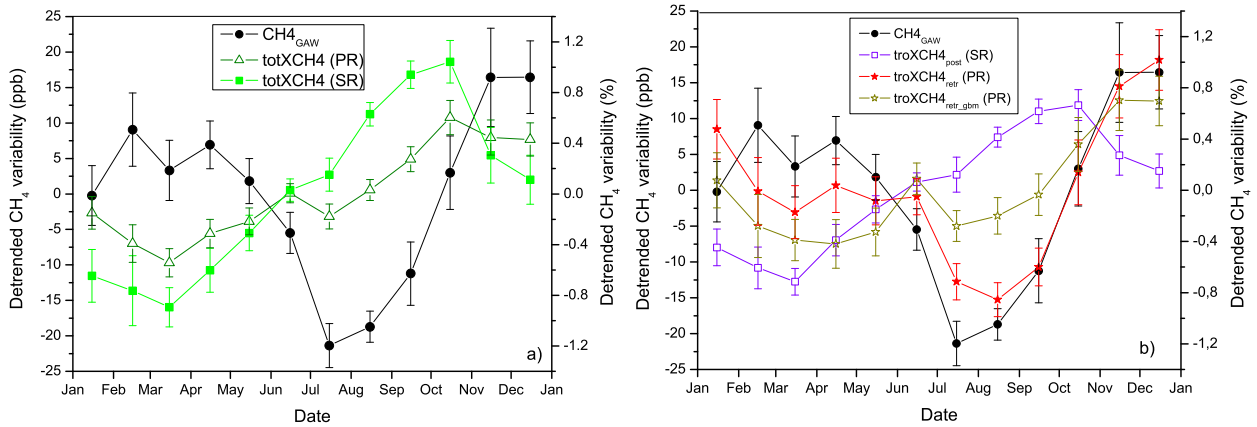

Fig. 12. The multi-annual mean annual cycles derived for data of the 2001–2010 period for the different $CH_{4_{GAW}}$ (black dots) and the different FTIR products: **(a)** total XCH_4 products; green squares for SR and green dark open triangles for PR; **(b)** tropospheric XCH_4 products: violet open squares for $troXCH_{4_{post}}$, red stars for $troXCH_{4_{retr}}$ and open dark yellow stars for $troXCH_{4_{retr\_gbm}}$. The error bars correspond to the standard error of the mean [2 x STD/sqrt(N)].

6 Outlook and conclusions

In the framework of the NDACC, ground-based FTIR experiments have recorded high-resolution mid-infrared solar absorption spectra for more than a decade at about 15 globally distributed sites. We examine two different CH_4 retrieval principles: first, a simple scaling of a fixed climatologic profile and, second, a CH_4 profile retrieval.

A scaling retrieval is indicated if there is no significant variation in the profile shape or if the variations in the profile shape are not reflected in the measured solar absorption spectra (e.g. due to limited spectral resolution or measurement noise). However, our study shows that the high quality NDACC spectra contain significant information about the typical vertical variability of CH_4 converting the smoothing error in the leads error component of the scaling retrieval. We estimate a theoretical precision of the total XCH_4 of 0.51 %. The smoothing error of total XCH_4 can be significantly reduced if performing a profile retrieval leading to an improved precision of 0.41 %. This good precision is empirically confirmed by a side-by-side intercomparison study applying two FTIR instruments in 2005. We document that only the profile retrieval produces total XCH_4 with high precision and should be used for producing data for scientific applications. We find, for instance, the annual XCH_4 cycle obtained by the scaling retrieval significantly differs from the cycle obtained by the profile retrieval.

While precise total XCH_4 FTIR data are an important reference for the validation of space-base XCH_4 experiments (e.g. SCIAMACHY, GOSAT, OCO-2), the total XCH_4

amounts are significantly affected by the variability of the stratospheric CH_4 contribution. We document that the annual cycle of total XCH_4 rather follows the annual cycle of the tropopause altitude and not the annual cycle of tropospheric CH_4 mole fraction. Our study shows that total XCH_4 is no valid proxy for tropospheric CH_4.

We investigate two methods for obtaining a tropospheric CH_4 proxy from the FTIR measurements. First, the often applied a posteriori correction method, which applies a CH_4 scaling retrieval and a posteriori corrects the stratospheric CH_4 contribution using HF total column amounts as stratospheric CH_4 proxy. This data set is called $troXCH4_{post}$ throughout the paper. Second, we directly retrieve tropospheric column-averaged XCH_4 amounts from the spectra applying the profile retrieval. This data set is called $troXCH4_{retr}$ throughout the paper.

Concerning $troXCH4_{post}$ we estimate a precision of 0.61 %. However, this estimation cannot be empirically confirmed by our comparison to the GAW CH_4 in-situ data (the scatter between $CH4_{GAW}$ and $troXCH4_{post}$ is as large as 1.24 %). The reason might be an underestimation of the smoothing error, a too optimistic assumption of the uncertainty of the b-value, or a seasonal variability of the fluorine partitioning. The scientific usefulness of $troXCH4_{post}$ data is rather doubtful. For instance, the data do not capture the full amplitude of the tropospheric CH_4 annual cycle.

For $troXCH4_{retr}$ we estimate a theoretical precision of 0.91 %. This value is consistent with the results of the side-by-side FTIR intercomparison study of 2005, and it is well confirmed by the comparison to the GAW CH_4 in-situ data (we obtain a scatter between $CH4_{GAW}$ and $troXCH4_{retr}$ of 0.97 %). Furthermore, we found that the FTIR/GAW scaling factor is very close to unity, suggesting that the NDACC FTIR network can provide tropospheric column-averaged CH_4 that is very consistent to the CH_4 data of the GAW in-situ network. The annual cycles of $troXCH4_{retr}$ and $CH4_{GAW}$ are very similar (phase and amplitude). For investigating the CH_4 interchange between atmosphere, biosphere, and ocean, we strongly recommend using the directly retrieved tropospheric XCH_4 instead of the tropospheric XCH_4 produced by the a posteriori correction method.

Although we do not perform a direct empirical validation of the total column-averaged XCH_4 obtained by the profile retrieval, it is important to recall that we observe, first, a good correlation of the retrieved tropospheric column-averaged XCH_4 amounts with the GAW data, and second, a good correlation of the retrieved lower stratospheric CH_4 concentrations with the HF data. These observations document the high quality of the retrieved CH_4 profile in the troposphere as well as in the stratosphere and thus strongly suggest a high quality for the total column-averaged XCH_4.

Due to its long-term characteristics, the NDACC tropospheric XCH_4 data set can make valuable contributions when investigating sources and sinks of CH_4. In our paper we exclusively investigate CH_4 retrievals applying mid-infrared NDACC spectra. In the future we plan a similar study for the near-infrared spectral region, which is recorded by the TCCON experiments. We plan to examine the practicability and benefits of a profile retrieval for obtaining highly precise total column-averaged XCH_4 amounts from TCCON spectra. Furthermore, we will use the Izaña GAW CH_4 in-situ data set for documenting the precision of possible TCCON tropospheric column-averaged CH_4 data and its level of consistency with the GAW CH_4 in-situ data.

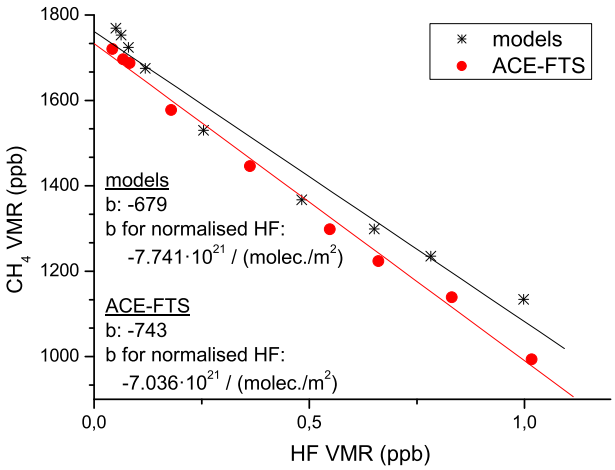

Fig. A1. HF volume mixing ratio versus CH_4 volume mixing ratio between the levels 10 and 100 hPa. The solid lines represent the regression line for models (black line) and ACE-FTS (red line). The b-values are also shown for the normalised HF profiles.

Appendix A

Using HF column amounts as proxy for the tropopause altitude

We calculate the CH_4-HF slope equilibrium (b-value) by applying three different approaches: (a) as Washenfelder et al. (2003) from the stratospheric CH_4 and HF VMR, (b) from the CH_4 and HF total columns and (c) fitting Eq. (3) (from the manuscript) but substituting the $troXCH4_{post}$ for $CH4_{GAW}$. For approaches (a) and (b) we determine the b-value by applying different datasets. We use model data (a CH_4 climatology for the 2004–2006 period from WACCM, and an HF climatology for the mid-2000s from KASIMA) as well as experimental data (a 2004–2008 climatology of CH_4 and HF profiles and for the latitude 25° N–35° N from the ACE-FTS satellite experiment; Jones et al., 2012). The three approaches give different b-values. The scatter between the different b-values can be used as the b-values uncertainty.

a. The b-value is determined by calculating the regression line between the stratospheric CH_4 and HF VMR profiles obtained from the ACE-FTS measurements

Table A1. $troCH_{4_{post}}$ calculated from $CH_{4_{col}}$ of the scaling retrieval.

Applied method to calculated the b-value	b-value	$troXCH_{4_{post}}$ vs. $CH_{4_{GAW}}$			
		R	MRD (%)	STD (%)	SF
Correlation of ACE VMRs (10 to 100 hPa)	−743	0.216	−2.01	1.24	0.9799
Correlation of ACE columns (shifts: −30 to +30 hPa)	−689	0.205	−2.21	1.25	0.9780
Correlation of modelled VMRs (10 to 100 hPa)	−679	0.203	−2.24	1.26	0.9776
Correlation of modelled columns (shifts: −30 to +30 hPa)	−901	0.247	−1.45	1.21	0.9855
fit: $CH_{4_{GAW}}$, $CH_{4_{FTIR}}$, HF_{FTIR}	−1368	0.344	0.21	1.12	1.0021

R: correlation coefficient; MRD: mean relative difference (FTIR-GAW)/GAW; STD: standard deviation; SF: scaling factor (FTIR/GAW).

Table A2. Same as Table A1 but for normalised HF time series.

Applied method to calculated the b-value	b-value $[(molec./m^2)^{-1}]$	$troXCH_{4_{post}}$ vs. $CH_{4_{GAW}}$			
		R	MRD (%)	STD (%)	SF
Correlation of ACE VMRs (10 to 100 hPa)	-7.036×10^{21}	0.193	−2.28	1.27	0.9772
Correlation of ACE columns (shifts: −30 to +30 hPa)	-6.529×10^{21}	0.185	−2.45	1.28	0.9755
Correlation of modelled VMRs (10 to 100 hPa)	-7.741×10^{21}	0.205	−2.04	1.25	0.9796
Correlation of modelled columns (shifts: −30 to +30 hPa)	-1.027×10^{22}	0.249	−1.19	1.21	0.9881
fit: $CH_{4_{GAW}}$, $CH_{4_{FTIR}}$, $HF_{FTIRnorm}$	-1.522×10^{22}	0.341	0.48	1.13	1.0048

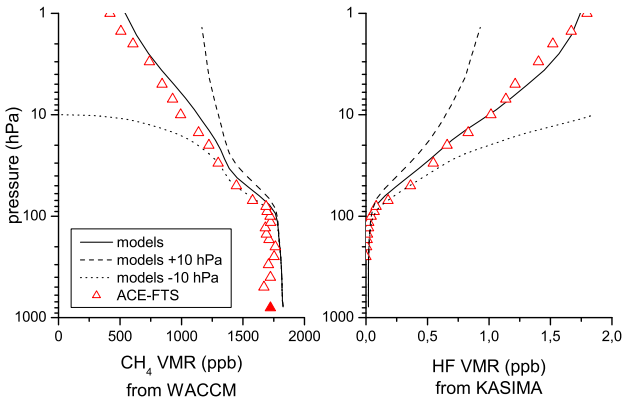

Fig. A2. Solid lines correspond to the modelled profiles for CH_4 (left panel) and HF (right panel). Dotted and dashed lines show the models mixing ratios for −10 hPa and +10 hPa vertical profile shifts, respectively. Red open triangles show the ACE-FTS mixing ratios (the red filled triangle is the CH_4 concentration that we use for the lower troposphere, where ACE-FTS is not sensitive anymore).

between the 10 and 100 hPa. We also determine a b-value from the modelled VMR profiles. The CH_4-HF correlation plots are depicted in Fig. A1. We calculate the correlations for the 10 to 100 hPa levels in agreement with Washenfelder et al. (2003), but in comparison to Washenfelder et al. (2003) we only determine one single b-value. Actually, the b-value changes with the increase of HF amounts by about 1 % per year. Consequently, using a single b-value representative for the 2004–2006/2008 time period for the whole time series (2001–2010) means an uncertainty of the b-value of up to 5 %. We obtain values of −743 and −679 for ACE-FTS profiles and models, respectively. For comparison Washenfelder et al. (2003) estimated a b-value for 1992 of about −950, which is in reasonable agreement with our b-values obtained for the mid-2000s.

In addition, we calculate a b-value from a normalised HF-profile. The normalisation means that the VMR values have been divided by the HF total column amounts. This b-value can then be applied in Eq. (3) together with a normalised HF time series. The normalisation allows using a b-value that is constant over time. We get values of $-7.036 \times 10^{21}\,(molec/m^2)^{-1}$ and $-7.741 \times 10^{21}\,(molec/m^2)^{-1}$ for ACE-FTS and models, respectively.

b. As can be seen in Fig. A1 between 10 and 100 hPa, the correlation is not perfectly linear. In particular for the model profiles assuming a linear correlation might cause an erroneous b-value. Therefore, we test an additional approach that determines the b-value from correlating CH_4 and HF total column amounts. The column amounts are calculated from profiles that are shifted vertically (between −30 hPa and +30 hPa; see Fig. A2). Figures A3 and A4 plot the correlations using ACE-FTS profiles and models

Table A3. Same as Table A1 but for $CH_{4_{col}}$ from profiling retrieval.

Applied method to calculated the b-value	b-value	troXCH$_{4_{post}}$ vs. CH$_{4_{GAW}}$			
		R	MRD (%)	STD (%)	SF
Correlation of ACE VMRs (10 to 100 hPa)	−743	0.519	−1.23	0.97	0.9877
Correlation of ACE columns (shifts: −30 to +30 hPa)	−689	0.510	−1.42	0.98	0.9858
Correlation of modelled VMRs (10 to 100 hPa)	−679	0.509	−1.45	0.98	0.9855
Correlation of modelled columns (shifts: −30 to +30 hPa)	−901	0.541	−0.67	0.96	0.9933
fit: $CH_{4_{GAW}}$, $CH_{4_{FTIR}}$, HF_{FTIR}	−1368	0.582	0.99	0.94	1.0099

Table A4. Same as Table A3 but for normalised HF time series.

Applied method to calculated the b-value	b-value [(molec./m^2)$^{-1}$]	troXCH$_{4_{post}}$ vs. CH$_{4_{GAW}}$			
		R	MRD (%)	STD (%)	SF
Correlation of ACE VMRs (10 to 100 hPa)	-7.036×10^{21}	0.499	−1.50	0.99	0.9851
Correlation of ACE columns (shifts: −30 to +30 hPa)	-6.529×10^{21}	0.492	−1.67	0.99	0.9833
Correlation of modelled VMRs (10 to 100 hPa)	-7.741×10^{21}	0.510	−1.26	0.98	0.9874
Correlation of modelled columns (shifts: −30 to +30 hPa)	-1.027×10^{22}	0.542	−0.41	0.96	0.9960
fit: $CH_{4_{GAW}}$, $CH_{4_{FTIR}}$, $HF_{FTIRnorm}$	-1.522×10^{22}	0.580	1.27	0.94	1.0130

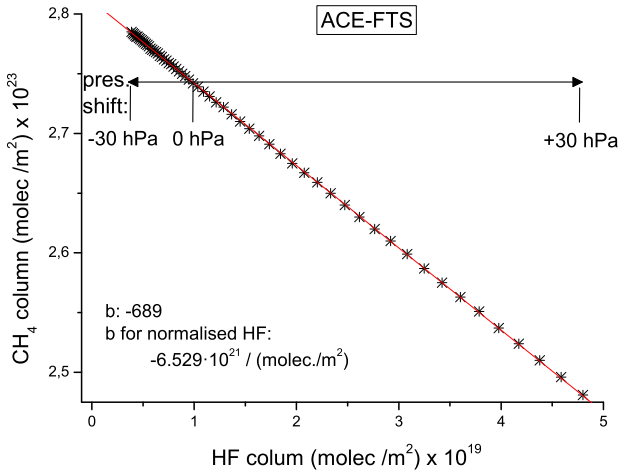

Fig. A3. Correlation plot between the CH_4 and HF total column amounts obtained for different vertical shifts of the CH_4 and HF ACE-FTS profiles.

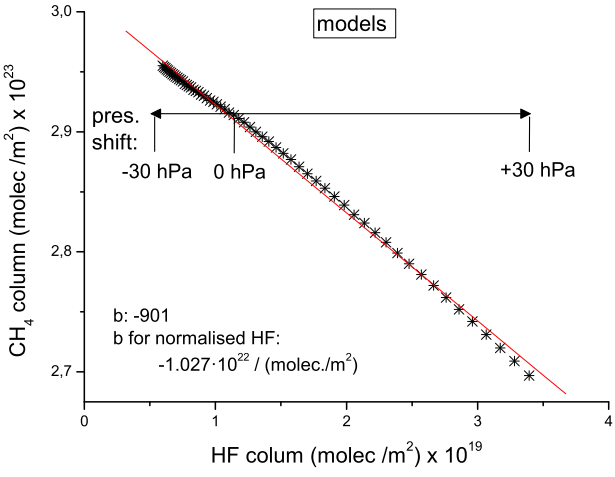

Fig. A4. Same as Fig. A3 but for model profiles.

profiles, respectively. We get b-values of −689 and −901 for ACE-FTS and models, respectively. For normalised profiles we get -6.529×10^{21} (molec/m^2)$^{-1}$ and -1.027×10^{22} (molec/m^2)$^{-1}$ for ACE-FTS and models, respectively.

c. Finally, we calculate an empirical b-value determined by fitting all the high quality data that are available at the Izaña Observatory: the FTIR CH_4 total column amounts determined from the profiling retrieval, the FTIR HF total column amounts, and the $CH_{4_{GAW}}$ data.

$$CH_{4_{col}}(t) = k \cdot \left(DPC(t) \cdot CH_{4_{GAW}}(t)\right) + b \cdot HF_{col}(t) \quad \text{(A1)}$$

The parameters b and k are obtained by least squares fit. The so-obtained b-value is the "best possible b-value". Applying this b-value in Eq. (3) produces a troXCH$_{4_{post}}$ with the best possible correlation to $CH_{4_{GAW}}$. This empirical value represents the best correction that is possible with the "HF-procedure". We get a b-value of −1368, and -1.522×10^{22} (molec/m^2)$^{-1}$ when it is applied for the normalised HF.

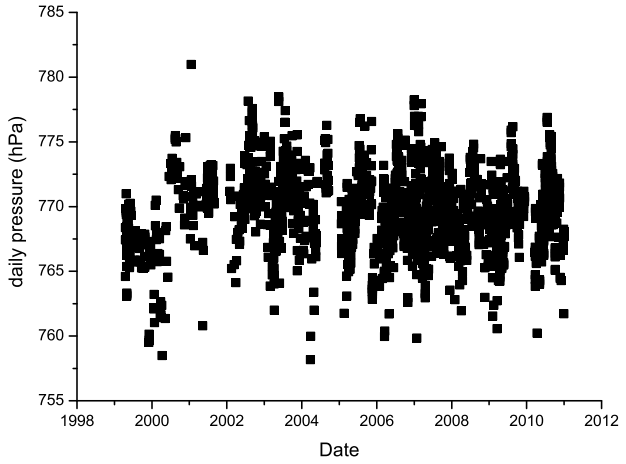

Fig. B1. Time series of the daily mean pressure at Izaña ground level.

According to Eq. (3) we calculate $troXCH4_{post}$ for the different b-values, considering the de-trended and normalised HF time series, and for CH_4 total columns obtained from the scaling retrieval. Tables A1 and A2 document the agreement between $troXCH4_{post}$ and $CH4_{GAW}$. We want to remark that the agreement between the $troXCH4_{post}$ and $CH4_{GAW}$ only slightly depends on the applied b-value. The correlation factor (R) and the standard deviation (STD) are roughly the same for the different b-values. Even for our empirical "best possible b-value", we get an agreement that is significantly poorer that the agreement between the directly retrieved tropospheric column-averaged CH_4 and $CH4_{GAW}$.

On the other hand, the agreement strongly depends on the quality of the applied CH_4 total column data. This is documented by Tables A3 and A4, which show the same as Tables A1 and A2 but using the CH_4 total column amounts obtained from the profile retrieval. These total column amounts are of higher quality than the CH_4 total column amounts obtained from the scaling retrieval (see error estimation section of the manuscript). We conclude that in the mid-infrared spectra, the leading error source of the "HF-procedure" is the uncertainty of the applied $CH4_{col}$ and not the uncertainty of the b-value.

Appendix B

Surface pressure measurements at Izaña Observatory

The 1999–2010 surface pressure measurement time series presents a jump at the beginning of 2001. The reason is that before and after 2001 two different types of pressure sensors have been applied: until 2001 a Thyas sensor ($\sim \pm 1$ hPa) and since 2001 a Setra sensor (± 0.3 hPa). Furthermore, the sensors were located at different positions and altitudes.

Figure B1 shows the time series of the daily mean pressure values acquired from both sensors at Izaña station. This jump will propagate into the $totXCH_4$ and $troXCH4_{post}$ with about 7 ppb and 8 ppb, respectively. Therefore, we decided to present CH_4 time series only from 2001 onward.

Acknowledgements. E. Sepúlveda enjoys a pre-doctoral fellowship from the Spanish Ministry of Education. M. Schneider is supported by the European Research Council under the European Community's Seventh Framework Programme (FP7/2007-2013)/ERC Grant agreement number 256961. The research leading to these results has received funding from the European Community's Seventh Framework Programme (FP7/2007-2013) within the NORS project (grant agreement no. 284421). We are grateful to the Goddard Space Flight Center for providing the temperature and pressure profiles of the National Centers for Environmental Prediction via the automailer system.

Edited by: D. Griffith

References

Bousquet, P., Ringeval, B., Pison, I., Dlugokencky, E. J., Brunke, E.-G., Carouge, C., Chevallier, F., Fortems-Cheiney, A., Frankenberg, C., Hauglustaine, D. A., Krummel, P. B., Langenfelds, R. L., Ramonet, M., Schmidt, M., Steele, L. P., Szopa, S., Yver, C., Viovy, N., and Ciais, P.: Source attribution of the changes in atmospheric methane for 2006–2008, Atmos. Chem. Phys., 11, 3689–3700, doi:10.5194/acp-11-3689-2011, 2011.

Dlugokencky, E. J., Bruhwiler, L., White, J. W. C., Emmons, L. K., Novelli, P. C., Montzka, S. A., Masarie, K. A., Lang, P. M., Crotwell, A. M., Miller, J. B., and Gatti, L. V.: Observational constraints on recent increases in the atmospheric CH_4 burden, Geophys. Res. Lett., 36, L18803, doi:10.1029/2009GL039780, 2009.

Frankenberg, C., Meirink, J. F., van Weele, M., Platt, U., and Wagner, T.: Assessing methane emissions from global spaceborne observations, Science, 308, 1010–8438, 2005.

Frankenberg, C., Aben, I., Bergamaschi, P., Dlugokencky, E. J., van Hees, R., Houweling, S., van der Meer, P., Snel, R., and Tol, P.: Global column-averaged methane mixing ratios from 2003 to 2009 as derived from SCIAMACHY: Trends and variability, J. Geophys. Res., 116, D04302, doi:10.1029/2010JD014849, 2011.

Gomez-Pelaez, A. J. and Ramos, R.: Improvements in the Carbon Dioxide and Methane Continuous Measurement Programs at Izaña Global GAW Station (Spain) during 2007–2009, Report of the 15th WMO/IAEA Meeting of Experts on Carbon Dioxide, Other Greenhouse Gases, and Related Tracer Measurement Techniques, 7–10 September 2009, GAW Report number 194, WMO TD 1553, available at: http://www.wmo.int/pages/prog/arep/gaw/gaw-reports.html (last access: 2 February 2012), Jena, Germany, 330 pp., 2011.

Gomez-Pelaez, A.J., Ramos, R., Cuevas, E., and Gomez-Trueba, V.: 25 years of continuous CO_2 and CH_4 measurements at Izaña Global GAW mountain station: annual cycles and interannual trends; Proceedings of the Symposium on Atmospheric Chemistry and Physics at Mountain Sites, ACP Symposium 2010, 8–10 June 2010, available at: http://www.izana.org/publications/

Abstract_25-year_CO2_and_CH4_Izana.pdf (last access: 2 February 2012), Interlaken, Switzerland, 157–159, 2010.

Gomez-Pelaez, A. J., Ramos, R., Gomez-Trueba, V., Campo-Hernandez, R., Dlugokencky, E., and Conway, T.: New improvements in the Izaña (Tenerife, Spain) global GAW station in-situ greenhouse gases measurement program; to be published in the proceedings of the 16th WMO/IAEA Meeting on Carbon Dioxide, Other Greenhouse Gases, and Related Measurement Techniques, 25–28 October 2011, GAW Report to be publish, Wellington, New Zealand, 2012.

Hase, F.: Inversion von Spurengas-profilen aus hochaufgelösten bodengebundenen FTIR-Messungen in Absorption, Forschungszentrum Kalrsruhe, FZKA 6512, 2000.

Hase, F.: Interactive comment on "Strategy for high-accuracy-and-precision retrieval of atmospheric methane from the mid-infrared FTIR network" by R. Sussmann et al., Atmos. Meas. Tech. Discuss., 4, C1048–C1048, 2011.

Hase, F., Blumenstock, T., and Paton-Walsh, C.: Analysis of the instrumental line shape of high-resolution Fourier transform IR spectrometers with gas cell measurements and new retrieval software, Appl. Optics, 38, 3417–3422, 1999.

Hase, F., Hannigan, J. W., Coffey, M. T., Goldman, A., Höpfner, M., Jones, N. B., Rinsland, C. P., and Wood, S. W.: Intercomparison of retrieval codes used for the analysis of high-resolution, ground-based FTIR measurements, J. Quant. Spectrosc. Ra., 87, 25–52, 2004.

IPCC: Climate Change 2007 – The Physical Science Basis: Contribution of Working Group I to the Fourth Assessment Report of the Intergovernmental Panel on Climate, Cambridge University Press, Cambridge, United Kingdom and New York, NY, USA, 2007.

Jones, A., Walker, K. A., Jin, J. J., Taylor, J. R., Boone, C. D., Bernath, P. F., Brohede, S., Manney, G. L., McLeod, S., Hughes, R., and Daffer, W. H.: Technical Note: A trace gas climatology derived from the Atmospheric Chemistry Experiment Fourier Transform Spectrometer (ACE-FTS) data set, Atmos. Chem. Phys., 12, 5207–5220, doi:10.5194/acp-12-5207-2012, 2012.

Keppler, F., Hamilton, T. G., Braß, M., and Rockmann, T.: Methane emissions from terrestrial plants under aerobic conditions, Nature, 439, 187–191, doi:10.1038/nature04420, 2006.

Olsen, S. C. and Randerson, J. T.: Differences between surface and column atmospheric CO_2 and implications for carbon cycle research, J. Geophys. Res., 109, D02301, doi:10.1029/2003JD003968, 2004.

Rigby, M., Prinn, R. G., Fraser, P. J., Simmonds, P. G., Langenfelds, R. L., Huang, J., Cunnold, D. M., Steele, L. P., Krummel, P. B., Weiss, R. F., O'Doherty, S., Salameh, P. K., Wang, H. J., Harth, C. M., M¨uhle, J., and Porter, L. W.: Renewed growth of atmospheric methane, Geophys. Res. Lett., 35, L22805, doi:10.1029/2008GL036037, 2008.

Rodgers, C. D.: Inverse Methods for Atmospheric Sounding: Theory and Praxis, World Scientific Publishing Co., Singapore, ISBN 981-02-2740-X, 2000.

Rothman, L. S., Gordon, I. E., Barbe, A., Chris Benner, D., Bernath, P. F., Birk, M., Boudon, V., Brown, L. R., Campargue, A., Champion, J.-P., Chance, K., Coudert, L. H., Dana, V., Devi, V. M., Fally, S., Flaud, J.-M., Gamache, R. R., Goldman, A., Jacquemart, D., Kleiner, I., Lacome, N., Lafferty, W. J., Mandin, J.-Y., Massie, S. T., Mikhailenko, S. N., Miller, C. E., Moazzen-Ahmadi, N., Naumenko, O. V., Nikitin, A. V., Orphal, J., Perevalov, V. I., Perrin, A., Predoi-Cross, A., Rinsland, C. P., Rotger, M., Simeckova, M., Smith, M. A. H., Sung, K., Tashkun, S. A., Tennyson, J., Toth, R. A., Vandaele, A. C., and Vander-Auwera, J.: The HITRAN 2008 molecular spectroscopic database, J. Quant. Spectrosc. Ra., 110, 533–572, doi:10.1016/j.jqsrt.2009.02.013, 2009.

Schneider, M., Blumenstock, T., Chipperfield, M. P., Hase, F., Kouker, W., Reddmann, T., Ruhnke, R., Cuevas, E., and Fischer, H.: Subtropical trace gas profiles determined by ground-based FTIR spectroscopy at Izaña (28° N, 16° W): Five-year record, error analysis, and comparison with 3-D CTMs, Atmos. Chem. Phys., 5, 153–167, doi:10.5194/acp-5-153-2005, 2005.

Schneider, M., Hase, F., and Blumenstock, T.: Water vapour profiles by ground-based FTIR spectroscopy: study for an optimised retrieval and its validation, Atmos. Chem. Phys., 6, 811–830, doi:10.5194/acp-6-811-2006, 2006.

Schneider, M., Toon, G. C., Blavier, J.-F., Hase, F., and Leblanc, T.: H_2O and δD profiles remotely-sensed from ground in different spectral infrared regions, Atmos. Meas. Tech., 3, 1599–1613, doi:10.5194/amt-3-1599-2010, 2010a.

Schneider, M., Romero, P. M., Hase, F., Blumenstock, T., Cuevas, E., and Ramos, R.: Continuous quality assessment of atmospheric water vapour measurement techniques: FTIR, Cimel, MFRSR, GPS, and Vaisala RS92, Atmos. Meas. Tech., 3, 323–338, doi:10.5194/amt-3-323-2010, 2010b.

Sussmann, R., Forster, F., Rettinger, M., and Jones, N.: Strategy for high-accuracy-and-precision retrieval of atmospheric methane from the mid-infrared FTIR network, Atmos. Meas. Tech., 4, 1943–1964, doi:10.5194/amt-4-1943-2011, 2011.

Washenfelder, R. A., Wennberg, P. O., and Toon, G. C.: Tropospheric methane retrieved from ground-based near-IR solar absorption spectra, Geophys. Res. Lett., 30, L017969, doi:10.1029/2003GL017969, 2003.

Zellweger, C., Klausen, J., and Buchmann, B.: System and performance audit for surface ozone, carbon monoxide, methane and nitrous oxide at the global GAW station Izana, Spain, March 2009, available at: http://gaw.empa.ch/audits/IZO_2009.pdf (last access: 2 February 2012), WCC-Empa Report 09/1, 2009.

7

TROPOSPHERIC CH_4 SIGNALS AS OBSERVED BY NDACC FTIR AT GLOBALLY DISTRIBUTED SITES AND COMPARISON TO GAW SURFACE IN-SITU MEASUREMENTS

Atmos. Meas. Tech. Discuss., 7, 633–701, 2014
www.atmos-meas-tech-discuss.net/7/633/2014/
doi:10.5194/amtd-7-633-2014

Atmospheric Measurement Techniques Discussions

Tropospheric CH_4 signals as observed by NDACC FTIR at globally distributed sites and comparison to GAW surface in-situ measurements

E. Sepúlveda[1,2], M. Schneider[3], F. Hase[3], S. Barthlott[3], D. Dubravica[3], O. E. García[1], A. Gomez-Pelaez[1], Y. González[1], J. C. Guerra[2], M. Gisi[3,*], R. Kohlhepp[3,], S. Dohe[3], T. Blumenstock[3], K. Strong[4], D. Weaver[4], M. Palm[5], A. Sadeghi[5], N. M. Deutscher[5,6], T. Warneke[5], J. Notholt[5], N. Jones[6], D. W. T. Griffith[6], D. Smale[7], G. W. Brailsford[7], J. Robinson[7], F. Meinhardt[8], M. Steinbacher[9], T. Aalto[10], and D. Worthy[11]**

[1]Izaña Atmospheric Research Center, Agencia Estatal de Meteorología (AEMET), Tenerife, Spain
[2]Department of Physics, University of La Laguna (ULL), Tenerife, Spain
[3]Institute for Meteorology and Climate Research, Karlsruhe Institute of Technology (KIT), Karlsruhe, Germany
[4]Department of Physics, University of Toronto (UofT), Toronto, Canada
[5]Institute of Environmental Physics, University of Bremen (UB), Bremen, Germany

[6]Centre for Atmospheric Chemistry, University of Wollongong (UOW), Wollongong, Australia
[7]National Institute of Water and Atmospheric Research (NIWA), Lauder, New Zealand
[8]Federal Environmental Agency Germany (UBA), Dessau-Roßlau, Germany
[9]Swiss Federal Laboratories for Materials Science and Technology (EMPA), Dübendorf, Switzerland
[10]Climate Change Research, Finnish Meteorological Institute (FMI), Helsinki, Finland
[11]Climate Research Division, Environment Canada (EC), Wellington, Canada
[*]now at: Bruker Optics GmbH, Ettlingen, Germany
[**]now at: Deutscher Wetterdienst, Offenbach, Germany

Received: 24 December 2013 – Accepted: 12 January 2014 – Published: 27 January 2014

Correspondence to: E. Sepúlveda (elisepul@ull.es)

Published by Copernicus Publications on behalf of the European Geosciences Union.

Abstract

We present lower/middle tropospheric column-averaged CH_4 mole fraction time series measured by nine globally distributed ground-based FTIR (Fourier Transform InfraRed) remote sensing experiments of the Network for the Detection of Atmospheric Composition Change (NDACC). We show that these data are well representative of the tropospheric regional-scale CH_4 signal, largely independent of the local small-scale signals of the boundary layer, and only weakly dependent on upper tropospheric/lower stratospheric (UTLS) CH_4 variations. In order to achieve the weak dependency on the UTLS, we use an a posteriori correction method. We estimate a typical precision for daily mean values of about 0.5 % and a systematic error of about 2.5 %. The theoretical assessments are complemented by an extensive empirical study. For this purpose, we use surface in-situ CH_4 measurements made within the Global Atmosphere Watch (GAW) network and compare them to the remote sensing data. We briefly discuss different filter methods for removing the local small-scale signals from the surface in-situ datasets in order to obtain the in-situ regional-scale signals. We find good agreement between the filtered in-situ and the remote sensing data. The agreement is consistent for a variety of time scales that are interesting for CH_4 source/sink research: day-to-day, monthly, and inter-annual. The comparison study confirms our theoretical estimations and proves that the NDACC FTIR measurements can provide valuable data for investigating the cycle of CH_4.

1 Introduction

Methane (CH_4) plays an important role in atmospheric chemistry, affecting the oxidizing capacity of the atmosphere, acting as a precursor of tropospheric ozone (O_3) and being the most important anthropogenic greenhouse gas after carbon dioxide (CO_2).

For many years, tropospheric greenhouse gases have been monitored at the Earth's surface by very precise in-situ techniques. However, surface measurements can be

strongly affected by local small-scale processes, and by this reason surface GAW stations have been located in very particular places where there is no influence of small-scale process at least part of the time in order to get regional representative measurements (especially for Global GAW stations).

Observations above the boundary layer are well representative of the lower tropospheric regional-scale evolution of CH_4 and thus they could well complement the surface in-situ datasets. For instance, Olsen and Randerson (2004) proposed using total column-averaged observations of CO_2 as valid input for inverse models. For CH_4, however, the strong vertical gradient in the stratosphere has a significant effect on the column averages. The CH_4 column average is therefore strongly dependent on the tropopause altitude, which means, for instance, that the seasonal cycle in column-averaged CH_4 can significantly differ from that in the free troposphere (e.g. Sepúlveda et al., 2012). The uncertainty in modeling the variations of the tropopause altitude and of stratospheric CH_4 significantly limits the usefulness of total column-averaged CH_4 observations for inverse modeling purposes.

Figure 1 gives an overview of the different atmospheric CH_4 signals. The grey bar indicates the very high and very local typical small-scale variability that might occur within the first few hundred meters above the surface. This signal is caused by local sources and sinks. In the upper troposphere/lower stratosphere (UTLS), the CH_4 mole fraction depend on the tropopause altitude. The blue area indicates the variability due to a ±100 hPa variability of the tropopause (e.g. Hoinka, 1998). This signal is mainly uniform over the whole UTLS, i.e. a tropopause shift causes strongly correlated variations from the tropopause up to the middle stratosphere.

The red area represents the typical variability in the free troposphere of about 2 %. Although the troposphere is typically well-mixed, the chemical activity of CH_4 (e.g. destruction by OH) can cause differences between lower/middle and upper tropospheric CH_4 mole fraction, and the vertical correlation of the tropospheric CH_4 variability is very likely limited to about 5–10 km. This tropospheric variability (or even better its lower tropospheric portion) would be a very suitable inverse model input. However, its

measurements by remote sensing techniques are difficult since this tropospheric signal is much smaller than the boundary layer or the UTLS signal.

Previous studies have shown tropospheric CH_4 mole fraction obtained by middle-infrared FTIR and in-situ techniques, e.g. Rinsland et al. (2005). Sepúlveda et al. (2012) documented theoretically and empirically that the ground-based FTIR experiments operated within the NDACC (Network for the Detection of Atmospheric Composition Change, http://www.acd.ucar.edu/irwg/, Kurylo and Zander, 2000) can provide some information on the vertical distribution of atmospheric CH_4. They empirically documented the quality of these profile data: first, for the lower tropospheric FTIR CH_4 data there is good agreement with coincident free tropospheric GAW in-situ observations and second, for the UTLS the FTIR measures CH_4 mole fraction that shows a strong anti-correlation with the stratospheric proxy HF. The profiling capability is not only important for CH_4 source/sink research applications, it is also an advantage when validating column-averaged CH_4 obtained from satellites, since it allows the vertical sensitivity of the satellite data to be accounted for. In this paper, we extend the Sepúlveda et al. (2012) study, which is limited to a subtropical site, to a set of nine globally-distributed NDACC FTIR stations covering polar, mid-latitudinal, and subtropical regions and we focus on the quality of the lower free tropospheric CH_4 FTIR data. We document that the data are largely independent of the local small-scale signals of the boundary layer, and only weakly dependent on upper tropospheric/lower stratospheric (UTLS) CH_4 variations. Furthermore, we find a reasonable consistency for the different NDACC FTIR sites.

This manuscript is organized as follows: Sect. 2 explains the ground-based NDACC FTIR technique, the CH_4 retrieval strategy, and an overview of the NDACC sites involved in this study. Section 3 discusses the different NDACC remote sensing and GAW in-situ datasets used in this work. Section 4 shows the comparison between the NDACC and GAW data and Sect. 5 provides a summary and conclusion.

2 Ground-based NDACC FTIR: experiment, tropospheric CH_4 retrieval setup, and error estimation

In this section we briefly describe the ground-based FTIR measurements performed within NDACC, the retrieval setup we have used for our study, the theoretical error analysis, and the locations of the participating stations.

2.1 NDACC FTIR experiments

NDACC is a global network community that monitors changes in atmospheric composition. It provides long-term observations of many trace gases and allows assessment of their impact on global climate. It is composed of more than 70 high-quality remote-sensing research stations operating several different measurement techniques. Currently, 22 NDACC sites operate with ground-based FTIR spectrometers. This study applies data obtained with the FTIR technique. The commercial Bruker IFS 125HR is one of the most modern FTIR instruments used in the network. Also the older version 120HR and the portable version 120M with slightly worse signal-to-noise ratio and less favourable instrumental line shape (ILS) characteristics and temporal stability are still in use.

The NDACC FTIR instrumentation consists of a high quality FTIR spectrometer and a high precision solar tracker controlled by a combination of astronomical calculations and a solar quadrant or more recently a digital camera (Gisi et al., 2011) for active tracker control. The experiments record direct solar spectra in the middle-infrared spectral region (740–4250 cm^{-1}, corresponding to 13.5–2.4 µm), with a resolution of 0.0035–0.005 cm^{-1} and work under clear sky conditions. This implies that the line of sight must be free of clouds and during night no measurements are possible. However, measurements with less sensitivity using the moon as the light source have been reported (Notholt et al., 1993; Notholt and Lehmann, 2003; Wood et al., 2004) but are not used in this study.

These high quality solar absorption spectra have been measured over many years and at many different sites (the first measurements started in the early nineties when the network was named the Network for the Detection of Stratospheric Change, NDSC). The measurements disclose significant information about the distribution of many different atmospheric trace gases. During recent years, the NDACC FTIR community has increased its efforts to monitor tropospheric mole fraction, including water vapour (Schneider et al., 2006a, b), and methane (e.g. Sussmann et al., 2012; Sepúlveda et al., 2012).

The ground-based NDACC FTIR stations involved in this study are nine globally distributed sites between the Arctic and the Antarctic. All of these stations contribute to the MUSICA project (MUlti-platform remote Sensing of Isotopologues for investigating the Cycle of Atmospheric water, Schneider et al., 2012). The stations are listed in Table 1 and site locations displayed in Fig. 2. The spectra for each station have been analysed in a uniform way, thereby ensuring good consistency of the ground-based CH_4 remote sensing data.

NDACC FTIR data are generally available on the NDACC database (http://www.ndsc.ncep.noaa.gov/data/). The CH_4 product presented here is not yet publicly available, however, we plan to make it available as part of the MUSICA project data that are currently published on the NDACC database in the project data section.

2.2 The tropospheric CH_4 profile retrieval setup

The measured spectra are analysed with the inversion code PROFFIT (PROFile FIT, Hase et al., 2004), which has been applied for many years by a part of the ground-based FTIR community for evaluating high resolution solar absorption spectra. The code simulates the spectra and the Jacobians by the line-by-line radiative transfer model PRFFWD (PRoFit ForWarD model, Hase et al., 2004; Schneider and Hase, 2009). It includes a ray tracing module (Hase and Höpfner, 1999) in order to precisely simulate how the radiation passes through the atmosphere.

The vertical structure of the atmosphere is discretised and the amount of the absorber x at altitude level z can be described in form of a vector $\boldsymbol{x}(z)$. Similarly the radiation spectrum is discretised and described by a vector $\boldsymbol{y}$ containing the radiances at the different spectral bins. PRFFWD accounts for the forward relation ($\mathbf{F}$), that connects the spectrum ($\boldsymbol{y}$) to the vertical distribution of the absorbers ($\boldsymbol{x}$) and to parameters ($\boldsymbol{p}$) describing the state of the atmosphere and instrumental characteristics:

$$\boldsymbol{y} = \mathbf{F}(\boldsymbol{x}, \boldsymbol{p}) \tag{1}$$

The retrieval adjusts the amount of the absorbers to obtain a best fit between the measured and simulated spectra. This is an under-determined problem, i.e. there are many different atmospheric states ($\boldsymbol{x}$) that produce almost identical spectra ($\boldsymbol{y}$). Consequently the problem requires some kind of constraint or regularisation. PROFFIT introduces the regularisation by means of a cost function:

$$[\boldsymbol{y} - \mathbf{F}(\boldsymbol{x}, \boldsymbol{p})]^{\mathrm{T}} \mathbf{S}_{\epsilon}^{-1} [\boldsymbol{y} - \mathbf{F}(\boldsymbol{x}, \boldsymbol{p})] + [\boldsymbol{x} - \boldsymbol{x}_{\mathrm{a}}]^{\mathrm{T}} \mathbf{S}_{\mathrm{a}}^{-1} [\boldsymbol{x} - \boldsymbol{x}_{\mathrm{a}}] \tag{2}$$

Here the first term is a measure for the difference between the measured spectrum ($\boldsymbol{y}$) and the spectrum simulated for a given atmospheric state ($\boldsymbol{x}$), whereby the actual measurement noise level is considered ($\mathbf{S}_{\epsilon}$ is the noise covariance). The second term is the regularisation term. It constrains the atmospheric solution state ($\boldsymbol{x}$) towards an apriori state ($\boldsymbol{x}_{\mathrm{a}}$), whereby the kind and the strength of the constraint are defined by the matrix ($\mathbf{S}_{\mathrm{a}}$). The constrained solution is reached at the minimum of the cost function Eq. (2).

Since the equations involved in atmospheric radiative transfer are non-linear, the cost function, Eq. (2), is minimised iteratively by a Gauss–Newton method. The solution for the $(i + 1)$th iteration is:

$$\boldsymbol{x}_{i+1} = \boldsymbol{x}_{\mathrm{a}} + \mathbf{S}_{\mathrm{a}} \mathbf{K}_i^{\mathrm{T}} (\mathbf{K}_i \mathbf{S}_{\mathrm{a}} \mathbf{K}_i^{\mathrm{T}} + \mathbf{S}_{\epsilon})^{-1} [\boldsymbol{y} - \mathbf{F}(\boldsymbol{x}_i) + \mathbf{K}_i (\boldsymbol{x}_i - \boldsymbol{x}_{\mathrm{a}})] \tag{3}$$

where $\mathbf{K}$ is the Jacobian matrix which samples the derivatives $\partial \hat{x} / \partial y$ (changes in the spectral fluxes y for changes in the vertical distribution of the absorber x). These

regularisation and iteration methods are standard in the field of remote sensing. An extensive treatment of this topic is given in the textbook of Rodgers (2000).

Our CH_4 retrieval strategy is essentially the one described in Sepúlveda et al. (2012), where we have presented CH_4 profile retrievals for the relatively dry high mountain site of Izaña. For this study we slightly change our microwindow selection in order to further reduce the impact of H_2O interferences, which might play a role for humid low-altitude sites. The chosen spectral microwindows are shown in Fig. 3. The new set of microwindows contains strong, not saturated, and well-isolated CH_4 absorption lines as well as H_2O and HDO lines, in order to better account for the H_2O and HDO interferences. Together with the spectral CH_4 signatures we consider H_2O, HDO, CO_2, O_3, N_2O, NO_2, HCl, and OCS signatures. We apply the HITRAN 2008 spectroscopy (with 2009 updates, Rothman et al., 2009), except for the target species CH_4, where we use line parameters obtained as a result of a current project of the Deutsche Forschungsgemeinschaft. IUP-Bremen, DLR-Oberpfaffenhofen, and KIT are involved in this activity. A preliminary linelist has been provided by D. Dubravica and F. Hase, KIT in December 2012 (see also, Dubravica et al., 2013) and it shows lower spectroscopic residuals than the HITRAN 2008 linelist.

The apriori knowledge for the interfering species are taken from the Whole Atmosphere Community Climate Model (WACCM version 5, provided by NCAR: National Centre for Atmospheric Research, J. Hannigan, personal communication, 2009). It is important to remark that we use station specific apriori data, but do not vary this apriori depending on season. This ensures that at an individual station all variability seen in our profiles comes exclusively from the measurement. We perform the inversion of the CH_4 profiles on a logarithmic scale (Hase et al., 2004; Schneider et al., 2006a) applying a Tikhonov–Phillips ad hoc constraint, that constrains the vertical slope of the profile (we do not apply diagonal constraints). The H_2O and HDO interferences are considered by including dedicated spectral H_2O and HDO windows and retrieving H_2O and HDO profiles, whereby we constrain the HDO/H_2O ratio (e.g. Schneider et al., 2006b). In order to account for the NO_2 signatures we scale the WACCM NO_2 profile.

For the rest of the minor interfering species, we simply simulate the spectral signatures according to the WACCM mole fraction. As in Sepúlveda et al. (2012), we calculate the tropospheric column-averaged CH_4 mole fraction directly from the measured spectra. Therefore, we average the retrieved CH_4 mole fraction for the first six atmospheric model levels above the station (i.e. we average the values within a lower tropospheric layer with a thickness of typically 2.5 km).

We use the NCEP analysis (National Centers for Environmental Prediction) at 12:00 UT as the temperature and pressure input profiles. In order to account for variations in the spectral baseline, we apply a second order fit for the continuum background.

We would like to remark that we apply exactly the same retrieval setup for all the FTIR stations.

2.3 Theoretical error estimation

In this section we present a theoretical quality assessment for the tropospheric CH_4 product. We do this in detail taking the Kiruna station as an example and in the form of an overview for the other stations. The error analysis is made according to the analytic method suggested by Rodgers (2000), where the difference between the retrieved and the real state, $(\hat{x} - x)$ the error, is linearised about a mean profile x_a (the applied apriori profile), the estimated model parameters $\hat{p}$, and the measurement noise ϵ:

$$(\hat{x} - x) = (\hat{\mathbf{A}} - \mathbb{I})(x - x_a) + \hat{\mathbf{G}}\hat{\mathbf{K}}_p(p - \hat{p}) + \hat{\mathbf{G}}\epsilon \quad (4)$$

Here $\mathbb{I}$ is the identity matrix, $\hat{\mathbf{A}}$ is the averaging kernel matrix, $\hat{\mathbf{G}}$ the gain matrix ($\mathbf{G} = (\mathbf{K}^T\mathbf{S}_\epsilon^{-1}\mathbf{K} + \mathbf{S}_a^{-1})^{-1}\mathbf{K}^T\mathbf{S}_\epsilon^{-1}$), and $\hat{\mathbf{K}}_p$ a sensitivity matrix to input parameters (instrumental line shape, spectroscopic parameters, etc). The gain matrix $\hat{\mathbf{G}}$ samples the derivatives $\partial\hat{x}/\partial y$ (changes in the retrieved CH_4-state $\hat{x}$ for changes at the spectral bin y).

Equation (4) identifies the three classes of errors. These are: (a) errors due to the inherent finite vertical resolution and the limited sensitivity of the observing system (smoothing error), (b) errors due to uncertainties in the input parameters applied in

the inversion procedure, and (c) errors due to measurement noise (with an assumed Gaussian noise with $\sigma = \epsilon$).

2.3.1 Vertical resolution and sensitivity (smoothing error)

When contemplating remotely-sensed vertical distribution profiles one must consider the inherent vertical resolution and the limited sensitivity of these data. The left panel of Fig. 4 shows typical averaging kernels (row kernels in the logarithmic scale) for the retrieved CH_4 profiles at Kiruna. The kernels correspond to a measurement made on 4 July 2012, with OPDmax (maximal optical path difference) of 180 cm, at a solar elevation angle of 42.8°, and with 8.1 mm of precipitable water vapour. We chose this observation since it is not exclusively representative for polar conditions (e.g. low solar elevation, low precipitable water vapour), instead it can also serve as an example for mid-latitudinal and/or subtropical observations. Lower/middle tropospheric kernels are depicted as red lines and kernels at and above the UTLS (> 11.5 km) are depicted as blue lines. We observe that the FTIR measurements contain information about the vertical distribution from the surface up to the middle stratosphere. The trace (sum of diagonal elements) of the averaging kernel matrix is a measure of the degrees of freedom for signal (DOFS) in the measurement. It indicates the number of independent layers present in the retrieved profile (for the example shown in the left panel of Fig. 4 we have a DOFS of 2.6).

We see that the vertical resolution is about 8 km (Full-Width-Half-Maximum, FWHM, of the individual kernels). The tropospheric kernels (red lines) peak mainly in the troposphere and the stratospheric kernels (blue lines) mainly in the stratosphere. However, the plot also indicates contributions of the UTLS to the retrieved tropospheric CH_4 (negative values between 12 and 25 km for the red tropospheric kernels). This means that the stratospheric CH_4 variations might significantly affect the retrieved tropospheric CH_4 signals, especially since in the UTLS the typical CH_4 variation (caused by tropopause altitude shifts) is larger than the small tropospheric CH_4 variation.

For calculating the smoothing error we separate the signals into the three rather independent atmospheric CH_4 signals as described in Fig. 1: the small-scale boundary layer signal, the regional-scale tropospheric signal, and the UTLS signal. We assume (a) that there are very local small-scale variations of 20 % in a 100 m thick boundary layer (described by the apriori covariance matrix $\mathbf{S}_{a,bl}$), (b) that free tropospheric CH_4 typically varies with 2 % with correlation length of 5 km (apriori covariance $\mathbf{S}_{a,tro}$), and (c) that the altitude variation of the tropopause is typically about 100 hPa corresponding to a UTLS CH_4 variation of about 10–20 % and we use a correlation length of 10 km (apriori covariance $\mathbf{S}_{a,utls}$). For defining the typical CH_4 tropopause, we use the WACCM simulations. We define the tropopause altitude as the lowermost altitude where the CH_4 mole fraction are less than 95 % of the lower/middle free tropospheric CH_4 mole fraction (at 3 km altitude). This is typically 11 km for the polar, 13.5 km for the mid-latitudinal, and 18 km for subtropical sites, respectively.

The corresponding CH_4 smoothing error covariance matrices can be calculated by:

$$\mathbf{S}_{sm,bl} = \mathbf{A}\mathbf{S}_{a,bl}\mathbf{A}^T \quad (5)$$

$$\mathbf{S}_{sm,tro} = (\mathbf{A} - \mathbb{I})\mathbf{S}_{a,tro}(\mathbf{A} - \mathbb{I})^T \quad (6)$$

$$\mathbf{S}_{sm,utls} = \mathbf{A}\mathbf{S}_{a,utls}\mathbf{A}^T \quad (7)$$

Here $\mathbf{A}$ and $\mathbb{I}$ are the averaging kernel and the identity matrix, respectively.

The square root values of the diagonal elements of $\mathbf{S}_{sm,bl}$, $\mathbf{S}_{sm,tro}$, and $\mathbf{S}_{sm,utls}$ are depicted in the left panel of Fig. 5 as black, red, and green lines, respectively. The red line documents that the FTIR can well resolve the tropospheric background CH_4 signals (2 % variability, 5 km correlation length) with a precision of 0.4–1.2 % between the surface and 6 km altitude (for a 3 km thick layer the precision is 0.8 %). However, we have to consider cross dependency on the small-scale boundary layer variability and on the UTLS variability caused by shifts in the tropopause altitude. While the former adds an uncertainty of less than 0.2 % (black line), the latter has a large influence on the retrieved tropospheric CH_4 amounts (green line). In fact, the contribution from the

stratospheric CH_4 signal is clearly the leading smoothing error and adds an uncertainty of up to 1.5 % to the lower tropospheric CH_4 product.

2.3.2 Propagation of uncertainties

The assumed uncertainty sources are listed in Table 2. These values are critical to the error estimation. They come from our experience (e.g. repeatability of ILS, instrumental line shape, measurements) or from references (e.g. the spectroscopic parameter uncertainties are from Rothman et al., 2005). To minimise errors due to uncertainties of the instrumental line shape we monitor and eventually correct line shape distortions regularly every two months. These measurements consist of independent detections of cell absorption signatures as described in Hase et al. (1999). Baseline offsets might be produced by detector non-linearities. Similarly to other studies (Schneider and Hase, 2008) we assume the following uncertainties for instrumental parameters: measurement noise of 4 ‰, ILS (instrumental line shape, modulation efficiency and phase error) of 0.01 at OPDmax/10 and 0.1 rad, baseline offset of 1 ‰, baseline amplitude of 1 ‰, line of sight (solar tracker misalignment) of 0.1°. For uncertainties of the intensity and spectral position of solar lines we assume 1 % and 1×10^{-6} cm^{-1}, respectively. We separate the uncertainties of the atmospheric temperature into three components: the lower troposphere (< 5 km) with an uncertainty of 2 K, the upper troposphere (> 5 km) with an uncertainty of 2 K, and the stratosphere (> 15 km) with an uncertainty of 5 K. For the atmospheric H_2O and HDO profiles, which are obtained from the MUSICA retrieval, we assume an uncertainty of 10 % and 2 km uncertainty correlation length. Finally for the spectroscopic HITRAN intensity and pressure broadening parameters we use uncertainties of 2 % for all absorbers.

The error propagation of the different uncertainty sources as listed in Table 2 can be described by the error covariance ($\mathbf{S}_e$):

$$\mathbf{S}_e = \mathbf{G}\mathbf{K}_p\mathbf{S}_p\mathbf{K}_p^T\mathbf{G}^T \quad (8)$$

where $\mathbf{G}$ is the gain matrix, $\mathbf{K}_p$ is the parameter Jacobian, which samples the derivatives $\partial y/\partial p$ (changes at the spectral bin y for changes in the parameter p), and $\mathbf{S}_p$ is the uncertainty covariance matrix for parameter p.

The left panel of Fig. 6 depicts the square root of the diagonal elements of ($\mathbf{S}_e$). For this calculation, the partitioning between statistical and systematic error (fourth column in Table 2) is not considered, i.e. for assessing the error impact effect on the statistical or systematic error budget one has to scale these values accordingly. All of the propagated measurement noise error (black line, noi) and much of the propagated baseline error (red line, bas) are statistical errors, i.e. they dominate the statistical error budget. The systematic errors are dominated by uncertainties in the spectroscopic line parameters (dark cyan line, spe).

2.3.3 A posteriori correction for optimal independence of retrieved tropospheric and stratospheric CH_4

The left panel of Fig. 5 reveals that the retrieved tropospheric CH_4 amounts are strongly affected by cross dependencies on the stratospheric CH_4 signals. These cross-dependencies can be the leading error source. In this subsection we show that the cross dependencies can be significantly reduced by an a posteriori correction method. The method consists of a simple matrix multiplication and can be easily applied to any CH_4 profile retrieval whenever the retrieved CH_4 state is provided together with the corresponding averaging kernel.

The correction matrix ($\mathbf{C}$) is constructed from entries of the averaging kernel matrix ($\mathbf{A}$), which can be written as:

$$\mathbf{A} = \begin{pmatrix} \mathbf{A}_{TT} & \mathbf{A}_{ST} \\ \mathbf{A}_{TS} & \mathbf{A}_{SS} \end{pmatrix} \quad (9)$$

where $\mathbf{A}_{TT}$ describes how the tropospheric CH_4 signal affects the retrieved tropospheric amounts and $\mathbf{A}_{SS}$ how the stratospheric CH_4 affects the retrieved stratospheric

amounts. The cross-entries $\mathbf{A}_{ST}$ and $\mathbf{A}_{TS}$ describe the cross dependencies of the retrieved tropospheric amounts on the stratospheric signal and of the retrieved stratospheric amounts on the tropospheric signal, respectively. The $\mathbf{A}_{ST}$ cross-entries are responsible for the large smoothing error in the retrieved tropospheric CH_4 (green line in left panel of Fig. 5).

These cross-entries can be used for $\mathbf{C}$ as follows:

$$\mathbf{C} = \begin{pmatrix} \mathbb{I} & -\mathbf{A}_{ST} \\ -\mathbf{A}_{TS} & \mathbb{I} \end{pmatrix} \tag{10}$$

If we now modify $\mathbf{A}$ by multiplication with $\mathbf{C}$, we get the a posteriori corrected averaging kernel $\mathbf{A}^*$:

$$\begin{aligned} \mathbf{A}^* &= \mathbf{CA} \\ &= \begin{pmatrix} \mathbb{I} & -\mathbf{A}_{ST} \\ -\mathbf{A}_{TS} & \mathbb{I} \end{pmatrix} \begin{pmatrix} \mathbf{A}_{TT} & \mathbf{A}_{ST} \\ \mathbf{A}_{TS} & \mathbf{A}_{SS} \end{pmatrix} \\ &= \begin{pmatrix} \mathbf{A}_{TT} - \mathbf{A}_{ST}\mathbf{A}_{TS} & \mathbf{A}_{ST} - \mathbf{A}_{ST}\mathbf{A}_{SS} \\ -\mathbf{A}_{TS}\mathbf{A}_{TT} + \mathbf{A}_{TS} & -\mathbf{A}_{TS}\mathbf{A}_{ST} + \mathbf{A}_{SS} \end{pmatrix} \end{aligned} \tag{11}$$

Similarly we can modify the retrieved CH_4 state ($\hat{x}$) and calculate an a posteriori corrected CH_4 state $\hat{x}^*$:

$$\hat{x}^* = \mathbf{C}(\hat{x} - x_a) + x_a \tag{12}$$

The a posteriori corrected averaging kernels $\mathbf{A}^*$ (row kernels) are depicted in the central panel of Fig. 4. The blue kernels are for altitudes at and above 11.5 km and the green kernels are for the troposphere (for altitudes < 11.5 km). The right panel of Fig. 4 depicts the tropospheric surface row kernels of $\mathbf{A}^*$ together with the respective kernel of $\mathbf{A}$. The region of improvement is marked in the graph with a dashed circle. We see that for the a posteriori corrected row kernel (green line) there is much less cross talk

from the UTLS than for uncorrected/original kernel (red line). At the same, time the sensitivity with respect to the lower middle troposphere is not modified. It is apparent that the a posteriori correction allows for generation of a product that ensures an optimal separation between the retrieved tropospheric and stratospheric amounts.

The smoothing error covariance matrices for the corrected state can be calculated by:

$$\mathbf{S}^*_{sm,bl} = \mathbf{CAS}_{a,bl}\mathbf{CA}^T \tag{13}$$

$$\mathbf{S}^*_{sm,tro} = (\mathbf{CA} - \mathbb{I})\mathbf{S}_{a,tro}(\mathbf{CA} - \mathbb{I})^T \tag{14}$$

$$\mathbf{S}^*_{sm,utls} = \mathbf{CAS}_{a,utls}\mathbf{CA}^T \tag{15}$$

For the corrected CH_4 state, the smoothing error caused by the stratospheric variability is significantly reduced in the troposphere if compared to the uncorrected state (compare green lines in the left and right panels of Fig. 5).

The error propagation for the a posteriori corrected state can be calculated by:

$$\mathbf{S}^*_e = \mathbf{CGK}_p\mathbf{S}_p\mathbf{K}_p^T\mathbf{G}^T\mathbf{C}^T \tag{16}$$

The right panel of Fig. 6 shows the square root of the diagonal elements of $\mathbf{S}^*_e$. We find that the a posteriori correction indeed only weakly affects the errors due to the parameter uncertainties of Table 2.

The a posteriori correction means an a posteriori optimisation of the retrieval constraints. The constraints are modified in order to get a tropospheric product that is optimally independent of the UTLS. A similar – although not equivalent – retrieval result might be achieved by already separating the tropospheric and stratospheric constraints in the original retrieval step. This has already been done, for instance, by Stiller et al. (1995), by means of a so-called "partitioning retrieval". The advantage of our a posteriori method is, that we get two products that are interesting: first, the optimally estimated profiles (no a posteriori correction), with good sensitivity from the lower troposphere up to the stratosphere, but with the UTLS cross talk on the tropospheric data. This is the

product that should be used for validating CH_4 total column measurements made by satellites. The second product is the optimally estimated tropospheric mole fraction. This product has slightly reduced sensitivity in the UTLS, where most satellites are sensitive, but it provides the best tropospheric CH_4 data quality and it is well-suited for tropospheric CH_4 source/sink research.

2.3.4 Error discussion

Table 3 summarizes the theoretical quality assessment of the CH_4 retrievals. The table lists DOFS values and the errors for the lower tropospheric column-averaged CH_4 product with and without applying the a posteriori correction as suggested in the previous subsection. The errors obtained if no a posteriori correction is applied are given in parenthesis.

At all stations, except Arrival Heights, we have typical DOFS close to or above 2.5. This means that we can estimate some details of the vertical distribution of the CH_4 mole fraction. However, we have to be aware that the lower tropospheric CH_4 signals (tropospheric CH_4 variations) are rather small compared to the UTLS signals (CH_4 variations due to variations of the tropopause altitude). This means that the small cross dependency of the retrieved lower tropospheric CH_4 mole fraction on the CH_4 state of the UTLS can significantly affect the quality of the lower tropospheric column-averaged CH_4 product. As a consequence, the UTLS smoothing error is a leading uncertainty source and dominates the overall smoothing errors in the lower troposphere (recall left panel of Fig. 5). This error is the more important, the lower the tropopause (it is more important for the polar than for the subtropical sites) and it can occasionally exceed 2 %, which is on the same order as the tropospheric CH_4 variations. In this context it is important to note that the UTLS smoothing error is actually not a purely random error. Since the tropopause altitude has a seasonal cycle this error will also depend on the season. It will mainly cancel out in the annual mean data but it will be responsible for major uncertainties in the lower tropospheric CH_4 seasonal cycles estimated from the FTIR observations. Therefore, if the objective is a precise tropospheric CH_4 product,

it is important to apply the a posteriori correction. The method reduces the cross talk for the stratosphere on the tropospheric CH_4 product at all sites, in particular at the polar regions (low tropopause altitude) where the cross dependency on the UTLS is particularly important. For the a posteriori corrected data we get for all stations (except Arrival Heights) total smoothing errors that are smaller than 1 %.

The relatively low DOFS values for Arrival Heights are explained by the lower signal to noise ratio of Arrival Heights spectra. Arrival Heights is the only site within our study where a Bruker 120M IFS is deployed. All the other sites use Bruker 120HR or 125HR, which offer higher signal to noise ratio as well as better ILS stability than the Arrival Heights 120M. For about 50 % of all Arrival Heights observations we get DOFS values of below 2.0. We exclude the respective spectra from this study, since they make independent lower tropospheric CH_4 retrievals rather difficult. The mean DOFS value for the remaining observations is 2.14, which allows determination of a lower tropospheric column-averaged CH_4 with a smoothing error of typically 1.1 % (but only if the a posteriori correction is applied).

We calculate the statistical and systematic errors for the uncertainty assumptions as listed in Table 2. The statistical errors sum up to about 1 % and are dominated by baseline uncertainties and measurement noise. We estimate a systematic error of about 2.5 %, which almost exclusively reflects the uncertainty in the spectroscopic CH_4 parameters. The a posteriori correction has nearly no effect on the statistical and systematic errors.

The values we report in Table 3 are for one individual measurement, which takes about 5–10 min. At most sites, several measurements are made per day and the statistical errors will be much smaller for the daily averages. The precision for daily mean data is likely better than 0.5 % at all sites (statistical error value of Table 3 multiplied by $1/\sqrt{N}$, with N being the number of measurements).

3 Pairing the ground-based FTIR and surface in-situ datasets

3.1 Surface in-situ measurement sites

We use surface in-situ CH_4 measurements obtained at different globally distributed sites. The data have been acquired by different institutions (please refer to Table 4). All of these sites are part of the GAW programme, which has been established by the World Meteorological Organization (WMO) in order to ensure consistent high quality standards. All GAW CH_4 site measurements are calibrated to the NOAA04 standard scale (Dlugokencky et al., 2005). Via this program, the activities of the observational in-situ network are coordinated: realisation of station audits, development of standard operational procedures or measurement guidelines, etc. The GAW data are publicly available through the World Data Center for Greenhouses Gases website (WDCGG, http://ds.data.jma.go.jp/gmd/wdcgg/).

The majority of the in-situ stations measure CH_4 by gas chromatography (GC) techniques with flame ionization detection (FID). This technique has been widely used by the in-situ community. In recent years, optical techniques like cavity ring-down spectroscopy (CDRS) or in-situ FTIR analysers have been introduced, showing similar or even better precisions than the traditional GC systems (e.g. Winderlich et al., 2010; Griffith et al., 2012; Hammer et al., 2013). The GAW CH_4 data are generally submitted to the WDCGG as hourly, daily and/or monthly mean and/or as event sampled data. Table 4 summarizes some information and Fig. 2 depicts the location of the in-situ stations that take part in our study.

The GAW CH_4 data are very high quality (compatibility between laboratories of ±2 ppb). However, even if the stations in the GAW network are chosen such that the observed atmospheric composition is regionally representative and usually free of significant local influences they can be affected by local small-scale processes (e.g. small-scale turbulences, very local sources and sinks) and therefore they are not always representative for background conditions. Only under some atmospheric situations we can

expect that the CH_4 surface in-situ data are representative for tropospheric regional-scale signals and thus comparable to the FTIR data.

To obtain in-situ time series from the GAW data that are representative of regional-scale signals, we apply a series of site specific filters. Figure 7 shows the paired FTIR (red stars) and the filtered regional-scale GAW (black squares) time series for each station. The WACCM apriori values used for the FTIR retrievals are shown as green lines. Please note that there are much more GAW regional-scale data points for the Izaña and Karlsruhe FTIR sites than for the other sites, since for the Izaña and Karlruhe sites we can reconstruct regional-scale GAW data on a daily time scale and for the other sites only on a monthly time scale. Details on the site specific GAW data filtering are explained in the following subsections.

We think that it is important to state here a fundamental difference between the GAW in-situ data and remote sensing data. The in-situ measurements provide pure, precise, and accurate CH_4 data (CH_4 is directly measured and referenced to WMO standards). On the contrary, a remote sensing system like the ground-based FTIR, measures spectral radiances, which are then interpreted with respect to the tropospheric CH_4 signal. This means that the FTIR CH_4 product is a mere proxy for the tropospheric CH_4 state, not to be confused with the true actual tropospheric CH_4 value.

3.2 FTIR Izaña vs. in-situ Izaña

Izaña is a subtropical high mountain observatory located on the Canary Island of Tenerife, Spain at 2367 m a.s.l. The NDACC FTIR has been in operation continuously since 1999 when a Bruker IFS 120M was installed. In March 2005 the instrument was replaced by a Bruker IFS 125HR. A good agreement between instruments has been found during an intercomparison campaign of few months (Sepúlveda et al., 2012; García et al., 2012). In this study we present results for the 2007–2012 period. On average we work with 70.2 days of FTIR measurements per year (251.2 measurements per year).

The in-situ CH_4 equipment is located only few tens of meters apart from the FTIR. It has measured in-situ CH_4 amounts by the gas chromatography technique with Flame Ionization Detection (GC-FID) continuously since 1984, and since then the data have been uploaded to the WDCGG. See Gomez-Pelaez and Ramos (2011) and references therein for information about the measurement system and the raw data processing scheme used in this global GAW site. Izaña is usually located above a strong subtropical temperature inversion layer. During daytime the strong diurnal insolation generates a slight upslope flow of air originating from below the inversion layer, but during nighttime the airmass at Izaña is well representative of the free troposphere (or at least of the lower part of the free troposphere). Due to this special situation we only work with Izaña's GAW CH_4 night-time data (from 20:00 UTC to 08:00 UTC), i.e. we work only with about 50 % of all available hourly mean data. This filter does typically provide one nighttime mean value every 24 h (typically 365 days of in-situ measurements per year). We calculate the GAW CH_4 mean of two consecutive night mean values and pair it with the FTIR daily median of the enclosed day. In addition we calculate a representative daily mean FTIR measurement time (mean time of the used FTIR data ensemble) and require that the FTIR's mean measurement time is between 10:00 UTC and 18:00 UTC (i.e. we exclude days when FTIR data have only been measured very early in the morning or very late in the evening).

3.3 FTIR Karlsruhe vs. in-situ Schauinsland

The Karlsruhe FTIR instrument, a Bruker IFS 125HR, is located in a continental flat terrain inside the Karlsruhe Institute of Technology (KIT), Campus North, Germany at 110 m a.s.l. It has been an official TCCON (Total Carbon Column Observing Network) station since 2010 and also measures down to the mid-infrared ($\approx 2000\,cm^{-1}$), a region that is traditionally covered by NDACC spectrometers. Information about the Karlsruhe instrument can be found in Gisi et al. (2011). On average we work with 104 days of FTIR measurements per year (462.3 measurements per year).

The closest GAW station that provides continuous in-situ CH_4 data is Schauinsland at 1200 m a.s.l., which is located about 130 km south of Karlsruhe. The station is situated on a mountain ridge in the Black Forest. During night the station is usually above the boundary layer, while during daytime, particularly in summer, the station mostly lies within the convective boundary layer. It has measured in-situ CH_4 amounts by GC-FID continuously since 1991.

In order to get in-situ data representative of regional-scale CH_4 signals, we have to filter the Schauinsland GAW CH_4 measurements (otherwise the data are strongly affected by local small-scale signals). A simple method consists in using local nighttime values (e.g. the nine hours between 22:00 and 07:00) and restrict on observation made at high wind-speed ($> 4\,m\,s^{-1}$). The nighttime filter removes about 60 % of all hourly data. The wind filter removes another 60 %. The two filters together remove almost 85 % of all available hourly data. This is a very high number and leaves us with only 35 % of all measurement days. In addition, we find that this filter does still not reasonably eliminate all the expected local small-scale signals (see Fig. A5 of Appendix A).

For this paper we developed a new method for detecting the regional-scale signals in the surface in-situ CH_4 data. It consists in combining the surface in-situ CH_4 data measured at two Central European sites, Schauinsland and Jungfraujoch. Jungfraujoch is a high mountain observatory located in the Swiss Alps at 3580 m a.s.l., about 150 km south of Schauinsland (see Fig. 2). We define the Schauinsland CH_4 background signal as the signal that remains after requiring common variability in the Schauinsland and Jungfraujoch data. This filter removes about 50 % of all available hourly mean data (leaves us with data for 65 % of all measurement days). The amount of removed data is significantly smaller than when using the nighttime/wind filter. Furthermore, the local small-scale signals are very effectively eliminated, thereby allowing the reconstruction of regional-scale in-situ signals. Please refer to Appendix A for details about this filter method.

We calculate daily medians and a representative daily mean measurement time (mean time of the used data ensemble) from the filtered in-situ data. The GAW daily

medians are then paired with the FTIR daily medians, but only if the GAW and FTIR representative measurement times agree within 6 h (i.e. we do not compare the data if, for instance, one instrument measures only in the morning and the other one only in the evening).

3.4 FTIR Eureka vs. in-situ Alert

The NDACC FTIR Eureka and GAW Alert stations are located on Ellesmere Island/Nunavut in the Canadian Arctic. The NDACC FTIR instrument is located at the Polar Environment Atmospheric Research Laboratory (PEARL) at 610 m a.s.l., operating throughout the sunlit period of the year (mid-February to mid-October). Its activities started in 1993 with a Bomem DA8 FTIR, which was replaced in July 2006 by a Bruker 125HR FTIR. In this study we present results only for the latter instrument and for a period of 6 yr. On average we work with 58 days of FTIR measurements per year (257 measurements per year). Details of the NDACC FTIR instrument, observations, and the PEARL site can be found in Batchelor et al. (2009).

The GAW measurements are made at the Dr. Neil Trivett GAW Observatory at Alert situated at 210 m a.s.l. on the northeastern tip of the island (about 460 km north of PEARL). It is the most northerly site within the GAW network and has measured in-situ CH_4 amounts by GC-FID continuously since 1988.

Both sites are far away from major anthropogenic activities and therefore we assume that they are well-suited for measuring regional-scale CH_4 signals. We work with the hourly GAW data but remove data where the standard deviation is greater than 0.5 % (hourly data are typically calculated from 4–5 individual measurements). This filter only removes 1 % of all available hourly mean data. Then, we calculate daily medians from the remaining hourly data, retaining data if the number of hourly data points is larger or equal than six and the respective standard deviation is smaller or equal than 1 %. From the remaining daily medians we calculate monthly medians and pair them with the coincident FTIR monthly medians. Here we compare only monthly and not daily datasets since there is a significant distance between the FTIR and the GAW sites

and we cannot reconstruct GAW regional-scale signals on a daily time scale that are representative for the FTIR site.

3.5 FTIR Ny-Ålesund vs. in-situ Ny-Ålesund

Ny-Ålesund is a small Norwegian settlement located in the north-west part of the island of Spitsbergen in the Svalbard archipelago, European Arctic. The NDACC FTIR experiment is situated at 21 m a.s.l. The FTIR spectra have been measured from the end of March to the end of September every year since 1990. In 1995, the Bruker 120M was replaced by a 120HR. We present results for the period 2005 to 2010. On average we work with 23 days of FTIR measurements per year (45 measurements per year). Details of the NDACC FTIR instrument and site can be found in Notholt et al. (1995).

The Ny-Ålesund GAW in-situ station is located slightly south from the FTIR on a small plateau of the Zeppelin Mountain at 475 m a.s.l. The GAW data are generally not influenced by local pollution from the settlement. Several flasks are collected per month (there are no CH_4 measurements on a daily basis) and all the samples are analysed for CH_4 at NOAA ESRL since 1994. We do not filter these in-situ data. We pair the GAW monthly mean data with the coincident FTIR monthly medians.

3.6 FTIR Kiruna vs. in-situ Pallas-Sammaltunturi

The NDACC FTIR Kiruna instrument is located at the Swedish Institute of Space Physics in the North of Sweden at 419 m a.s.l. A Bruker IFS 120HR has been operated continuously since 1996 and in July 2007 the instrument was upgraded to a 125HR. Information about the instrument can be found in Blumenstock et al. (2006). The period covered in this study is from 2004 to 2010. On average we work with 51 days of FTIR measurements per year (98.9 measurements per year).

The closest GAW in-situ site that provides CH_4 data is Pallas-Sammaltunturi situated in northern Finland at 560 m a.s.l. and about 250 km east of the Kiruna NDACC FTIR. Pallas-Sammaltunturi is on the top of a hill about 100 m above the tree line and it

is considered free of large local and regional pollution sources. From 2004 to 2008, the in-situ CH_4 amounts were measured by the traditional GC-FID system but since January 2009 the CDRS optical technique has been applied.

The in-situ station provides hourly data and in order to obtain the large-scale monthly median signal, we perform the same data treatment as for the Alert site (please refer to Sect. 3.4), i.e. there are only about 1 % of all available hourly data removed. We pair the GAW monthly medians with the coincident FTIR monthly medians. Here we compare only monthly and not daily datasets since there is a significant distance between the FTIR and the GAW sites.

3.7 FTIR Bremen vs. in-situ Mace Head

The NDACC FTIR Bremen instrument is located in the Institute of Environmental Physics at the University of Bremen, Germany at an altitude of 27 m a.s.l. A Bruker 125HR has been operated since June 2004. We work with data until 2011. On average we work with 29 days of FTIR measurements per year (50.9 measurements per year). Information about the instrument can be found in Velazco et al. (2007).

The Mace Head Research Station is located on the west coast of Ireland, County Galway at 5 m a.s.l., and about 1000 km east from Bremen. It is representative of background marine boundary layer conditions when the air masses arrive from the North Atlantic ocean (on average over 60 %, from meteorological records). The in-situ CH_4 amounts has been measured by GC-FID system. The station provides event and monthly mean data since 1987. We do not apply any filter to the dataset. We pair the GAW monthly mean data with the coincident FTIR monthly medians since there is a significant distance between the FTIR and the GAW sites.

3.8 FTIR Wollongong vs. in-situ Cape Grim

The NDACC FTIR Wollongong site is located at the University of Wollongong, Australia at 30 m a.s.l. Its activities started in 1994 with a Bomem DA3, which was upgraded to

a Bomen DA8 in 1996. Since 2007, a Bruker IFS 125HR has been in operation. Here, we only use data from this new instrument and for a period of 5 yr. On average we work with 66 days of FTIR measurements per year (350 measurements per year). Details of the current FTIR instrument can be found in Kohlhepp et al. (2012).

For our comparison with the FTIR data, we use the GAW CH_4 measurements acquired at the Cape Grim Baseline Air Pollution Station. This site is located in the northwestern point of Tasmania, Australia, at 94 m a.s.l. and about 1000 km south of Wollongong. The air that arrives at Cape Grim station from the southwest is essentially marine air. The in-situ GAW CH_4 measurements started in 1981 with a GC-FID system. For this work we use the values measured continuously since January 2007.

In order to ensure that the Cape Grim CH_4 signals are also representative for the Wollongong area we look in addition at data measured at Cape Ferguson, located towards the northest tip of Australia at 2 m a.s.l. and about 1500 km north of Wollongong. There flasks are collected several times per month since 1991. We combine the data gathered at two different GAW stations and look for common variability. This method is similar to the one we use for Central Europe (see Appendix A). In the case of Australia we first calculate daily means from the continuous Cape Grim data and for the several times per month acquired Cape Ferguson data. Then we pair the daily coincidences from both stations. Between August 2007 and August 2011 there are 76 daily coincidences. This number is determined by the rather low number of Cape Ferguson data. We define the in-situ CH_4 regional-scale signal as the signal that remains after requiring common variability in these coincident Cape Grim and Cape Ferguson data. This filter leaves as with 66 Cape Grim daily mean data (i.e. about 15 % of the data are filtered out) that should be well representative for the whole east coast of Australia (extension from north to south of 2500 km).

Finally we calculate the monthly medians from the retained Cape Grim data and pair them with the coincident FTIR monthly medians. Here we compare only monthly and not daily datasets since there is a significant distance between the FTIR and the GAW sites.

3.9 FTIR Lauder vs. in-situ Lauder

The NDACC FTIR Lauder experiment is located at the National Institute of Water and Atmospheric Research (NIWA) station in Central Otago, New Zealand at an altitude of 370 m a.s.l. The ground-based remote sensing FTIR activities started in 1986 with a Bomem DA2 operated in campaign mode. Long term full time measurements started in 1990 with the temporary instalment of a Bruker 120HR which was replaced in late 1991 with a Bruker 120M (Griffith et al., 2003). Since 2001 a later model Bruker 120HR has been in operation. We present results for the period 2007 to 2012. On average we work with 52 days of measurements per year (87 measurements per year). Details of the current FTIR instrument can be found in Morgenstern et al. (2012).

Surface in-situ CH_4 measurements at Lauder started in 2007 with the installation of an in-situ FTIR spectrometer trace gas analyser. Since here we present the Lauder in-situ FTIR data for the first time in a peer review article we provide some details on its measurement principle and data quality in the Appendix B.

For the purposes of this study in order to obtain a regional-scale CH_4 signal we filter the in-situ data for conditions that are indicative for a well-mixed boundary layer: first, we only work with afternoon data (hourly mean between 15:00 LT and 16:00 LT, if standard deviation is within 0.5 %). This removes more than 96 % of all available data. Second, we require the wind speed to be above 5 m s^{-1}, which removes another 72 %. We apply a filter that removes in total almost 99 % of all available in-situ data. For the remaining data we only have 19 daily coincidences of the in-situ measurements with the ground-based FTIR mesurements. This is a very low number and we decided to work with monthly coincidences. For this purpose we calculate monthly medians from the remaining in-situ data and pair it with the coinciding FTIR monthly medians. Please note that we have 47 monthly coincidences but only 19 daily coincidences since we define as a monthly coincidence each month that has at least one in-situ and one FTIR measurement at any day during the month, whereas for a daily coincidence we require that the in-situ and the ground-based FTIR data are obtained at exactly the same day.

3.10 FTIR Arrival Height vs. in-situ Arrival Height

The Arrival Heights atmospheric laboratory is located 3 km north of McMurdo and Scott Base stations on Hut Point Peninsula, Ross Island, Antarctica at 184 m a.s.l. Campaign based MIR-FTIR measurements started in 1988 when NIWA operated a Bomen DA2 FTIR in the austral spring. Full time measurements were initiated in 1991 with an Eocom 7101 FTIR and in 1996 a Bruker 120M replaced the Eocom. Unlike the prior FTIR systems the Bruker 120M contains a complete NDACC compliant filter set allowing the collection of solar spectra (August to March) over the wavenumber range 700 cm^{-1} to 4200 cm^{-1}. Details of the Arrival Heights NDACC site and FTIR instrumentation can be found in Wood et al. (2002). For this study we work with the spectra that have been measured since 2002 until 2011. On average we work with 10.5 days of measurements per year (11.5 measurements per year).

The GAW CH_4 data is measured by flasks since 1989 (Lowe et al., 1997). The fortnightly flask samples are taken only when the wind is from the northerly direction and the wind speed is greater than 5 m s^{-1} (there are no CH_4 measurements on a daily basis). This is to avoid any possible contamination from Scott Base and McMurdo station anthropogenic emissions. We use these data only if the event data are calculated as the mean of at least five individual measurements and if the respective standard deviation is within 0.5 %. The removes about 5 % of all the data available on the GAW database. From these remaining dataset we calculate monthly medians and pair it with the FTIR monthly medians.

4 Comparison of the ground-based FTIR and surface in-situ datasets

Table 5 summarizes the sites involved in the comparison, the time scale of the compared data, the filters applied for ensuring regional-scale GAW data, and the number of coincidences.

4.1 Daily datasets

For Izaña and Karlsruhe we have daily GAW in-situ data that are representative of regional-scale CH_4 signals (see explanation in Sects. 3.2 and 3.3). This offers unique opportunities for extensive comparison studies between the GAW in-situ and the Izaña and Karlsruhe FTIR remote sensing data. Figure 7 gives an overview of this large amount of data, covering almost six years for Izaña (2007–2012) and three years for Karlsruhe (2010–2012).

Figure 8 shows correlation plots for the daily coincidences. For Izaña there are 225 and for Karlsruhe there are 162 daily coincidences. We observe a reasonable correlation. However, the FTIR values are systematically higher than the GAW in-situ values. This systematic difference of about 2 % is very likely due to uncertainties in the applied spectroscopic parameters of CH_4. As mentioned in Sect. 2.2, further improvement of the CH_4 spectroscopic parameters is the subject of a current project.

For analysing the time series on different time scales we fit the measured time series to a time series model, which is similar to the one used in Gardiner et al. (2008); Sepúlveda et al. (2012). The model considers a mean CH_4 value and CH_4 variations on different time scales: a linear trend, intra-annual variations (Fourier series with three frequencies and phases), and inter-annual variations (Fourier series with frequencies lower than $1\,yr^{-1}$). For this analysis we work with the CH_4 values in the logarithmic scale. Since the tropospheric CH_4 variations (typically smaller than 50 ppb) are much smaller than the climatological CH_4 reference value (typically about 1850 ppb) we can interpret the variations on logarithmic scale ($\Delta \ln[CH_4]$) as the variations relative to the climatological reference value ($\Delta[CH_4]/[CH_4]$):

$$\Delta \ln[CH_4] \approx \Delta[CH_4]/[CH_4] \quad (17)$$

In order to investigate de-trended seasonal cycles we reconstruct a time series that only considers variation on the time scales longer than the seasonal cycle, i.e. we use the fit results obtained for the mean CH_4 value, the linear trend, and the inter-annual variations. This reconstructed time series does not reflect seasonal variations

and can be interpreted as the climatological long-term reference. We subtract it from the measured time series. Since we work with $\ln[CH_4]$ values the difference can be interpreted as the seasonal variation relative to the climatological long-term reference (see approximation 17). Then we calculate the mean and standard errors of the mean for these differences for each month (independently from the year). These mean values and standard errors of the mean are shown as the dots and error bars in Fig. 9. They represent the de-trended seasonal cycles (GAW: black squares; FTIR: red stars) relative to the climatological long-term reference. For both sites, we find generally good agreement between the seasonal cycles of FTIR and GAW (amplitude and phase). The shapes of the seasonal cycles at Izaña and Karlsruhe are different. At Izaña we observe no significant CH_4 changes between November and May and a rather sharp minimum in July. At Karlsruhe the tropospheric CH_4 mole fraction decrease continuously between February and August, when the minimum value is reached. These differences between the seasonal cycles at the two sites are observed consistently in the FTIR and the GAW data.

In addition to the seasonal time scale we look on day-to-day and long-term (biannual) time scales. For the separation into the different time scales we use the aforementioned time series model. The day-to-day time scale signal is calculated as the difference (on logarithmic scale) between the measured time series and the modeled time series (whereby all fitted time scales are considered: mean value, linear trend, seasonal cycle, and inter-annual cycle). Thereby we include all the variations (linear trend, seasonal cycle, and inter-annual cycle) when defining the climatological CH_4 reference. The so-calculated day-to-day time scale variations represent the variations that take place within a few weeks, relative to the this climatological CH_4 reference (see approximation 17).

In order to calculate the long-term (biannual) time scale signal we reconstructed a time series that only considers the fit results obtained for the mean CH_4 and the seasonal cycle and define it as climatological reference. Then we subtract it from the measured time series and obtain CH_4 values relative to the climatological reference

(see approximation 17). By this measure we get a de-seasonalised time series, for which we then calculate the biannual mean values.

In Fig. 10 we correlate the different time scale signals obtained for the GAW and the FTIR data. We find a good consistency for the correlations for all the different time scales. This clearly documents that GAW and NDACC FTIR consistently detect intra-monthly, seasonal, and long-term CH_4 variations.

4.2 Monthly datasets

For the NDACC FTIR sites of Eureka, Ny-Ålesund, Kiruna, Bremen, Wollongong, and Arrival Heights we cannot calculate daily GAW in-situ data that are representative for regional-scale CH_4 signals. Due to the different sampling characteristics of FTIR and GAW we cannot perform meaningful inter-comparisons on a daily basis for these sites and therefore we restrict the inter-comparison to monthly means, i.e. to large-scale signals. We then compare the GAW CH_4 monthly medians to the monthly FTIR medians, but only if the mean measurement times (mean time of the used daily data ensembles) do not differ by more than 15 days. An overview of the data amount that is compared is given in Fig. 7.

Figures 11–13 show the respective FTIR vs. GAW comparisons analogous to Figs. 8–10. The number of monthly coincidences are naturally smaller than the number of daily coincidences. For instance we have only 65 monthly coincidences for Bremen and 21 monthly coincidences for Arrival Heights. We observe essentially the same as for the Izaña and Karlsruhe comparisons: good correlations (on different time scales), reasonable agreement of seasonal cycles, and a systematic difference of about 2 %.

In particular for Arrival Heights we observe that the FTIR seasonal cycle has a significantly larger amplitude than in-situ seasonal cycle (see Figs. 7 and 12). This is mainly due to the interference from the UTLS. At Arrival Heights the vertical resolution is more limited than at other sites (i.e. resulting in a lower DOFS) and in addition the UTLS is rather close to the FTIR, i.e. we cannot completely eliminate influences of the UTLS on our tropospheric FTIR product. There is an anti-correlation between the real UTLS

CH_4 and the retrieved tropospheric FTIR CH_4. This is predicted by the kernels (see right panel in Fig. 4) and the reason for the large amplitude as observed by the FTIR. In summer (high CH_4 in the UTLS), the retrieved tropospheric FTIR CH_4 is too low and in winter (low CH_4 in the UTLS) it is too high. The a posteriori correction method reduces this effect but cannot completely eliminate it (because of the low DOFS). Something similar is observed for Ny-Ålesund.

4.3 Network-wide data consistency

Latitudinal gradients of CH_4 contain valuable source/sink information. In this subsection we examine whether the FTIR and GAW data observe similar site specific long-term CH_4 evolutions. For this purpose we look at de-seasonalised biannual mean data. Because the WACCM apriori data are station specific, i.e. they change from FTIR station to FTIR station, the differences between the FTIR data obtained at the different stations are due to a combination of the differences in the applied apriori data and the differences actually measured by the FTIR instruments. In order to reduce the influence of the apriori on our consistency assessment, we remove the WACCM apriori data and compare FTIR-WACCM with GAW-WACCM for each station. Hence we investigate whether the FTIR and GAW measurements allow a consistent improvement of a global model such as WACCM.

Since the seasonal cycles have been well studied in the previous sections and in order to investigate the average situation we work here with de-seasonalised biannual mean GAW and FTIR data, i.e. we remove the seasonal cycles as plotted in Figs. 9 and 12. Then we calculate the differences to the station specific WACCM data (i.e. calculate GAW-WACCM and FTIR-WACCM). This is done on a logarithmic scale. Since the CH_4 values are much larger than the difference with respect to the WACCM model approximation 17 applies and we can interpret the difference on logarithmic scale as the relative difference. In Fig. 14 we correlate the GAW-WACCM and FTIR-WACCM data. Both the GAW and FTIR data show similar differences with respect to the WACCM climatological mean data. The statistic for the

difference ([GAW – WACCM] – [FTIR – WACCM] = [GAW] – [FTIR]) for the deseasonalised biannual means for the different sites is 2.18 % ± 0.65 % (mean ± standard deviation). We observe that the data are described well by a straight line, meaning that both networks (GAW in-situ and NDACC FTIR) observe similar differences with respect to the model. Figure 14 also show a linear regression line (yellow), for which we obtain a correlation coefficient R^2 of 0.69. We think that this is a conservative documentation of the data consistency since it still has to be taken into account that some of the GAW data are measured several hundreds of kilometres away from the FTIR sites, and that local small-scale effects on the GAW data cannot be fully excluded.

As already observed and discussed in previous sections there is a systematic difference of about 2 % (the dashed line is the diagonal + 2 %). This systematic difference can be removed by calibrating the CH_4 spectroscopy to the GAW observations (calibration factor of 0.98). The calibration factor of 0.98 is also found in Wunch et al. (2010) showing an analogous comparison between TCCON CH_4 and total column in-situ measurements on the NOAA scale. Although, in this study and in the work of Wunch et al. (2010) different quantities are compared (TCCON vs. NDACC and total column vs. surface in-situ), we think that this does add some good weight to the spectroscopy vs. in-situ CH_4 comparison in general (e.g. if the line strengths were off by the same 2 % in both regions).

5 Conclusions

In this work we present a lower tropospheric regional-scale CH_4 product obtained from the ground-based FTIR remote sensing measurements made within the NDACC. The work extends the study of Sepúlveda et al. (2012), which was limited to the subtropical site of Izaña, to a set of nine globally distributed FTIR sites situated in polar regions, the mid-latitudes, and the subtropics. In order to minimise potential humidity interferences at humid sites like Wollongong, Bremen, or Karlsruhe, we slightly modify our spectral microwindow selection. Furthermore we use new spectroscopic CH_4 parameters,

which are currently produced within a project of the Deutsche Forschungsgemeinschaft (D. Dubravica and F. Hase, personal communications, 2012, work still in progress).

We demonstrate that the retrieved lower tropospheric CH_4 mole fraction can be significantly affected by CH_4 variations in the UTLS caused by tropopause altitude shifts. This is a severe problem and strongly compromises the scientific value of the tropospheric CH_4 data product. For instance, it means that the retrieved lower tropospheric seasonal cycle might mainly reflect the seasonal cycle of the tropopause altitude thus offering rather limited information for investigating CH_4 source/sink processes. We show that this dependency on UTLS variations can be significantly reduced by an a posteriori correction method. The correction consists of a simple matrix multiplication applied to the retrieved CH_4 state and is strongly recommended for polar sites. When applying this correction, we demonstrate that the NDACC FTIR experiments can observe lower tropospheric CH_4 mole fraction largely independent of the variation in the UTLS region. We estimate a precision for the daily mean data of about 0.5 %. We estimate a systematic error of about 2.5 % (Table 3) due to the uncertainty in the applied spectroscopic parameters (intensity and pressure broadening coefficient) of CH_4.

In contrast to the pure CH_4 measurements provided by GAW, the remote sensing CH_4 product is a mere proxy for the true actual tropospheric CH_4 value. This paper uses the GAW data in order to demonstrate that the NDACC FTIR CH_4 proxy reasonably picks up the actual CH_4 variability and so it can be recommended, for instance, for the purpose of satellite validation or for assimilation into a model. In these applications the limitations introduced by the applied constraints can be taken properly into account.

The Izaña nighttime GAW data are well representative for the lower free troposphere (subtropical island on a mountain). At Karlsruhe we use Schauinsland data, whose regional-scale signal is obtained by requiring correlation to the Jungfraujoch data. For this reason we think that for the Izaña and Karlsruhe NDACC FTIR site, we can generate a regional-scale GAW signal on a daily time scale that serves as a reasonable reference for the FTIR data. We show that both the remote sensing and in-situ data observe very similar lower tropospheric regional-scale CH_4 signals. The good agreement

is demonstrated for the different time scales that are interesting for CH_4 source/sink research: daily, seasonal, and long-term biannual mean evolution. For the other seven sites, we compare FTIR and regional-scale GAW data on a monthly time scale. The comparisons for these sites confirm the results obtained for the Izaña and Karlsruhe study. We demonstrate that both networks observe consistent latitudinal CH_4 gradients. The observed systematic difference of about 2 % is within the estimated systematic error due to the uncertainty of the spectroscopic parameters. This systematic difference can be removed by calibrating the CH_4 spectroscopy to the GAW observations (calibration factor of 0.98).

Appendix A

Combination of data from two nearby GAW stations

Central Europe offers the opportunity to combine two GAW datasets measured at two nearby stations at different altitudes within the free troposphere. The two stations are Schauinsland (47.97° N, 24.12° E, 1210 m a.s.l.) and Jungfraujoch (46.55° N, 7.99° E, 3580 m a.s.l.). Their location is depicted together with the location of the Karlsruhe FTIR instrument in Fig. A1. The stations should measure the same large-scale CH_4 signal when no local influences affect them. We combine the two central European GAW datasets to filter out the small-scale signals and thus, obtain a regional-scale signal.

The applied method is as follows:

- we pair the original hourly mean data of both stations (this large dataset is shown in Fig. A2).
- We calculate the time series of the differences between the Schauinsland and Jungfraujoch data.

- We fit a modeled time series to the measured difference. The model considers a systematic difference and an annual cycle of the difference.
- We calculate the residual (difference between modeled and observed differences).
- We only retain Schauinsland data when this residual is smaller than 1 %.

This data treatment gives some very interesting insight into Central European's CH_4 variations. Figure A3 shows that the annual CH_4 cycles at both stations are not in phase and that the Schauinsland mole fraction are systematically about 2 % larger than the Jungfraujoch mole fraction. Both can be expected due to the relatively high altitude of Jungfraujoch compared to Schauinsland.

Figure A4 shows an example for the behaviour of this filter for November 2010. After removing the local signals we can still observe some increased CH_4 mole fraction with a periodicity of about 10 days. We think that these are regional-scale CH_4 signals that are related to the synoptical-scale situation of Europe in this period.

Figure A5 shows the advantage of this filter in comparison to another possible filter method. It shows comparisons of Schauinsland in-situ data to coincident Karlsruhe FTIR data. The left panel for unfiltered in-situ data, the middle panel uses nighttime data filtered additionally by the wind criteria (wind speed $> 4\,m\,s^{-1}$), and the right panel shows the situation when applying the filter discussed here, which searches for common signals at Schauinsland and Jungfraujoch. We apply the filters on the hourly mean data, where the nighttime/wind filter removes about 85 % of all data and then calculate daily medians whenever there remains at least one hourly mean data for the day after filtering. The nighttime/wind filtered dataset leads to only 90 daily coincidences, i.e. about 65 % less daily coincidences than the unfiltered dataset, where we have 258 daily coincidences. The filter that works with common signals at Schauinsland and Jungfraujoch removes about 50 % of all hourly mean data and it leads to about 38 % less daily mean data (N = 162) than the unfiltered dataset (N = 258), i.e. it removes significantly less data than the nighttime/wind filter. When applying the filter for common signals

we observe a reasonable correlation between the Schauinsland in-situ and the Karlsruhe FTIR data (correlation coefficient of about 0.6). For the nighttime/wind filter the respective correlation coefficient is 0.26 (if we remove an outlier it is 0.47).

In summary, the here proposed filter for common signals removes significantly less data than the simple nighttime/wind filter. In addition it seems to very efficiently remove local small-scale signals, whereas the simple nighttime/filter does not that efficiently remove these local small-scale signals.

Appendix B

The Lauder in-situ FTIR dataset

The Lauder FTIR analyser is a prototype of that described in Griffith et al. (2012); Hammer et al. (2013). Continuous 10 min measurements of CO_2, CH_4, CO and N_2O are made from air drawn from an inlet located at the top of a 10 m mast. A roughing pump delivers sample air to a manifold at a rate of 10 L min^{-1} from this the FTIR analyser draws off sample air at 0.5 L min^{-1}. Daily measurements of a single working tank (prepared by NIWA-Gaslab, New Zealand) allow calibration of the atmospheric sample to the NOAA04 CH_4 scale. The precision of the measurements is 0.2 ppb. Due to the large operational pressure range a residual pressure sensitivity (Hammer et al., 2013) of 0.0285 ppb hPa^{-1} was experimentally derived and applied to sample measurements.

To assess the performance of the FTIR analyser against a standard in-situ measurement technique fortnightly flask samples have been taken at Lauder since mid-2009. Analysed at the NIWA-Gaslab, the resultant GC/FID derived CH_4 flask sample concentrations are also calibrated to the NOAA04 scale. A comparison of 71 flask samples and coincident FTIR analyser measurements over the period 2009 to 2013 show a −0.67 ppb bias (with a 1 sigma sd of 2.03 ppb) in the FTIR analyser measurements. This bias is not seasonally dependent and within the GAW network comparability recommended limit of ±2 ppb (WMO, 2012).

Additionally, in accordance with the recommendations of a WMO audit of the Lauder site GAW measurements conducted in 2010 (Zellweger et al., 2010) it is envisaged both the Lauder FTIR analyser and flask CH_4 in-situ datasets will be submitted to the GAW WDCGG database in the first half of 2014.

Acknowledgements. We would like to thank the many different technicians, PhD students, postdocs, and scientists from the different research groups that have been involved in the NDACC-FTIR activities during the last two decades. Thanks to their excellent work (maintenance, calibration, observation activities, etc.) high quality long-term datasets can be generated.

The Eureka measurements were made at the Polar Environment Atmospheric Research Laboratory (PEARL) by the Canadian Network for the Detection of Atmospheric Change (CANDAC), led by James R. Drummond, and in part by the Canadian Arctic ACE Validation Campaigns, led by Kaley A. Walker. They were supported by the AIF/NSRIT, CFI, CFCAS, CSA, EC, GOC-IPY, NSERC, NSTP, OIT, PCSP, and ORF.

The authors wish to thank Rebecca Batchelor, Rodica Lindenmaier, PEARL site manager Pierre F. Fogal, the CANDAC operators, and the staff at Environment Canadas Eureka weather station for their contributions to data acquisition, and logistical and on-site support.

We thank the Alfred Wegener Institut Bremerhaven for support in using the AWIPEV research base, Spitsbergen, Norway.

We would like acknowledge funding from the EU-Project InGOS and the Senate of Bremen for supporting the measurement program at Bremen.

We would like to thank Uwe Raffalski and Peter Völger for technical support at IRF Kiruna.

Measurements at Wollongong are supported by the Australian Research Council, grant DP110103118.

We would like to thank Antarctica New Zealand and the Scott Base staff for providing logistical support for the NDACC-FTIR measurement and in-situ program at Arrival Heights. The NIWA measurements at Lauder and Arrival heights is core funded through the Ministry of Business, Innovation and employment. The authors would like to thank Dr Vanessa Sherlock for her input and helpful comments.

The Advanced Global Atmospheric Gases Experiment (AGAGE) is funded by NASA grant NNX11AF17G to MIT. Funding for AGAGE measurements at Mace Head, Ireland comes from the above NASA grant to MIT and the UK Department of Energy and Climate Change. AGAGE measurements at Cape Grim, Tasmania are supported by the above NASA grant to MIT and

by the Australian Bureau of Meteorology and CSIRO Marine and Atmospheric Research. Flask measurements from Cape Ferguson, Australia are funded by CSIRO Marine and Atmospheric Research.

In-situ CH_4 measurements at Jungfraujoch are run by Empa in collaboration with the Swiss Federal Office for the Environment (FOEN). Empa and FOEN acknowledge the International Foundation High Altitude Research Station Jungfraujoch and Gornegrat (HFSJG) for providing access to Jungfraujoch facilities.

The Izaña in-situ GAW measurements have been carried out and financed by the Izaña Atmospheric Research Center (AEMET).

At Ny-Alesund and Izaña, the FTIR work has received funding from the European Community's Seventh Framework Programme ([FP7/2007–2013]) under grant agreement no. 284421 (see Article II.30. of the Grant Agreement). At Izaña has also received funding from the Ministerio de Economía and Competitividad from Spain for the project CGL2012-37505 (NOVIA project).

This study has strongly benefited from work made in the framework of the project MUSICA, which is funded by the European Research Council under the European Community's Seventh Framework Programme (FP7/2007–2013)/ERC Grant agreement number 256961.

E. Sepúlveda enjoyed a pre-doctoral fellowship thanks to the Spanish Ministry of Education.

References

Batchelor, R. L., Strong, K., Lindenmaier, R., Mittermeier, R. L., Fast, H., Drummond, J. R., and Fogal, P. F.: A new Bruker IFS 125HR FTIR spectrometer for the Polar Environment Atmospheric Research Laboratory at Eureka, Canada – measurements and comparison with the existing Bomem DA8 spectrometer, J. Atmos. Ocean. Tech., 26, 1328–1340, 2009. 655

Blumenstock, T., Kopp, G., Hase, F., Hochschild, G., Mikuteit, S., Raffalski, U., and Ruhnke, R.: Observation of unusual chlorine activation by ground-based infrared and microwave spectroscopy in the late Arctic winter 2000/01, Atmos. Chem. Phys., 6, 897–905, doi:10.5194/acp-6-897-2006, 2006. 656

Dlugokencky, E. J., Myers, R. C., Lang, P. M., Masarie, K. A., Crotwell, A. M., Thoning, K. W., Hall, B. D., Elkins, J. W., and Steele, L. P.: Conversion of NOAA atmospheric dry air CH_4 mole fractions to a gravimetrically prepared standard scale, J. Geophys. Res., 110, D18, doi:10.1029/2005JD006035, 2005. 651

Dubravica, D., Birk, M., Hase, F., Loos, J., Palm, M., Sadeghi, A., and Wagner, G.: Improved spectroscopic parameters of methane in the MIR for atmospheric remote sensing, in: High Resolution Molecular Spectroscopy 2013 meeting, 25–30 August 2013, Budapest, Hungary, available at: http://lmsd.chem.elte.hu/hrms/abstracts/D16.pdf (last access: 5 December 2013), 2013. 641

García, O. E., Schneider, M., Redondas, A., González, Y., Hase, F., Blumenstock, T., and Sepúlveda, E.: Investigating the long-term evolution of subtropical ozone profiles applying ground-based FTIR spectrometry, Atmos. Meas. Tech., 5, 2917–2931, doi:10.5194/amt-5-2917-2012, 2012. 652

Gardiner, T., Forbes, A., de Mazière, M., Vigouroux, C., Mahieu, E., Demoulin, P., Velazco, V., Notholt, J., Blumenstock, T., Hase, F., Kramer, I., Sussmann, R., Stremme, W., Mellqvist, J., Strandberg, A., Ellingsen, K., and Gauss, M.: Trend analysis of greenhouse gases over Europe measured by a network of ground-based remote FTIR instruments, Atmos. Chem. Phys., 8, 6719–6727, doi:10.5194/acp-8-6719-2008, 2008. 661

Gisi, M., Hase, F., Dohe, S., and Blumenstock, T.: Camtracker: a new camera controlled high precision solar tracker system for FTIR-spectrometers, Atmos. Meas. Tech., 4, 47–54, doi:10.5194/amt-4-47-2011, 2011. 638, 653

Gomez-Pelaez, A. J. and Ramos, R.: Improvements in the Carbon Dioxide and Methane Continuous Measurement Programs at Izaña Global GAW Station (Spain) during 2007–2009, Report of the 15th WMO/IAEA Meeting of Experts on Carbon Dioxide, Other Greenhouse Gases, and Related Tracer Measurement Techniques, 7–10 September 2009, Jena, Germany, GAW Report number 194, WMO TD 1553, available at: http://www.wmo.int/pages/prog/arep/gaw/gaw-reports.html (last access: 2 February 2012), 2011. 653

Griffith, D. W. T., Jones, N. B., McNamara, B., Walsh, C. P., Bell, W., and Bernardo, C.: Intercomparison of NDSC ground-based solar FTIR measurements of atmospheric gases at Lauder, New Zealand, J. Atmos. Ocean. Tech., 20, 1138–1153, 2003. 659

Griffith, D. W. T., Deutscher, N. M., Caldow, C., Kettlewell, G., Riggenbach, M., and Hammer, S.: A Fourier transform infrared trace gas and isotope analyser for atmospheric applications, Atmos. Meas. Tech., 5, 2481–2498, doi:10.5194/amt-5-2481-2012, 2012. 651, 669

Hammer, S., Griffith, D. W. T., Konrad, G., Vardag, S., Caldow, C., and Levin, I.: Assessment of a multi-species in situ FTIR for precise atmospheric greenhouse gas observations, Atmos. Meas. Tech., 6, 1153–1170, doi:10.5194/amt-6-1153-2013, 2013. 651, 669

Hase, F. and Höpfner, M.: Atmospheric raypath modelling for radiative transfer algorithms, Appl. Optics, 38, 3129–3133, 1999. 639

Hase, F., Blumenstock, T., and Paton-Walsh, C.: Analysis of the instrumental line shape of high-resolution Fourier transform IR spectrometers with gas cell measurements and new retrieval software, Appl. Optics, 38, 3417–3422, 1999. 645

Hase, F., Hanningan, J. W., Coffey, M. T., Goldman, A., Höpfner, M., Jones, N. B., Rinsland, C. P., and Wood, S. W.: Intercomparison of retrieval codes used for the analysis of high-resolution ground-based FTIR measurements, J. Quant. Spectrosc. Ra., 87, 25–52, 2004. 639, 641

Hoinka, P. K.: Statistic of the global tropopause pressure, Mon. Weather Rev., 126, 3303–3325, 1998. 636

Kohlhepp, R., Ruhnke, R., Chipperfield, M. P., De Mazière, M., Notholt, J., Barthlott, S., Batchelor, R. L., Blatherwick, R. D., Blumenstock, Th., Coffey, M. T., Demoulin, P., Fast, H., Feng, W., Goldman, A., Griffith, D. W. T., Hamann, K., Hannigan, J. W., Hase, F., Jones, N. B., Kagawa, A., Kaiser, I., Kasai, Y., Kirner, O., Kouker, W., Lindenmaier, R., Mahieu, E., Mittermeier, R. L., Monge-Sanz, B., Morino, I., Murata, I., Nakajima, H., Palm, M., Paton-Walsh, C., Raffalski, U., Reddmann, Th., Rettinger, M., Rinsland, C. P., Rozanov, E., Schneider, M., Senten, C., Servais, C., Sinnhuber, B.-M., Smale, D., Strong, K., Sussmann, R., Taylor, J. R.,

Vanhaelewyn, G., Warneke, T., Whaley, C., Wiehle, M., and Wood, S. W.: Observed and simulated time evolution of HCl, $ClONO_2$, and HF total column abundances, Atmos. Chem. Phys., 12, 3527–3556, doi:10.5194/acp-12-3527-2012, 2012. 658

Kurylo, M. J. and Zander, R.: The NDSC–Its status after 10 yr of operation, in: Proceedings of XIX Quarennial Ozone Symposium, Hokkaido University, Sapporo, Japan, 167–168, 2000. 637

Lowe, D. C., Manning, M. R., Brailsford, G. W., and Bromley, A. M.: The 1991–1992 atmospheric methane anomaly: Southern Hemisphere 13C decrease and growth rate fluctuations, Geophys. Res. Lett., 24, 857–860, 1997. 660

Morgenstern, O., Zeng, G., Wood, S. W., Robinson, J., Smale, D., Paton-Walsh, C., Jones, N. B., and Griffith, D. W. T.: Long-range correlations in Fourier transform infrared, satellite, and modeled CO in the Southern Hemisphere, J. Geophys. Res., 117, D11301 doi:10.1029/2012JD017639, 2012. 659

Notholt, J. and Lehmann, R.: The moon as light source for atmospheric trace gas observations: measurement technique and analysis method, J. Quant. Spectrosc. Ra., 76, 435–445, 2003. 638

Notholt, J., Neuber, R., Schrems, O., and v. Clarmann, T.: Stratospheric trace gas concentrations in the Arctic polar night derived by FTIR-spectroscopy with the moon as IR light source, Geophys. Res. Lett., 20, 2059–2062, 1993. 638

Notholt, J., Meier, A., and Peil, S.: Total column densities of tropospheric and stratospheric trace gases in the undisturbed Arctic summer atmosphere, J. Atmos. Chem., 20, 311–332, 1995. 656

Olsen, S. C. and Randerson, J. T.: Differences between surface and column atmospheric CO_2 and implications for carbon cycle research, J. Geophys. Res., 109, D02301, doi:10.1029/2003JD003968, 2004. 636

Rinsland, C. P., Goldman, A., Elkins, J. W., Chiou, L. S., Hannigan, J. W., Wood, S. W., Mahieu, E., and Zander, R.: Long-term trend of at northern mid-latitudes: comparison between ground-based infrared solar and surface sampling measurements, J. Quant. Spectrosc. Ra., 97, 457–466, 2005. 637

Rodgers, C.: Inverse Methods for Atmospheric Sounding: Theory and Praxis, World Scientific Publishing Co., Singapore, 2000. 641, 642

Rothman, L. S, Jacquemart, D., Barbe, A., Benner, D. C., Birk, M., Brown, L. R, Carleer, M. R., Chackerian Jr., C., Chance, K., Coudert, L. H., Dana, V., Devi, V. M., Flaud, J.-M.,

Gamache, R. R., Goldman, A., Hartmann, J.-M., Jucks, K. W., Maki, A. G., Mandin, J.-Y., Massie, S. T., Orphal, J., Perrin, A., Rinsland, C. P., Smith, M. A. H., Tennyson, J., Tolchenov, R. N., Toth, R. A., Auwera, J. V., Varanasi, P., and Wagner, G.: The HITRAN 2004 molecular spectroscopic database, J. Quant. Spectrosc. Ra., 96, 139–204, 2005. 645

Rothman, L. S., Gordon, I. E., Barbe, A., Benner, D. C., Bernath, P. F., Birk, M., Boudon, V., Brown, L. R., Campargue, A., Champion, J.-P., Chance, K., Coudert, L. H., Dana, V., Devi, V. M., Fally, S., Flaud, J.-M., Gamache, R. R., Goldmanm, A., Jacquemart, D., Kleiner, I., Lacome, N., Lafferty, W., Mandin, J.-Y., Massie, S. T., Mikhailenko, S. N., Miller, C. E., Moazzen-Ahmadi, N., Naumenko, O. V., Nikitin, A. V., Orphal, J., Perevalov, V. I., A. Perrin, A. P.-C., Rinsland, C. P., Rotger, M., Šimečková, M., Smith, M. A. H., Sung, K., Tashkun, S. A., Tennyson, J., Toth, R. A., Vandaele, A. C., and Auwera, J. V.: The HITRAN 2008 molecular spectroscopic database, J. Quant. Spectrosc. Ra., 110, 533–572, 2009. 641

Schneider, M. and Hase, F.: Technical Note: recipe for monitoring of total ozone with a precision of around 1 DU applying mid-infrared solar absorption spectra, Atmos. Chem. Phys., 8, 63–71, doi:10.5194/acp-8-63-2008, 2008. 645

Schneider, M. and Hase, F.: Improving spectroscopic line parameters by means of atmospheric spectra: theory and example for water vapour and solar absorption spectra, J. Quant. Spectrosc. Ra., 110, 1825–1839, 2009. 639

Schneider, M., Hase, F., and Blumenstock, T.: Water vapour profiles by ground-based FTIR spectroscopy: study for an optimised retrieval and its validation, Atmos. Chem. Phys., 6, 811–830, doi:10.5194/acp-6-811-2006, 2006a. 639, 641

Schneider, M., Hase, F., and Blumenstock, T.: Ground-based remote sensing of HDO/H_2O ratio profiles: introduction and validation of an innovative retrieval approach, Atmos. Chem. Phys., 6, 4705–4722, doi:10.5194/acp-6-4705-2006, 2006b. 639, 641

Schneider, M., Barthlott, S., Hase, F., González, Y., Yoshimura, K., García, O. E., Sepúlveda, E., Gomez-Pelaez, A., Gisi, M., Kohlhepp, R., Dohe, S., Blumenstock, T., Wiegele, A., Christner, E., Strong, K., Weaver, D., Palm, M., Deutscher, N. M., Warneke, T., Notholt, J., Lejeune, B., Demoulin, P., Jones, N., Griffith, D. W. T., Smale, D., and Robinson, J.: Ground-based remote sensing of tropospheric water vapour isotopologues within the project MUSICA, Atmos. Meas. Tech., 5, 3007–3027, doi:10.5194/amt-5-3007-2012, 2012. 639

Sepúlveda, E., Schneider, M., Hase, F., García, O. E., Gomez-Pelaez, A., Dohe, S., Blumenstock, T., and Guerra, J. C.: Long-term validation of tropospheric column-averaged CH_4 mole

fractions obtained by mid-infrared ground-based FTIR spectrometry, Atmos. Meas. Tech., 5, 1425–1441, doi:10.5194/amt-5-1425-2012, 2012. 636, 637, 639, 641, 642, 652, 661, 665

Stiller, G., von Clarmann, T., Wegner, A., Baumann, M., Frank, E., and Oelhaf, H.: Retrieval of tropospheric versus stratospheric partitioning of HCl from ground-based MIPAS FTIR spectra, J. Quant. Spectrosc. Ra., 54, 899–912, 1995. 648

Sussmann, R., Forster, F., Rettinger, M., and Bousquet, P.: Renewed methane increase for five years (2007–2011) observed by solar FTIR spectrometry, Atmos. Chem. Phys., 12, 4885–4891, doi:10.5194/acp-12-4885-2012, 2012. 639

Velazco, V., Wood, S. W., Sinnhuber, M., Kramer, I., Jones, N. B., Kasai, Y., Notholt, J., Warneke, T., Blumenstock, T., Hase, F., Murcray, F. J., and Schrems, O.: Annual variation of strato-mesospheric carbon monoxide measured by ground-based Fourier transform infrared spectrometry, Atmos. Chem. Phys., 7, 1305–1312, doi:10.5194/acp-7-1305-2007, 2007. 657

Winderlich, J., Chen, H., Gerbig, C., Seifert, T., Kolle, O., Lavrič, J. V., Kaiser, C., Höfer, A., and Heimann, M.: Continuous low-maintenance CO_2/CH_4/H_2O measurements at the Zotino Tall Tower Observatory (ZOTTO) in Central Siberia, Atmos. Meas. Tech., 3, 1113–1128, doi:10.5194/amt-3-1113-2010, 2010. 651

WMO: Brailsford, G. (Ed.), Report of the 16th WMO/IAEA Meeting on Carbon Dioxide, Other Greenhouse Gases, and Related Measurement Techniques (GGMT-2011), GAW Report No. 206, Wellington, New Zealand, 2012. 669

Wood, S. W., Bodeker, G. E., Boyd, I. S., Jones, N. B., Connor, B. J., Johnston, P. V., Matthews, W. A., Nichol, S. E., Murcray, F. J., Nakajima, H., and Sasano, Y.: Validation of version 5.20 ILAS HNO_3, CH_4, N_2O, O_3, and NO_2 using ground-based measurements at Arrival Heights and Kiruna, J. Geophys. Res., 107, D24, ILS 5-1–ILS 5-11, doi:10.1029/2001JD0005812002, 2002. 660

Wood, S. W., Batchelor, R. L., Goldman, A., Rinsland, C. P., Connor, B. J., Murcray, F. J., Stephen, T. M., and Heuff, D. N.: Ground-based nitric acid measurements at Arrival Heights, Antarctica, using solar and lunar Fourier transform infrared observations, J. Geophys. Res.-Atmos., 109, D18, doi10.1029/2004JD004665, 2004. 638

Wunch, D., Toon, G. C., Wennberg, P. O., Wofsy, S. C., Stephens, B. B., Fischer, M. L., Uchino, O., Abshire, J. B., Bernath, P., Biraud, S. C., Blavier, J.-F. L., Boone, C., Bowman, K. P., Browell, E. V., Campos, T., Connor, B. J., Daube, B. C., Deutscher, N. M., Diao, M., Elkins, J. W., Gerbig, C., Gottlieb, E., Griffith, D. W. T., Hurst, D. F., Jiménez, R., Keppel-Aleks, G., Kort, E. A., Macatangay, R., Machida, T., Matsueda, H., Moore, F., Morino, I.,

Park, S., Robinson, J., Roehl, C. M., Sawa, Y., Sherlock, V., Sweeney, C., Tanaka, T., and Zondlo, M. A.: Calibration of the Total Carbon Column Observing Network using aircraft profile data, Atmos. Meas. Tech., 3, 1351–1362, doi:10.5194/amt-3-1351-2010, 2010. 665

Zellweger, C., Steinbacher, M., Buchmann, B., and Scheel, H. E.: System and Performance Audit of Surface Ozone, Methane, Carbon Dioxide, Nitrous Oxide and Carbon Monoxide at the Global GAW Station Lauder, New Zealand, March 2010, WCC-Empa Report 10/3, available at: http://gaw.empa.ch/audits/LAU_2010.pdf (last access: 10 December 2013), 2010. 670

Table 1. Ground-based NDACC FTIR contributing sites.

Site (acronym)	Location	Altitude a.s.l. [m]	Instrument	Contributor
Eureka, EU	80.1° N, 86.4° W	610	125HR	University of Toronto
Ny-Ålesund, NA	78.9° N, 11.9° W	15	120HR	University of Bremen and Alfred Wegener Institute
Kiruna, KI	67.8° N, 20.4° E	419	120/5HR	Karlsruhe Inst. of Tech. and Inst. for Space Phys. Kiruna
Bremen, Br	53.1° N, 8.9° E	27	125HR	University of Bremen
Karlsruhe, KA	49.1° N, 8.9° E	111	125HR	Karlsruhe Inst. of Tech.
Izaña, IZ	28.3° N, 16.5° E	2367	120/5HR	Karlsruhe Inst. of Tech. and Meteorological State Agency of Spain
Wollongong, WO	34.4° S, 150.9° E	30	125HR	University of Wollongong
Lauder, LA	45.1° S, 169.7° E	370	120HR	National Institute of Water and Atmospheric Research
Arrival Heights, AH	77.8° S, 166.7° E	250	120M	National Institute of Water and Atmospheric Research and University of Denver

Table 2. Uncertainty sources used for our error estimation. The third column gives the uncertainty value and the fourth column the partitioning of this uncertainty between statistical and systematic sources.

Error source	Acronym	Uncertainty	Statistical/ Systematic
Measurement Noise	noi	0.4 %	100/0
Baseline (Channeling and Offset)	bas	0.1 % and 0.1 %	50/50
Mod. Eff. and Pha. Err.	ils	10 % and 0.1 rad	50/50
Temperature Profile	tem	2–5 K	70/30
Line Of Sight	los	1°	90/10
Solar Lines (Intensity and ν-scale)	sol	1 % and 10^{-6}	80/20
Humidity Profile	hum	10 % (2 km corr. length)	50/50
Spectroscopic Parameters (S and γ)	spe	2 %	0/100

Table 3. Typical DOFS for the CH_4 FTIR retrievals and typical smoothing errors (root-square-sum of bl, tro, and utls), total statistical errors, and total systematic errors for the lower tropospheric column-averaged CH_4 amounts. The error values are calculated according to the assumed uncertainty and statistical/systematic partitions as given in Table 2 and are for the a posteriori corrected retrievals as described in Sect. 2.3.3. The error values obtained without the a posteriori correction are given in parentheses.

Station	DOFS	Smoothing [%]	Statistical [%]	Systematic [%]
Eureka, EU	2.51	0.83 (1.52)	0.91 (0.92)	2.56 (2.58)
Ny-Ålesund, NA	2.27	0.95 (1.75)	0.69 (0.70)	2.29 (2.27)
Kiruna, KI	2.61	0.82 (1.51)	0.98 (1.00)	2.59 (2.60)
Bremen, BR	2.48	0.91 (1.40)	0.86 (0.88)	2.42 (2.40)
Karlsruhe, KA	2.57	0.93 (1.39)	1.07 (1.10)	2.54 (2.52)
Izaña, IZ	2.51	0.84 (1.14)	1.28 (1.29)	2.53 (2.51)
Wollongong, WO	2.60	0.97 (1.15)	1.06 (1.06)	2.53 (2.52)
Lauder, LA	2.52	0.93 (1.22)	1.21 (1.22)	2.66 (2.65)
Arrival Heights, AH	2.14	1.10 (2.23)	0.70 (0.72)	2.34 (2.30)

Table 4. In-situ surface contributing sites. Instrument acronym: GC, Gas Chromatography; FID, Flame Ionization Detection; CRDS, Cavity Ringdown Spectroscopy. Interval time means the time frequency of the data available used in this study.

Site, acronym	Location	Altitude a.s.l. [m]	Measurement method	Sampling type	Interval time	Contributor (acronym)
Alert, AL	82.45° N, 62.52° W	210	GC-FID	Continuous	hourly	Environment Canada (EC)
Ny-Ålesund, NA	78.90° N, 11.88° E	475	GC-FID	Flasks	monthly	Earth System Research Laboratory, NOAA (NOAA/ESRL)
Pallas-Sammaltunturi, PS	67.97° N, 24.12° E	560	GC-FID: 2004–2008; CRDS: since 2009	Continuous	hourly	Finnish Meteorological Institute (FMI)
Mace Head, MH	53.33° N, 9.90° W	8	GC-FID	Continuous	monthly	Advanced Global Atmospheric Gases Experiment Science Team (AGAGE)
Schauinsland*, SC	47.92° N, 7.92° E	1205	GC-FID	Continuous	hourly	Federal Environmental Agency Germany (UBA)
Jungfraujoch, JU	46.55° N, 7.99° E	3580	GC-FID: 2005–2009; CRDS: since 2010	Continuous	hourly	Swiss Federal Laboratories for Materials Science and Technology (EMPA)
Izaña, IZ	28.30° N, 16.50° W	2367	GC-FID	Continuous	hourly	Izaña Atmospheric Research Center, Meteorological State Agency of Spain (AEMET)
Cape Ferguson*, CF	19.28° S, 147.05° E	2	GC-FID	Flasks	event	Commonwealth Scientific and Industrial Research Organisation (CSIRO)
Cape Grim, CG	40.68° S, 144.68° E	94	GC-FID	Continuous	event	Advanced Global Atmospheric Gases Experiment Science Team (AGAGE)
Lauder, LA	45.1° S, 169.7° E	370	in-situ FTIR	Continuous	hourly	National Institute of Water and Atmospheric Research (NIWA)
Arrival Height*, AH	77.80° S, 166.67° E	184	GC-FID	Flask	event	National Institute of Water and Atmospheric Research (NIWA)

* indicate a GAW regional site, the rest sites are global sites.

Table 5. NDACC FTIR vs. GAW tropospheric CH_4 data comparison: stations, time scales, filter applied for obtaining regional-scale GAW data, and number of coincidences.

NDACC site	GAW site	Time scale	Filter applied to GAW data	Coincidences
Eureka	Alert	monthly	standard deviation	33
Ny-Ålesund	Ny-Ålesund	monthly	no filter	22
Kiruna	Pallas-Sammaltunturi	monthly	standard deviation	51
Bremen	Mace Head	monthly	no filter	65
Karlsruhe	Schauinsland	daily	combination of stations	162
Izaña	Izaña	daily	night time	225
Wollongong	Cape Grim	monthly	combination of stations	36
Lauder	Lauder	monthly	time, wind $\geq 5\,m\,s^{-1}$, and standard deviation	47
Arrival Heights	Arrival Heights	monthly	standard deviation	21

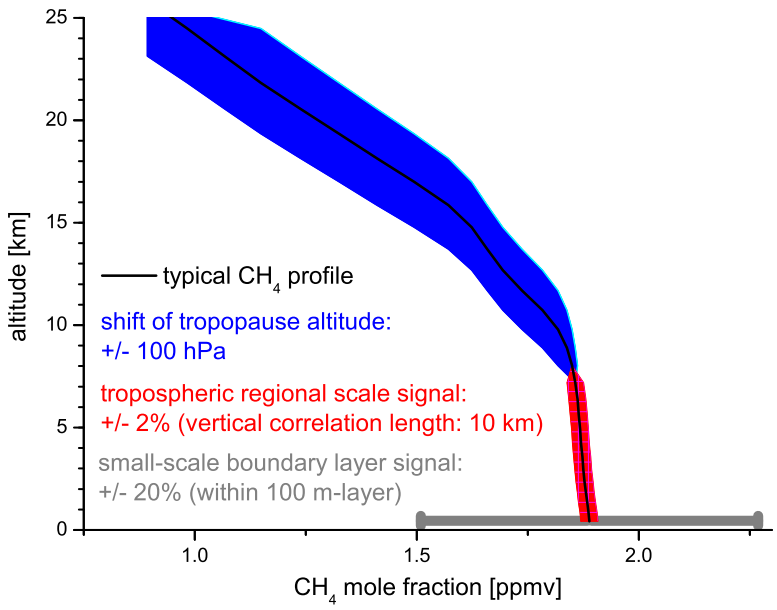

Fig. 1. Typical atmospheric CH_4 signals. Grey bar: near-surface boundary layer variability; red area: tropospheric regional-scale variability; blue area: UTLS variability caused by shifts in the tropopause altitude.

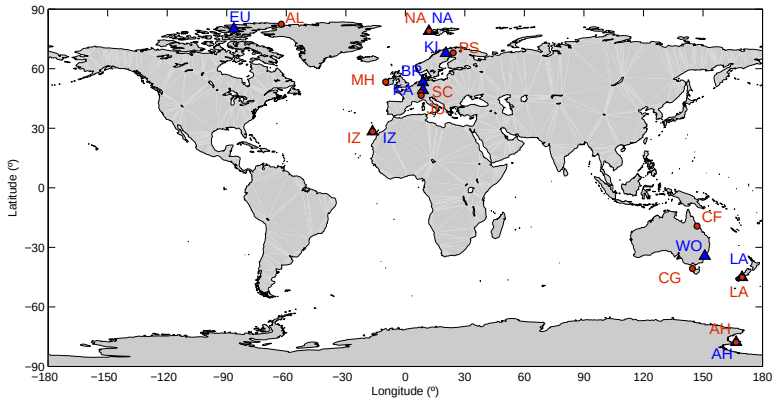

Fig. 2. NDACC FTIR stations in blue solid triangles and GAW in-situ stations in orange solid circles. See Tables 1 and 4 for the full station names.

Discussion Paper | Discussion Paper | Discussion Paper | Discussion Paper |

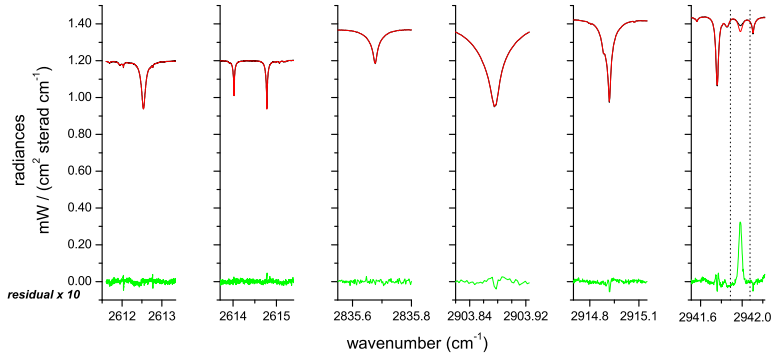

Fig. 3. Spectral microwindows applied to retrieve the tropospheric CH_4 mole fraction. It shows measured spectrum (black), simulated spectrum (red), and residuals multiplied by a factor of 10 (green). The black dashed lines in the last microwindow delimit an absorption line that is not included in the retrieval process.

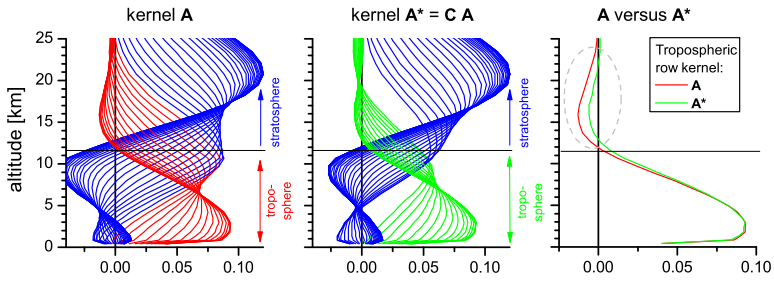

Fig. 4. Row averaging kernels of the CH_4 product for a typical observation at the subarctic site of Kiruna. Left panel: kernels $\hat{\mathbf{A}}$ obtained from the Tikhonov–Phillips profile retrieval (red: tropospheric kernels, blue: UTLS kernels). Central panel: kernels $\mathbf{A}^*$ obtained after applying the a posteriori optimisation of Eq. (11) (green: tropospheric kernels, blue: UTLS kernels). Right panel: comparison of the surface row kernels $\hat{\mathbf{A}}$ (red line) and $\mathbf{A}^*$ (green line). The typical altitude where the UTLS starts is indicated by the horizontal black line (11.5 km).

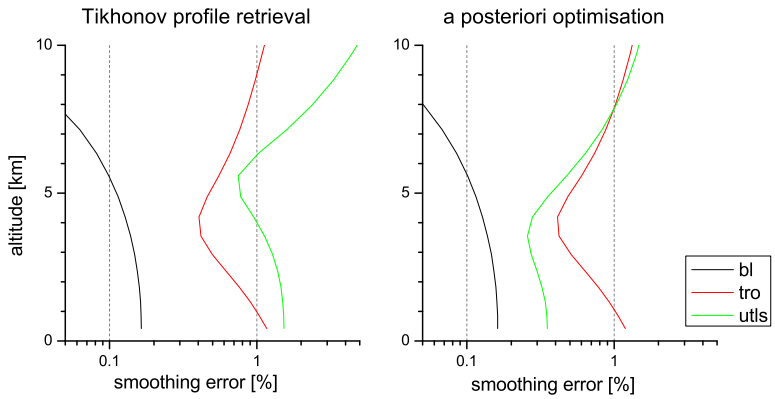

Fig. 5. Estimated smoothing errors for CH_4 for small-scale boundary layer variability (black line), tropospheric variability (red line), and variability in the UTLS due to a tropopause altitude shift (green line). Left panel: for the Tikhonov–Phillips profile retrieval. Right panel: after applying the a posteriori optimisation.

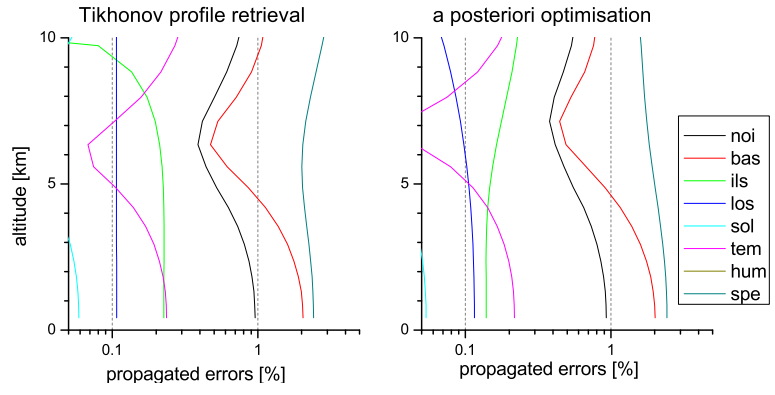

Fig. 6. Errors propagation for CH_4 due the uncertainties as listed in Table 2 in the third column. Error sources as given in the legend: noi (measurement noise), bas (baseline), ils (instrumental line shape), los (line of sight), sol (solar lines), tem (atmospheric temperature), hum (cross dependency on humidity; this error is smaller than 0.02 %), and spe (spectroscopic parameters). Left panel: for the Tikhonov–Phillips profile retrieval. Right panel: after applying the a posteriori optimisation.

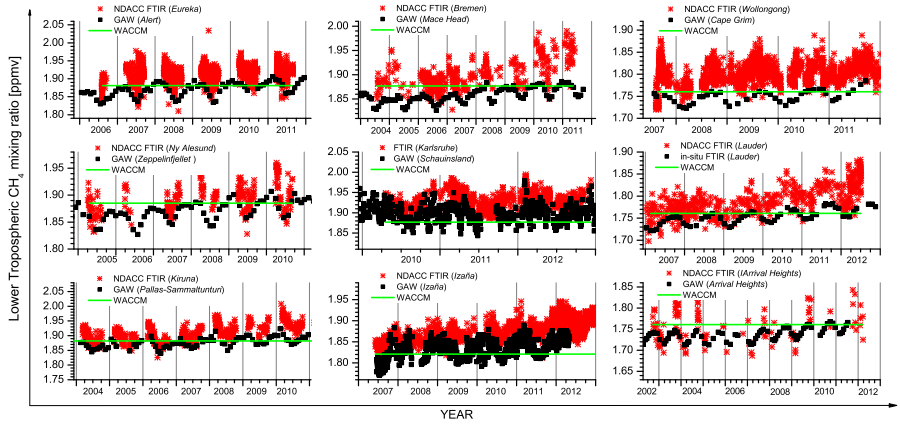

Fig. 7. Tropospheric column-averaged CH_4 mole fraction measured by NDACC FTIR (red stars) and GAW in-situ (black squares) at the nine different sites. Shown are all FTIR data and the GAW data that are representative for regional-scale signals (the filter methods are described in Sects. 3.2–3.10). These are daily data for Schauinsland and Izaña and monthly data for the rest of the GAW stations. The green line represents the WACCM apriori mole fraction applied for the NDACC FTIR retrievals.

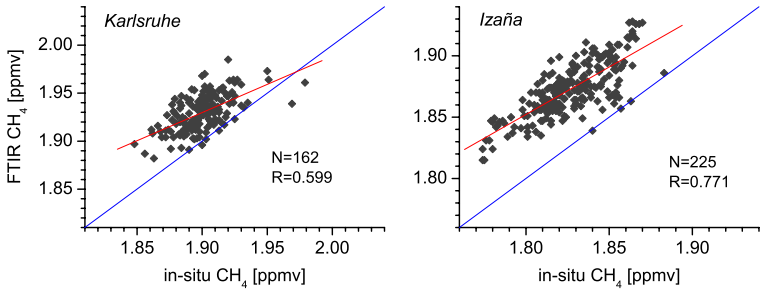

Fig. 8. Correlation plot between coincident tropospheric CH_4 daily medians obtained by NDACC FTIR and in-situ GAW for the Karlsruhe (left graph) and Izaña (right graph) FTIR sites. The blue lines indicate the 1 : 1 diagonal.

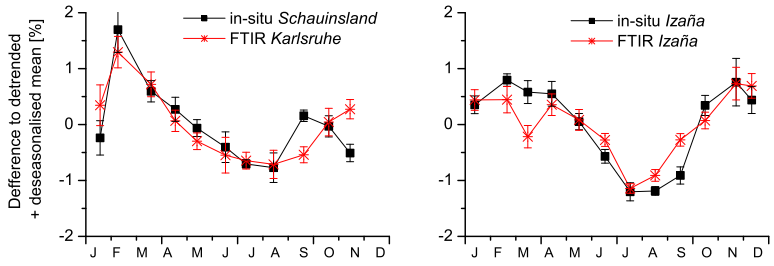

Fig. 9. Seasonal cycle for Karlsruhe (left graph) and Izaña (right graph) stations obtained by NDACC FTIR (red stars) and in-situ GAW CH_4 mole fraction (black squares), respectively.

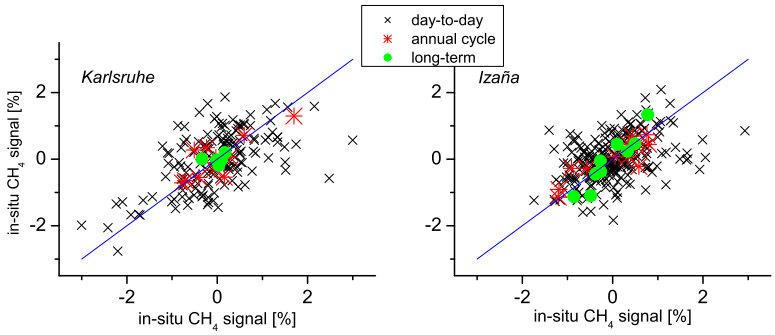

Fig. 10. NDACC FTIR/GAW correlation plots for CH_4 variations/signals on different time scales. Left graph: for Karlsruhe; right graph: for Izaña. The day-to-day variation is shown as black crosses, the monthly variation (annual/seasonal cycle) as red stars, and the long-term variation as green circles.

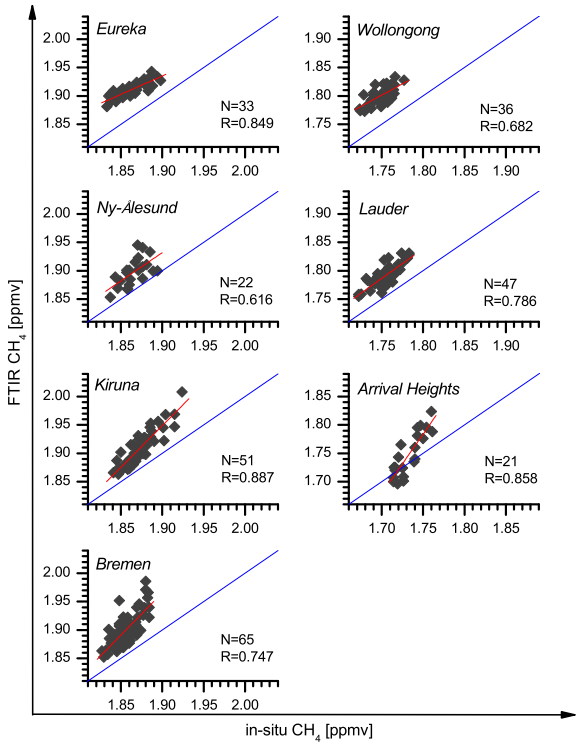

Fig. 11. Same as Fig. 8 but for the rest of the stations and for coincident data within ±15 days. The corresponding station name is shown in each graph.

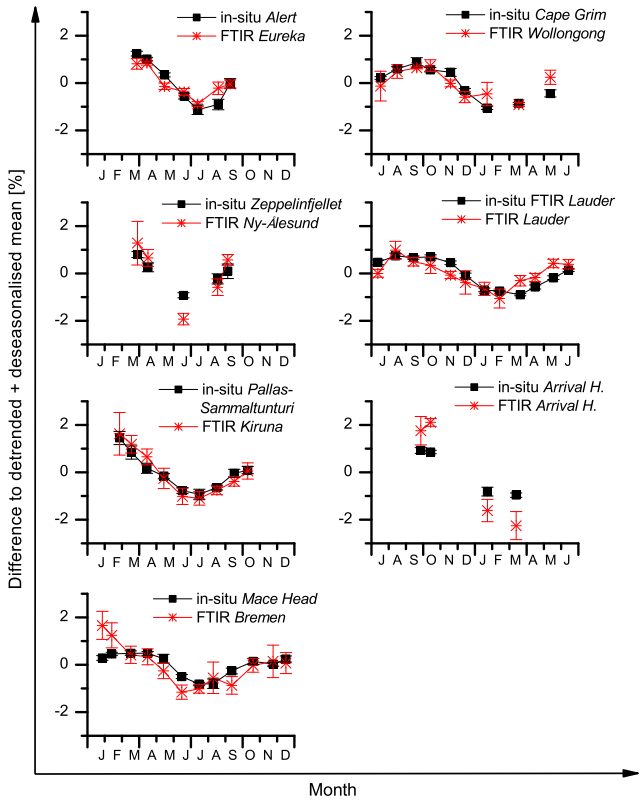

Fig. 12. Same as Fig. 9 but for the rest of the stations. The stations names are shown in each graph.

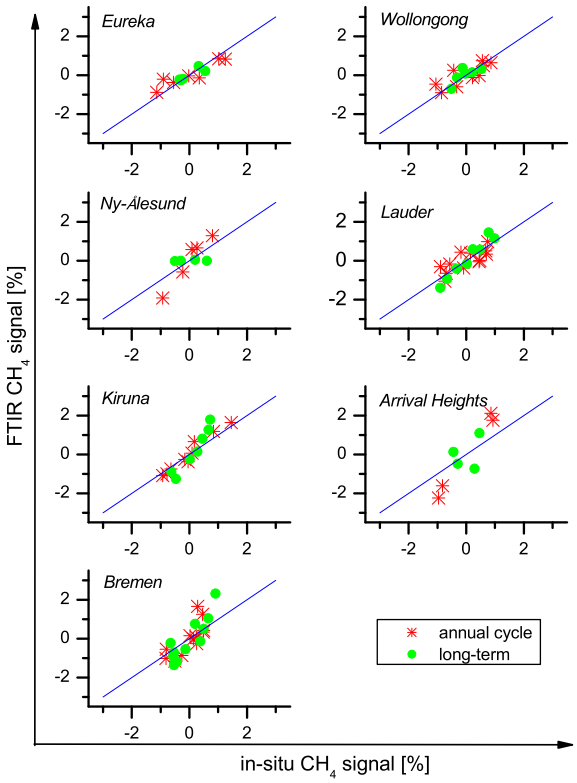

Fig. 13. Same as Fig. 10 but for the rest of the stations and only for the seasonal/annual cycle variability and the long-term variability.

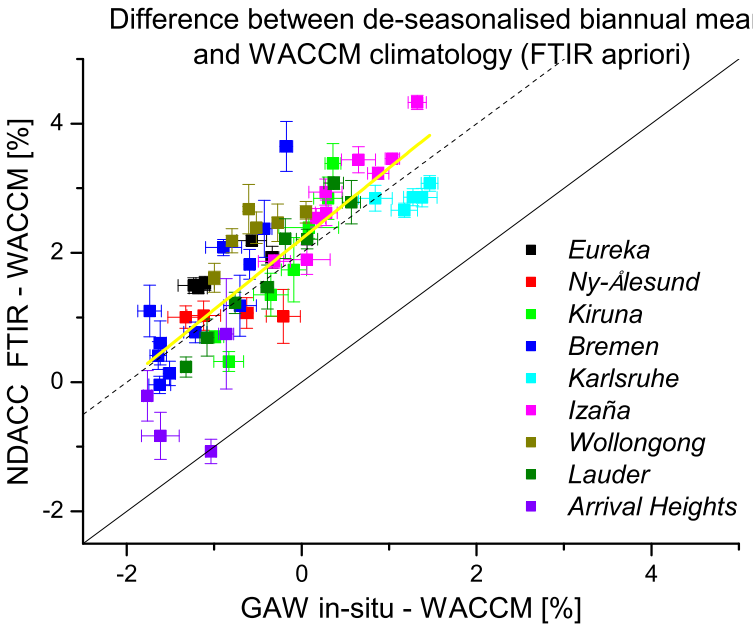

Fig. 14. Network consistency between GAW and NDACC FTIR. Plotted are the difference between the de-seasonalised biannual mean data and the WACCM climatology (FTIR apriori) for GAW and NDACC FTIR at the nine stations. The solid and dashed black lines indicate the 1 : 1 diagonal, being the dashed line + 2 % off. The solid yellow line shows the regression line.

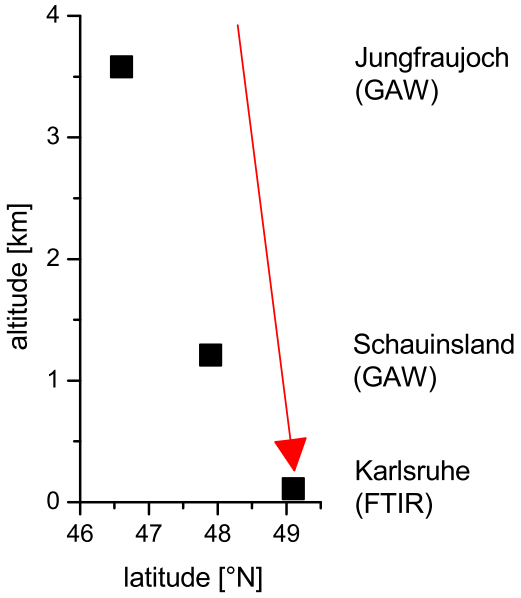

Fig. A1. Location of the Central European GAW stations and the Karlsruhe FTIR instrument. Red arrow is indicative for the line of sight of the FTIR instrument.

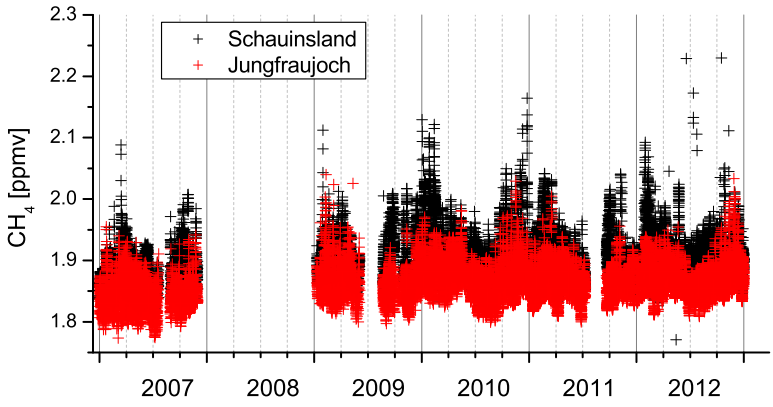

Fig. A2. Overview of the coincident Schauinsland and Jungfraujoch in-situ CH_4 time series.

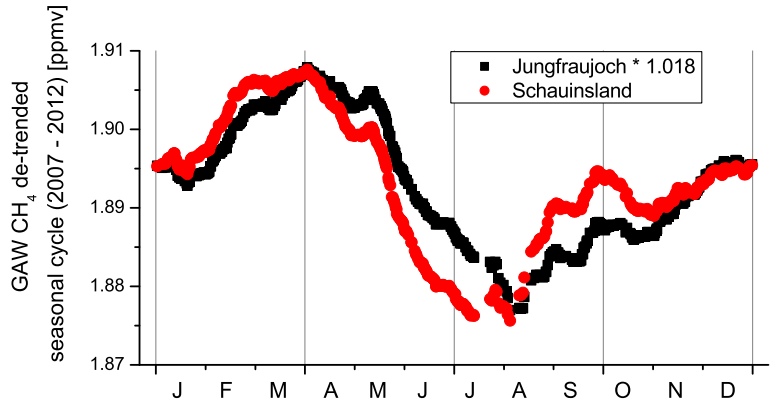

Fig. A3. De-trended seasonal cycles observed in the in-situ data of Schauinsland and Jungfraujoch. The Jungfraujoch CH_4 mole fraction are roughly 2 % lower than the Schauinsland mole fraction.

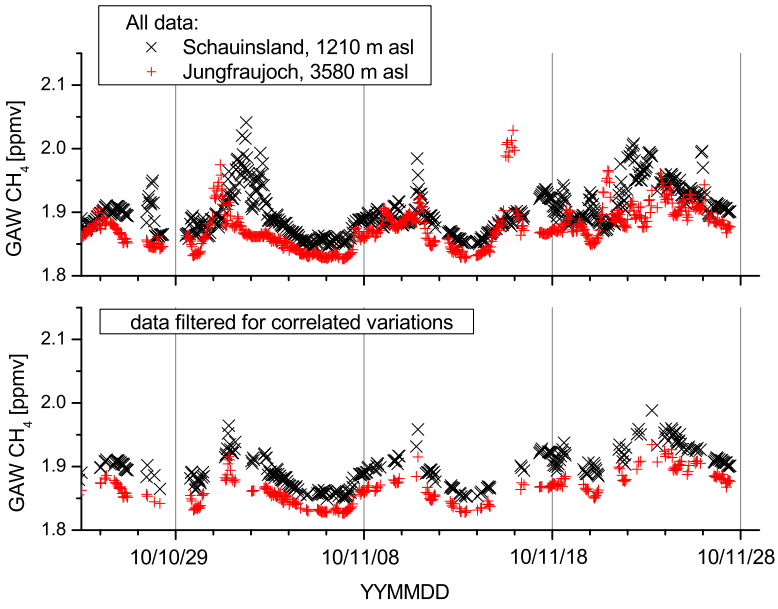

Fig. A4. Example of Schauinsland and Jungfraujoch CH_4 in-situ data for a period in November 2010. Upper panel: all data. Lower panel: data retained after applying the filter for common signals.

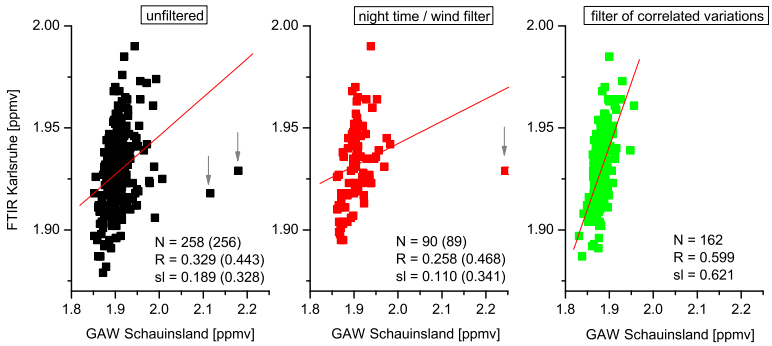

Fig. A5. Comparison of coincident Schauinsland in-situ and Karlsruhe FTIR CH_4 data for different in-situ data filters. Left panel: unfiltered data; central panel: nighttime/wind filter; right panel: filter for common signals in the Jungfraujoch and Schauinsland data. The regression lines are shown as red line. The number of achieved daily coincidences (N), the correlation coefficient (R), and the slope of the regression line (sl) is written in each graph. The N, R, and sl values after removing outliers (which are marked by arrows) are given in parentheses. Please note that the plot on the right panel is also shown in Fig. 8 (left panel) but there on an optimised scale.